Mechanisms associated with deep tissue injury induced by sustained compressive loading

Please check the document version of this publication:

Mechanisms associated with deep tissue injury induced by sustained compressive loading

Mechanisms associated with deep tissue injury induced by sustained compressive loading

Proefschrift

ter verkrijging van de graad van doctor aan de
Technische Universiteit Eindhoven, op gezag van de
Rector Magnificus, prof.dr.ir. C.J. van Duijn, voor een
commissie aangewezen door het College voor
Promoties in het openbaar te verdedigen
op dinsdag 22 november 2005 om 16.00 uur

door

Anke Stekelenburg

geboren te Raamsdonksveer

Dit proefschrift is goedgekeurd door de promotoren:

prof.dr. D.L. Bader
en
prof.dr. K. Nicolay

Copromotor:
dr.ir. C.W.J. Oomens

Anyone who isn't confused really doesn't understand the situation.
-Edward R. Murrow

Contents

x

Summary

Pressure ulcers, also termed decubitus, are localised areas of degenerated skin and/or underlying soft tissues, caused by sustained mechanical loads. They represent a serious health and financial problem. Prevalence figures are high, ranging between 8% and 23% depending on the severity of wounds included in the survey and the subject group under investigation. Prevalence is generally considered to be highest among elderly patients and those with impaired sensations, such as occurs following spinal cord injury. In addition, in situations where orthoses and prostheses are used to support soft tissues, pressure ulcers may occur.

Pressure ulcers can be initiated either at the skin layer and progress towards deeper layers, or progress from the underlying tissues towards the skin. The latter are generally referred to as deep pressure ulcers, which necessarily involve deep tissue injury recently defined as "A pressure-related injury to subcutaneous tissues under intact skin". This definition instantly reveals one of the major problems associated with their early detection. By the time a deep pressure ulcer becomes visible at the skin surface, effective clinical intervention may prove problematic and prognosis is variable. In addition, the underlying mechanisms leading to deep tissue injury following compressive loading are not well understood. The focus of the present thesis is therefore on deep tissue injury, and specifically on damage that starts in muscle tissue. Our hypothesis is that initial damage to muscle fibres is induced mechanically by local excessive deformation and subsequent disruption of muscle fibres.

Research on deep pressure ulcers has been hampered by a lack of non-invasive techniques to examine initial pathological changes in deep tissues. However, new techniques have become available which allow non-invasive examination of deeper tissues. In the present thesis, magnetic resonance imaging (MRI) was used to study the damage initiation and development in muscle tissue of Brown Norway rats, during and after compressive loading. An MR-compatible loading device was designed and built, which allowed simultaneous application of indentation and collection of MR-data. This offered the opportunity to measure the moment of damage initiation and the subsequent temporal development of damage using T2-weighted MRI. The loading device also enabled the use of different MR-techniques, such as contrast-enhanced MRI to obtain information of the perfusion status, and tagging MRI to measure deformation of the tissue during indentation. In order to distinguish between different factors that contribute to muscle damage several loading protocols, incorporating combinations of

ischaemia and compressive loading, were used. To study the relevance of the sustained deformation of cells, the location of damage, indicated by an increase in T2, was compared to local strain fields determined from MR tagging data. In addition, the preliminary stages of a dedicated finite element (FE) model were developed. Such a model might prove to be a valuable tool in both defining objective damage thresholds and design criteria for optimal pressure relief strategies.

The results showed that the effect of 2 hours of pure ischaemia on the T2 of muscle tissue was reversible within 40 minutes after unloading, which was confirmed by the histological examination showing only minor abnormalities. Compression of the tissue for 2 hours did lead to persistently increased T2 values up to 20 hours and localised regions of necrosis as indicated by histology. This implied that the deformation, superimposed on the ischaemia, was a major trigger for the initiation of damage. An increase in T2 during ischaemic loading did reveal tissue changes due to ischaemia alone. These tissue changes will most probably accelerate and/or increase the damage development during and after compressive loading. The importance of deformation was further confirmed by the correlation between regions of high shear strain calculated from tagging MR data and damage location.

In conclusion, this thesis presents a selection of MRI methodologies, each designed to identify specific mechanisms associated with the temporal profile of tissue damage in an animal model. Derived MR parameters were examined in conjunction with histological analysis and FE simulation. The importance of deformation was indicated by the location of damage, the histological appearance of the damage and the differences in response to pure ischaemia versus compression.

Chapter 1

Introduction

1.1 Problem definition

Pressure ulcers, also termed decubitus, may be defined as localized areas of degenerated skin and underlying soft tissues, caused by sustained mechanical loads. They represent a serious and increasing health problem to an ever-ageing population. Prevalence figures are very high, ranging between 8% and 23% depending on the severity of wounds included in the survey and the subject group under investigation [1, 2, 3]. Prevalence is generally considered to be highest among elderly patients [2, 4] and those with impaired sensations, such as occurs following spinal cord injury [5, 6]. In addition, in situations where orthoses and prostheses are used to support soft tissues, pressure ulcers may occur.
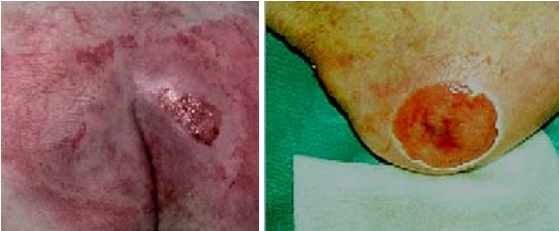
Different classification systems have been developed for pressure ulcers [7, 8, 9, 10]. Following the deliberations of the European Pressure Ulcer Advisory Panel (EPUAP) [11, 12], pressure ulcers are classified in four grades (table 1.1). Other systems define different stages in pressure ulcers. This, however, leads to confusion as pressure ulcer classification is only appropriate for defining the maximum depth of tissue involvement, and not the state of healing or progression of a pressure ulcer. Thus reverse grading cannot be used to describe the healing of a pressure ulcer [13, 14], as grade 4 pressure ulcers cannot become grade 3, grade 2, and/or subsequently grade 1 ulcers. Classification systems focus on visible signs of skin and, in advanced ulcers, of underlying tissues. It is, however, known that pressure ulcers can be initiated either in the superficial skin layers or within deeper tissues [15, 16]. Clearly those ulcers which initiate within deeper tissues are not fully accommodated with the current classification systems. By the time a deep pressure ulcer becomes visible, clinical intervention may be too late and, as a result, prognosis is variable. Deep pressure ulcers inevitably involve deep tissue injury which was recently defined as "A pressure-related injury to subcutaneous tissues under intact skin". The fact that deep tissue injury cannot be defined by staging systems was also the topic of the US National Pressure Ulcer Advisory Panel (NPUAP) debate in 2005 [17] entitled "Should we include deep tissue injury in pressure ulcer staging systems?". Part of this debate was a discussion about the causes of deep tissue injury, and whether or not these injuries are truly pressure ulcers. It raised a number of contrasting views and it is clear that the underlying mechanisms of deep tissue injury require further investigation.

The focus of the present thesis is therefore on deep tissue injury, and specifically on damage that starts in muscle tissue and its subsequent progression.

Most of the current knowledge on the aetiology of pressure ulcers has been provided by animal models. These studies, which are reviewed in chapter 2 [18], have mainly focused on the effects of both the magnitude and duration of loading and its nature, in particular, continuous versus intermittent loading. Early studies focussed on determining the minimal degree of loading that will lead to persistent tissue damage.

These studies all demonstrate an inverse relationship between the magnitude and duration of loading, indicating that the higher loads require less time to initiate tissue breakdown. Furthermore, it was demonstrated that intermittent loading was more damaging compared to continuous loading [19]. Hypotheses associated with the pathogenesis of pressure ulcers involve localised ischaemia [20, 21, 22], reperfusion injury [23], impaired interstitial fluid flow and lymphatic drainage [24, 25, 26, 27], and sustained deformation of cells [28, 29, 30]. In reality, each of these mechanisms can contribute to the causation of pressure ulcers, although their individual and combined role in tissue breakdown will undoubtedly vary depending on the nature of the mechanical insult and patient characteristics, such as illness and age [31]

Table 1.1 *Classification of pressure ulcers [11, 12] Adapted from PUCLAS software package developed by the EPUAP [32]*

Grade 1
Non-blanchable erythema of intact skin. Discolouration of the skin, warmth, oedema, induration or hardness may also be used as indicators, particularly on individuals with darker skin

Grade 2
Partial thickness skin loss involving epidermis, dermis or both. The ulcer is superficial and presents clinically as an abrasion or blister

Grade 3
Full thickness skin loss involving damage to or necrosis of subcutaneous tissue that may extend down to, but not through underlying fascia

Grade 4
Extensive destruction, tissue necrosis, or damage to muscle, bone, or supporting structures with or without full thickness skin loss

In order to be able to reduce the prevalence of pressure ulcers it is essential to improve and expand the knowledge of the aetiology in terms of both basic science and clinical experience. Research on deep tissue injury has been limited, in part, due to the difficulty in assessing initial pathological changes in the deep tissues with currently available techniques. In addition, it is not known how external loads are transferred to local internal stresses and strains and, more importantly, how they result in tissue damage. What is evident is that surface pressures alone are not representative of the internal mechanical conditions inside the tissue, which are most relevant for tissue breakdown. This is particularly relevant for complex tissue composition and geometry, where surface pressures result in highly inhomogeneous internal mechanical conditions, as is the case adjacent to bony prominences, such as the trochanter and the ischial tuberosity.

The primary focus in pressure ulcer prevention and treatment has traditionally concentrated on skin. This was certainly appropriate when considering that a high proportion of pressure ulcers initiate in the superficial skin layer [33]. However, the focus on skin was also out of necessity, due to the difficulty in assessing initial pathological changes in the deep tissues with established techniques, such as laser Doppler and transcutaneous gas monitoring. New techniques have, however, become available which allow non-invasive examination of deeper tissues. These include high-frequency ultrasonography [34], elastography [35, 36] and magnetic resonance imaging (MRI) [37]. The latter has been used in a limited number of human studies on pressure ulcers [38, 39], and proved to be useful in identifying pathological tissue changes related to deep pressure ulcers. It was demonstrated by Bosboom [40], using an animal model, that MRI could also be used to study the underlying mechanisms leading to muscle damage.

1.2 Magnetic Resonance Imaging

In the present thesis several MRI methodologies were used to study the underlying mechanisms in deep tissue injury after compressive loading. In particular, T2-weighted MRI was used to determine tissue status during and after loading. For an introduction to the physics of MRI, the reader is referred to the internet-book by Hornak [41] and textbooks by Vlaardingerbroek et al. [42] and Haacke et al. [43]. A brief description of MRI [44] is given below to explain the basis of MRI and illustrate what is measured by T2-weighted MRI, and how changes in tissue status can influence T2 values.

The nuclear magnetic resonance signal that is most frequency used for MRI arises from the magnetic properties of hydrogen nuclei in tissue water and fat molecules. Following placement in a strong magnetic field (figure 1.1a), the hydrogen nuclei are excited by an intense radio frequency (RF) pulse delivered at the resonant frequency (figure 1.1b). This pulse causes the nuclei to oscillate together (phase-coherent

oscillation) and, following the pulse, to generate a detectable magnetic signal that can be recorded electronically.

Immediately following the excitation pulse, the nuclei begin to dephase and the signal begins to decay. Decay of the nuclear magnetic resonance signal because of loss of phase coherence is termed transverse, or T2, relaxation (figure 1.2a). T2 is the time constant of the signal decay. The longitudinal relaxation time T1 describes the exponential recovery of magnetisation towards equilibrium (figure1.2b), and depends on the main magnetic field strength. This component of the MR signal reflects structural aspects, but is relatively insensitive to changes in the state of muscle. In contrast, T2 is essentially independent of magnetic field strength and very sensitive to tissue changes. A common used pulse sequence used for imaging is the spin-echo sequence (figure 1.3). A 90º pulse is first applied to the spin system. The 90º pulse rotates the magnetisation down to the xy plane. The transverse magnetisation begins to dephase. At some point in time after the 90º pulse, a 180º pulse is applied. This pulse rotates the magnetisation by 180º about the x axis. The 180º pulse causes the magnetisation to, at least partially, rephrase and to produce a signal called an echo. The echo time (TE) is defined as the time between the 90º pulse and the maximum amplitude in the echo. The intensity of the nuclear magnetic resonance signal is dependent on TE and on two properties of the tissue, namely, the concentration of hydrogen nuclei and the T2 of the nuclei in the magnetic environment of the tissue. Regardless of magnetic field strength, T1 is always greater than T2. For skeletal muscle tissue T1 and T2 are in the order of 1.5 s, at a field strength of 6.3 Tesla, and 30 ms, respectively.
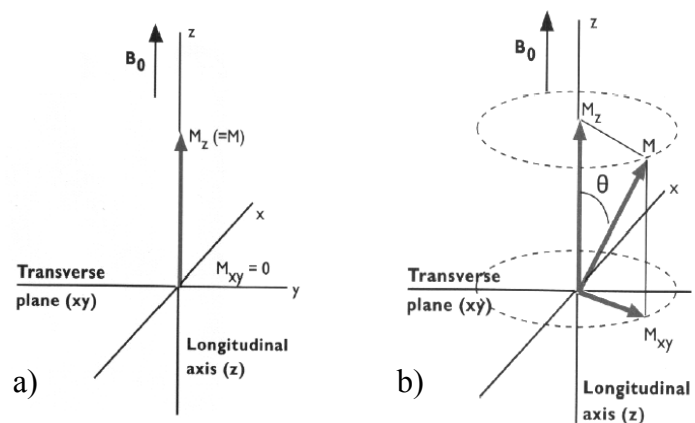
Figure 1.1 *a) Net magnetisation M_z due to main magnetic field. b) Direction of magnetisation is changed by radio frequency (RF) pulse.*

The intensity of the MR signal for a repeated spin echo sequence is given in first approximation by

$$I \approx Ne^{-TE/T2}(1-e^{-TR/T1}), \tag{1.1}$$

where N is the proton density, TE the echo time or signal delay time, and TR the radio-frequency pulse repetition time. When TR in an MR sequence is chosen long and the echo time (TE) is chosen short compared to T2, the contrast is mainly determined by the proton-density, yielding a so-called proton density weighted image. When TR is chosen short compared to T1 and TE short relative to T2, contrast is obtained on the basis of differences in T1, and the image is called a T1-weighted image. When TE is in the order of T2 and TR long relative to T1, contrast is obtained on the basis of differences in T2, resulting in a so-called T2-weighted image.
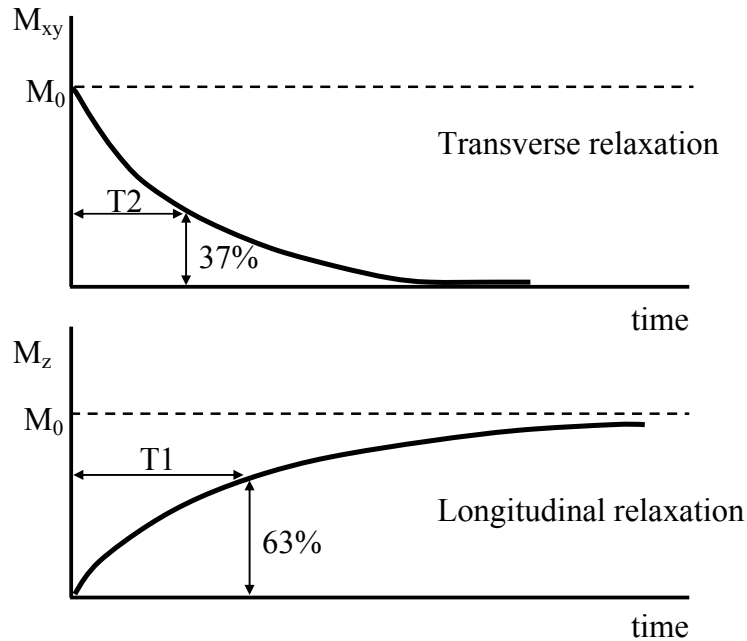
Figure 1.2 *a) Transverse relaxation time T2 describes the exponential decrease of the magnetisation in the transverse plane, which is perpendicular to the static magnetic field. b) Longitudinal relaxation time T1 describes the exponential recovery of magnetisation towards equilibrium.*

Although T2 relaxation is a single exponential process in water, the interpretation of the T2 relaxation of water in a protein matrix, such as muscle cytoplasm, is considerably more challenging. In concentrated protein solutions such as muscle, magnetic interactions between neighboring molecules cause local field variations that shorten the T2 relaxation time. In regions in which the motion of water is restricted, for example hydrogen bonding around proteins and other macromolecules, these magnetic interactions contribute to phase dispersion and signal decay. In addition, muscle tissue contains both intracellular and extracellular spaces, which increases the complexity of the T2 analysis. Thus changes in tissue status can cause osmotically driven shifts of muscle water that strongly influence the T2 relaxation time. An increase in the transverse relaxation time T2 is generally accepted as a measure of tissue damage [45].
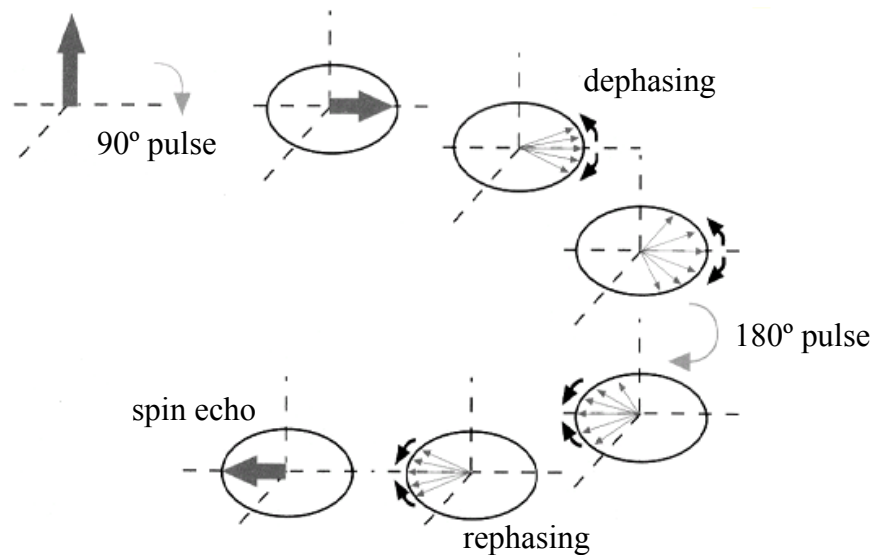
Figure 1.3 *Magnetisation in spin-echo sequence*

1.3 Rationale

From the first section in this chapter, it is clear that there is a great need for more fundamental research on the mechanisms leading to deep pressure ulcers. The focus in the present thesis is on damage that starts in the muscle tissue and its subsequent progression. In order to learn more about the aetiology of deep tissue injury different aspects should be examined. Indeed, when damage develops in muscle tissue after sustained compressive loading, three critical questions arise:

1. What type of damage is found in the muscle tissue?
2. At which location is the tissue damaged? and
3. How does this damage progress with time?

MRI can provide information on the spatial and temporal development of damage in muscle tissue and histology can reveal the type of damage. The use of histological examination is indispensable in as much as T2-weighted MRI is rather non-specific. A combination of both methods was therefore chosen to be able to answer the above questions. Besides measuring location of damage using T2-weighted MRI, alternative methodologies, such as tagging MRI and contrast-enhanced MRI, can be used to study the underlying mechanisms.

The aim of the present thesis is to identify some of the critical factors which are associated with the initiation and subsequent development of deep pressure ulcers, and to distinguish between the effects of these factors on muscle tissue damage after compressive loading.

1.4 Outline

In chapter 2, animal studies examining the aetiology of pressure ulcers are described with particular emphasis on the factors that influence the development of pressure ulcers. In chapter 3 the animal model used in the present thesis is detailed and a new MR-compatible loading device is presented that was developed to enable application of load and the simultaneous collection of MR data. These loading methods were employed in the animal model to examine their effects on muscle damage, using T2-weighted MRI correlated with histological examination (chapter 4). Chapter 5 describes contrast-enhanced MRI measurements which provided information on perfusion status during and after loading. Two loading protocols were used to discriminate between the effects of compression versus pure ischaemia. The importance of deformation in the initiation of deep tissue injury was studied using MR tagging measurements and a dedicated finite element model and is discussed in chapter 6. Finally a summary and discussion of the methods and results is provided, and the clinical relevance and recommendations are described in chapter 7.

The contents of chapter 3, 4 and 5 were written in journal format. Therefore, these chapters can be read independently. Inevitably, this will lead to some repetition and overlap between these chapters, particularly in the introductory sections.

Chapter 2

Compression induced tissue damage: animal models

"Compression induced tissue damage: animal models"

A Stekelenburg, CWJ Oomens, DL Bader

2.1 Introduction

To gain insight in the aetiology of pressure ulcers, different kinds of studies have been performed in de last 50 years. From experimental studies, using animal models and humans, to theoretical and numerical studies. In this chapter animal studies on the aetiology of pressure ulcers and on factors that influence the development of pressure ulcers are described, particularly studies performed in the last decade. A clear trend is visible in studies performed in the last years. They focus less on deriving pressure/time curves and more on practical aspects like the influence of temperature, medicine, nutrition and the way of pressure-relieve.

To be able to investigate the role of tissue (re)perfusion and lymph flow as well as the interaction between tissue layers in bulk tissue, animal experiments are needed. However, the number of animal experiments is fortunately being reduced by the recent trend in using in-vitro model systems such as tissue-engineered skin or muscle for studies on the effect of mechanical loading on tissues. In-vitro models are, however, never conclusive with respect to the results because in-vitro cultures behave differently from animals or humans. Furthermore, new technologies which are non-invasive, such as MRI, also reduce the number of animals needed

2.2 General requirements

The aetiology of pressure ulcers has been the topic of several studies for over half a century. Many animal models have been developed since then, but is has proven very difficult to develop a suitable animal model for ubiquitous investigation. This can be illustrated by three seminal studies. Groth [46] studied the effect of constant local pressure on the gluteal muscle of rabbits, Husain [47] attached a pressure cuff to the legs of rats and guinea pigs, and Kosiak [48] applied external pressure over the femoral trochanter and ischial tuberosity of dogs. These studies contributed much to the present state of knowledge related to the aetiology of pressure ulcers. Kosiak's work was reported to be "the cornerstone of modern pressure ulcer research" [20]. However, the clinical relevance to human pressure ulcers was limited because the skin of rabbits and dogs differs anatomically and physiologically from the human.

Animals can be conveniently divided into 2 broad groups, loose skin and fixed skin animals, based on anatomic, embryologic, and physiologic characteristics of their skin. Since 1970, the animals most used for pressure ulcer research are swine (fixed skin) and rats (loose skin). A major exception involved a study involving the greyhound dog [49]. These dogs are particularly susceptible to the development of pressure ulcers, because of their angular conformation, short hair, and thin skin. Therefore, they can serve as an appropriate model to study pressure ulcers.

The use of swine has long been considered to be an acceptable model for pressure ulcer research primarily as a result of the similarity of skin structure and cardiovascular system in swine and humans. For example, swine have a relatively fixed skin and there are further similarities to the human when considering the soft tissue coverage of bony protuberances. The possibility of inducing model conditions such as radiation damage, paraplegia, and diabetes, in both domestic and miniature swine, has allowed for the modulation of these parameters to simulate clinical situations in humans. The most common relevant site used to create pressure-induced damage in animal model has typically involved the greater femoral trochanters [20, 23, 48, 50, 51].

However, the use of a large animal model precludes the possibility of conducting a large number of individual experiments. By contrast, the rat represents a common small animal model offering the advantages of small initial cost and maintenance [19, 52]. It is thus highly efficient from a financial standpoint and well suited for extensive experimental trials. As an example, Salcido and colleagues [52, 53, 54] developed a fuzzy rat animal model for production of pressure ulcers. In contrast to the normal rat, this breed of rat is essentially hypotrichotic and, therefore, does not require depilation or prior treatment of the skin, which might contribute to the formation of damage artefacts. Another major reason they selected the rat as their animal model of choice was that more is known about the pharmacological effects on absorption, distribution, and metabolism of drugs in rats than in any other species. In the research of Bosboom et al. [28] rats were also used. One of the goals of their research was to reconstruct the loaded muscle underneath the compressed skin using magnetic resonance imaging and finite element modelling, and that required a small animal.

The advantages and disadvantages of using swine or rats as an animal model in pressure ulcer research are summarised in table 2.1. When studying skin damage and superficial wounds, it is obvious that swine as an animal model is more suitable because of the similarities in skin between pig and human. Many studies, however, have shown that damage caused by application of pressure can also start at deeper levels (muscle tissue) and extends to the surface. For studying muscle damage, and the influence of possible predisposing factors such as (re)perfusion on damage evolution, rats can be used as an animal model as well.

To study the aetiology of pressure ulcers using animal models various methods/interventions are required such as anaesthesia, fixation and/or skin indentation. The methods most commonly used entail sedation or anaesthesia of animals during pressure application. It is, however, undesirable to anaesthetise animals for prolonged periods and on more than one occasion. Furthermore, the physiological consequences of anaesthesia may compromise the true effects of pressure on unanaesthetised animals. Hyodo and colleagues [50] developed a method that avoids the need for animal anaesthesia. This method used a specially designed pressure applicator which was secured into the bone (the greater trochanter of a pig) and compressed the skin with a spring-loaded disk (figure 2.1d). Peirce [19] also developed

a model in which the animal was not anaesthetised during periods of skin ischaemia and reperfusion. She produced injury by applying and removing a permanent magnet to a dorsal region of rat skin under which a ferromagnetic steel plate was implanted (figure 2.1e). These methods do not require anaesthesia during pressure application, however, they allow free movement of the animal, which reduces the techniques that can be used, e.g. MRI.

Table 2.1 *Advantages and disadvantages of using swine or rats as an animal model in pressure ulcer research.*

animal model	advantages	disadvantages
swine	- skin properties comparable to human skin - relatively fixed skin - cardiovascular system comparable to that of human - susceptible to conditions such as e.g. diabetes and paraplegia - large surface areas for pressure application	- large animal; reduce possibility large scale experiments - relatively expensive - require large experimental set-ups
rat	- small animal; easy to handle - well suited for large scale experiments - relatively inexpensive - a lot is known about effects of drugs in rats	- loose skin - skin properties not comparable to those of human skin

Pressure ulcers are a continuing clinical problem for the spinal cord injury injured subject. This has resulted in a number of pressure ulcer related studies involving paraplegic animals. For example, Groth [46] applied pressure to the gluteus muscle of both normal and spinal cord transected rabbits. His conclusion was that pressure necrosis occurred in paralysed animals in a comparable manner as in controls. Dinsdale [55] analysed the effects of pressure in the production of pressure ulcers for both normal and paralysed swine. He also found a similarity in the pathological changes which were present in normal swine and swine which had been paraplegic for 8 days. It has been suggested by Daniel [56] that in order to examine realistic effects associated with paraplegic animals, a period of time is required in order for the animal weight to increase twofold and manifest extensive atrophy of muscle and subcutaneous tissue. Indeed after a 6-week period, the paraplegic swine exhibited a pressure time response which was of similar form to that of normal swine, as illustrated in figure 2.2. However, damage in the former animal model occurred over a shorter time scale [56]. These findings were attributed to impaired mobility and sensation and incontinence in paraplegic swine leading to skin maceration, and the atrophy of soft tissues resulting in an effective increase in interface pressures at bony prominences. However the invasive

procedures involving spinal cord transection, performed by Daniel and colleagues, incritably caused bowel and urinary dysfunction and increased rates of both complications and morbidity. In an attempt to reduce the complications and mortality associated with the previous models, Hyodo et al. [50] developed monoplegic pigs created by surgical resection of unilateral lumbar nerve roots in the spinal canal and applied pressure to the denervated skin over the trochanteric area. Muscle atrophy in the denervated limb was obvious within 7 days after denervation. No bladder and bowel dysfunction occurred through the experimental period. Hyodo began pressure application 1 to 2 weeks after transection.

2.3 Pressure-delivery systems

Different methods for the application of pressure to induce pressure-induced damage have been developed. The early study by Groth [46] utilised a balance beam, whereas more recent studies involve advanced computer-controlled surface pressure delivery systems [23, 52].

For the simple balanced beam, as illustrated in figure 2.1a, weights applied to one arm caused the other arm, which consisted of circular discs, to apply pressure. There was no reported measurement of applied or transmitted pressure. Dinsdale [55] also used a mechanical arm. Weights were added to a spindle at one end of a beam, and a metal applicator applied the force. Applied pressure was measured with a strain gauge before and after each experiment. An alternative method employed by Husain [47], involved the application of a cuff to the limb of an animal. This effectively produces a hydrostatic pressure. As illustrated in figure2.1b, Kosiak [48] applied pressure by means of inverted 20 cc syringes driven by compressed air. He reported a 10% variation in pressure measured between the compressed air system and the point of pressure application. Tissue pressure was measured by a hydraulic needle transducer.

Associated with the application of constant pressure, several authors have described monitoring systems for applied pressures and other parameters, such as perfusion and temperature. Daniel et al. [20] developed an electro-mechanical system for pressure application. It was composed of a computer-controlled servomotor whose rotational output was converted to a linear driven indenter by means of a mechanical interface. A force transducer was mounted in line with the indenter to provide feedback control.

In the computer-controlled surface pressure delivery systems of Salcido [52] and Sundin [57] both the force and the pressure-induced reduction of cutaneous blood perfusion using a fiber optic laser Doppler flowmeter were measured. Goldstein [51] and Houwing [23] also used computer-controlled devices. The former study involved the application of a constant normal force to the skin and, simultaneously, a cyclic shear force. The apparatus involved was a load applicator device positioned on a universal joint and hydraulic lift. A normal force was applied by lowering the hydraulic

lift and a shaker motor and power amplifier were used to deliver cyclic shear forces. To be able to measure skin temperature, a thermistor probe was placed in the pressure applicators in the devices used by Houwing [23] and Patel [58].
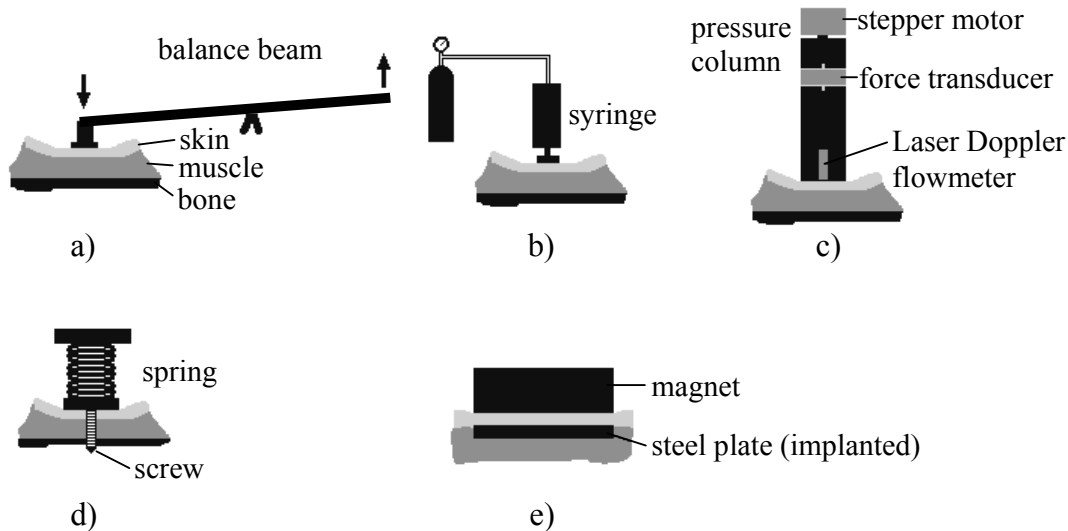
Figure 2.1 *Schematic drawings of indenter systems. a) balance beam used by Groth [46], b) inverted syringes driven by compressed air used by Kosiak [48], c) pressure column used by Salcido [52], d) pressure applicator secured into bone used by Reger [59] and Hyodo [50], and e) magnet compressing skin used by Peirce [19].*

An important part of the pressure delivery systems is the pressure applicator itself. Investigators have been using a range of pressure applicators, precluding the direct comparison of results. Pressure is most often applied by an indenter, but pressure cuffs [47], magnets [19] and air bladders [57] have also been used. The size of the used indenter is generally matched to the site of indentation and the size of the animal. Thus Goldstein [51], Hyodo [50] and Houwing [23], who applied pressure to the skin above the greater femoral trochanter of pigs, used animals of different sizes, with weights of 6, 18 and 30 kg, respectively, and associated indenter sizes of 7x8 mm, 30 and 50 mm diameter.

2.4 Relationship between pressure and time

The objectives of many studies have involved the establishment of threshold values for external loads that will predict the onset of tissue damage. These values can be derived either by analysing (retrospectively) clinical cases or by performing animal models. Reswick and Rogers [60] developed a pressure/time curve (figure 2.2) that has been used as a clinical guideline clue in the early 1970's. They monitored the skin-cushion interface pressures on 800 volunteer normal human subjects and patients.

In the animal model experiments soft tissues are loaded, generally by compressing the soft tissues between an indenter and the underlying bone, while the magnitude and the duration of the compressive loads are varied. Groth [46] was the first who published an extensive systematic study on the primary causes of pressure ulcers using histological techniques. He examined the load-induced evolution of damage by indenting the gluteus muscles of rabbits with a range of forces and application periods. After a period of observation, typically a few days, post-mortem analysis and histological examination were performed. The findings suggested that all loads cause degenerative changes, but there is a point where these changes become irreversible. Groth defined the threshold level as the point where changes became macroscopically visible and thus was able to define a pressure/time curve. Above this level damage would occur, below it any damage was defined as reversible.

Husain [47] also performed pressure experiments with varying degree and duration of pressure. He attached a pressure cuff to the legs of rats and guinea pigs. Using a hydrostatic form of pressure, a threshold pressure of 100 mmHg (13.3 kPa) applied for 2 hours was observed to produce definite microscopic changes in the leg muscles of rats. Furthermore, Husain suggested that a low pressure maintained for long periods of time induce a more extensive amount of tissue damage than high pressures for short periods. With the guinea pig model, cuff pressures of 100, 200 and 300 mmHg (13.3, 26.7 and 40 kPa) were applied for up to 3 hours. Tissue changes, such as oedema, vascular congestion, cellular infiltration and muscle degeneration, were first observed at a pressure of 200 mmHg applied for 2 hours.

Using a canine model Kosiak and colleagues [48] applied pressures of different intensities for various durations over two locations, namely the femoral trochanter and ischial tuberosity. After release of pressure, oedema and cellular infiltration were observed immediately, and these features persisted for 1 or 2 days. Kosiak also reported that intense pressures of short duration are as injurious to tissues as low pressures applied for longer periods, as indicated in figure 2.2. In a later experiment on a rat model, Kosiak [21] applied a constant load and equal amounts of intermittent loads and reported a higher susceptibility of tissue to the constant load. Although no changes were noted in the animals that were subjected to pressures of 35 mmHg (4.7 kPa) for periods up to four hours, the application of 70 mmHg (9.3 kPa) produced changes after 2 hours. By contrast, the application of pressures up to 190 mmHg (25.3 kPa) for one hour did not produce any noticeable microscopic change in the tissue.

Several investigations have been published since those seminal studies. For example, Lindan [61] compressed rabbit ears and found that pressures of 90 mmHg (12 kPa) applied for a period of 13 hours resulted in tissue necrosis. Dinsdale et al. [22] applied pressures to the posterior superior iliac of normal and paraplegic swine. He also found an inverse relationship between the magnitude of pressure and the duration of pressure in the production of pressure ulcers. It is of interest to note that for paraplegic swine no ulcerations occurred when pressure was less than 480 mmHg (64 kPa) applied for 3

hours. In 1981, Daniel and colleagues [20] experimentally produced pressure ulcers in swine. The animals were subjected to localised pressures ranging from 30 mmHg to 1000 mmHg (4 to 133.3 kPa) for periods between 2 and 18 hours. The indenter was placed over the greater femoral trochanter. With their results, they were also able to plot a critical pressure/time curve for pressure ulcers in swine (figure 2.2). In his fuzzy rat model, Salcido [52] applied pressure for a six-hour period on each of two consecutive days. This resulted in tissue damage at a pressure of 145 mmHg (19.3 kPa).
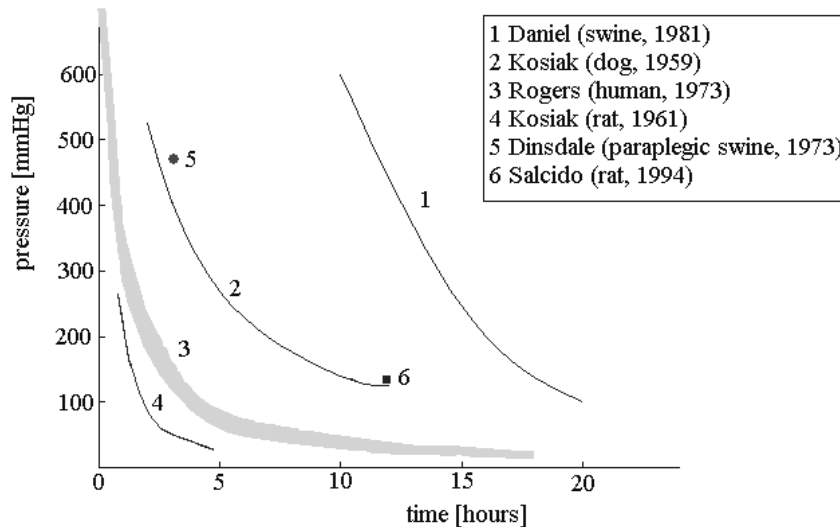
Figure 2.2 *Risk curves with regard to pressure-ulcers. Time/pressure combinations above the curve result in tissue breakdown.*

Although animal experiments have the relative advantage over clinical studies of being defined and more controllable, a large variation exists in the threshold values for tissue damage found in the different studies. This variation arises from diversity in experimental conditions, animal models, loading methods and regions/locations of load application. A means of overcoming the diversity in animal models and interpreting the differences between the results could be to relate the applied external load to the local loads inside the tissues, whereas these local loads determine the tissue state and hence the occurrence of tissue damage (figure 2.3) [28]. Bosboom compared the maximum shear strain distributions in the tissue, calculated using FE modelling, and the amount and location of initial tissue damage in the skeletal muscle beneath the indented skin. Their first results (figure 2.4) showed that the shear strain distribution showed some coincidence with the area of tissue damage, but more measurements and calculations are needed.
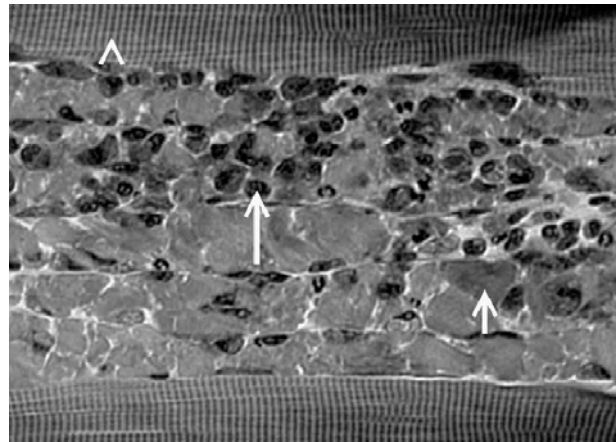
Figure 2.3 *Longitudinal section of muscle, showing the typical cross-striated appearance of skeletal muscle (arrowhead), loss of cross-striation of muscle fibres in the damaged area (small arrow) and the infiltration of mononuclear cells (large arrow). Reproduced with permission from Bosboom [28].*

Sacks [62] calculated a theoretical pressure versus time curve for the onset of pressure sores, which was based upon the use of dimensional analysis. He assumed that there is a definable pressure that will initiate a pressure ulcer, and that it will depend primarily upon the physical properties of the tissue in question (tissue density and elastic modulus) and the blood flow through it, as well as the time of exposure. Comparison with available experimental data from humans and dogs and swine indicated that this approach agreed well with experiment.
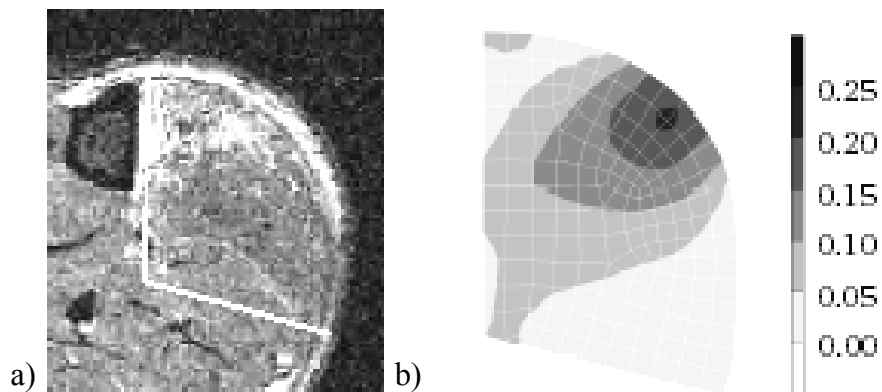
Figure 2.4 *Comparison of the area of muscle damage in a) transverse MR image with b) maximum shear strain distribution for the reference model [28].*

2.5 Influence of shear forces

A number of animal models have been developed to study the influence of pressure, but relatively few have examined the influence of shear forces. Of these, Reichel [63] was probably the first who pointed out the danger of shear stress. From anatomical observations he concluded that shear occludes blood vessels more easily than normal stress on its own. This led to the work of Dinsdale [22] who combined the application of normal loads and friction on pig skin and measured their effects on blood flow. This combined loading was found to be more effective in blood flow cessation. However, it was postulated that friction-induced ulceration was not caused by ischaemia, but was a direct result of tearing apart of the top layers of skin, in particular the stratum corneum.

Goldstein et al. [51] also studied the influence of shear forces. They applied different normal and shear forces for relatively short periods to the greater femoral trochanter and the tibialis anterior of swine. Shear forces between 1 and 5 N and normal forces between 2 and 15 N were applied. Their results confirmed the clinical observations that shear forces injure skin and body wall tissues and that there is a more rapid onset of damage at increased shear forces. In addition, it was noted that tissue breakdown occurred at a normal force of 14 N in the presence of a 2.5 N shear force. However, when the shear force was increased to 4 N, tissue breakdown occurred at a normal force of only 7 N. These data also confirmed previous studies that shear force alone did not induce tissue breakdown [64].

2.6 Ischaemia-reperfusion injury

Ischaemia-reperfusion (I/R) injury can be a factor in the formation of pressure ulcers. Clinical observations of pressure ulcers showed that ulcers typically occur after, rather than during, a period in which pressure is applied to the body. I/R injury can be defined as cellular injury resulting from the reperfusion of blood to tissue areas, which had been previously exposed to an ischaemic insult. Reperfusion injury to skeletal muscle is characterised by a number of features, which include muscle necrosis, endothelial cell swelling, and release of intracellular enzymes and proteins [65, 66]. Reperfusion injury is mediated through free radicals. Production of oxygen free radicals may initiate a cascade of biochemical events that may significantly contribute to or result in the production of pressure ulcers [19, 23]. Under normal circumstances oxygen free radicals are buffered by free radical scavengers, such as reduced glutathione and glutathione. However, in tissues undergoing oxidative stress, there is a decrease in the levels of these enzymes. As a consequence, during reperfusion the oxygen free radicals are buffered to a lesser degree and this is reflected in an increase in concentration of hydrogen peroxide [65, 67, 68].

Several recent studies have examined the effects of reperfusion on the formation of pressure ulcers in animal models. Peirce et al. [19] induced ischaemia-reperfusion

injury by implanting a ferromagnetic steel plate in the dorsal region of rat skin, followed by applying and removing a permanent magnet over the region. The application of the magnet compressed the skin and reduced blood flow, thus causing ischaemia, while removal of the magnet allowed reperfusion of blood to the ischaemic region. A pressure of 50 mmHg (6.7 kPa) was chosen as representative of a clinically relevant interface pressure. Different numbers of I/R cycles were applied to the skin tissues, each cycle consisting of 2 hours of ischaemia and 0.5 hour of reperfusion. The results indicated that 5 I/R cycles, equivalent to a total ischaemic period of 10 hours, were more damaging to the skin than one continuous compression induced ischaemic period of 10 hours. The extent of the damage was indicated by an increase in both necrotic area and the degree of leukocyte extravasation in the I/R group compared to the ischaemia-alone group. Houwing and colleagues [23] also studied the influence of ischaemia and reperfusion. A pressure of 375 mmHg (50 kPa) was applied for two hours on the skin above the greater femoral trochanters of eight-week-old pigs. Specimens taken immediately after cessation of pressure application showed no histopathological signs. Early signs of damage in the muscles and subcutaneous tissue under the pressure device appeared only after a reperfusion period in excess of one hour. The observed damage distal to the pressure applicator was identical to the damage immediately below the applicator, suggesting that the process followed a vascular pattern and was a result of ischaemia. Thus it was concluded that although pressure resulted in damage, the observed damage was not a direct result of pressure per se.

Several substances are thought to prevent free radical formation or to scavenge free radicals once they are formed. These substances include superoxide dismutase, catalase and allopurinol, which function at the enzymatic level, and dimethylsulfoxide, deferoxamine and vitamin E, which function non-enzymatically [67]. Houwing et al. [23] investigated the effect of one such scavenger, vitamin E. The study showed that pre-treatment with 500 mg of vitamin E prevented damage caused by pressure to a large degree. Although vitamin E does not prevent oxidative stress during the application of pressure, as reflected in the decrease in reduced glutathione and total glutathione, it does prevent the excess production of oxygen free radicals and hydrogen peroxide during reperfusion.

The role of allopurinol and deferoxamine was examined by Sundin et al. [57]. They applied pressure to the scapulae of pigs in a 4-hour cycle, consisting of 210 minutes of an applied pressure of 150 mmHg (20 kPa) followed by a zero pressure for 30 minutes. This cycle was repeated continuously for 48 hours. Both biochemical markers improved cutaneous blood flow and tissue oxygenation, but only deferoxamine significantly reduced necrosis of cutaneous and skeletal muscle tissues. Indeed a significant decrease in the extent of muscle infarction was evident in the deferoxamine group compared to the control group. According to the authors, the protective effect of deferoxamine can be explained in several ways. Deferoxamine has a relatively low molecular weight, which facilitates its entry into cells. In addition, deferoxamine has a

high binding affinity for iron which, under ischaemic conditions, becomes more available. By binding iron, deferoxamine inhibits the formation of the hydroxyl radical (OH) from superoxide radicals (O_2). Salcido et al. [54] tested the effect of a potent anti-inflammatory agent, ibuprofen, on the development of on pressure ulcers. Their hypothesis was that transcutaneous pressure intervention, resulting in the production of experimental pressure ulcers, may be mechanistically similar to the vascular damage resulting from burns injury, which has shown to be responsive to ibuprofen intervention. The effect of ibuprofen intervention before, during and after the application of pressure (145 mmHg (19.3 kPa) for five consecutive daily pressure sessions, each of 6 hours' duration) to the fuzzy rat model was examined. However, their results suggested that ibuprofen intervention was not effective in reducing the incidence or severity of pressure ulcers and may, in some cases, be detrimental.

Another known way to diminish reperfusion injury is the gradual reperfusion of the ischaemic tissues. Ünal and colleagues [69] investigated the effect of gradual increase in blood flow on ischaemia-reperfusion injury of the skeletal muscle. They induced ischaemia by applying clamps to the femoral vessels of rats. Three groups of rats were used,

- a control group, no ischaemia was induced,
- a conventional clamp release group, 150 minutes of ischaemia was followed by immediately release of the clamps, and
- a gradual clamp release group, 150 minutes of ischaemia was followed by a gradually release of the clamps (blood flow velocity recovered in 120 seconds)

Histological examination was performed and malonyldialdehyde (MDA) and myeloperoxidase (MPO) levels were measured (figure 2.5). MPO is a sign of neutrophil accumulation and MDA is a by-product of radical-induced lipid disintegration.

Inflammatory cell infiltration and loss of striation of the muscle were noticeably less in the gradual reperfusion group compared to the conventional group. The values of tissue MPO and MDA of the conventional reperfusion group were significantly greater than of the gradual reperfusion group. They demonstrated that gradual reperfusion decreases neutrophil accumulation, superoxide radical occurrence, and tissue infarction in the rat hind limb model.

2.7 Influence of temperature

Since the work of Groth, Kosiak and others, it has become clear that tissue breakdown is a multi-dimensional process. Besides pressure, factors that (may) have influence are shear, friction, moisture, age, nutrition, physiologic abnormalities, sensory loss, mobility, and/or temperature.
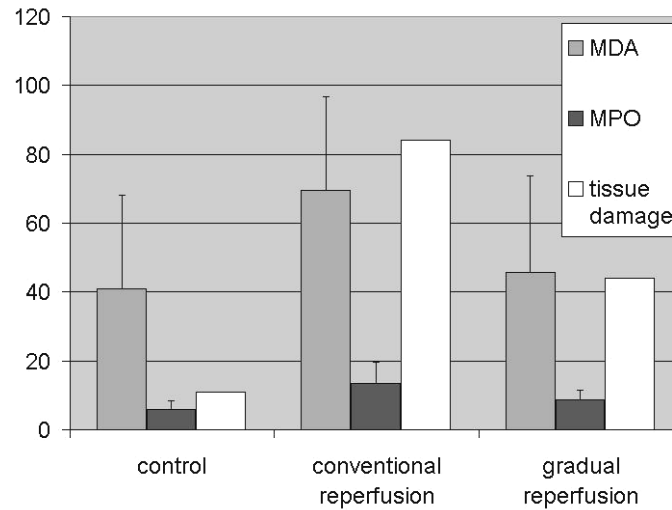
Figure 2.5 *Mean tissue myeloperoxidase (MPO) levels (measured in units per gram protein), mean malonyldialdehyde (MDA) levels (measured in nanomolecules per gram) and histopathological tissue injury scores (percent tissue damage) for the three different groups [69].*

The role of temperature in the causation of pressure ulcers has only been examined in a few studies. It is, however, known that, in general, an increase of 1 °C in skin temperature results in an approximately 13 % increase in tissue metabolic requirements [70]. The heightened need for nutrients and oxygen cannot be fulfilled, however, because of tissue compression and in tissues which are subjected to pressure-induced ischaemia. Studies indicating an increase in local skin temperature caused by both pressure application [71] and the insulating effect of specific foam cushions and mattresses [72] appear to affirm temperature as an important factor in pressure ulcer development.

Kokate et al. [73] described a porcine model for the creation and assessment of temperature-modulated pressure-induced damage to tissues. A device was developed which was capable of applying both pressure and temperature. Applied pressure was 100 mmHg (13.3 kPa) and applied temperatures were 25, 35, 40 and 45°C, the latter temperature representing a commonly accepted upper bound for thermal therapies applied to skin, such as water beds. The local application of 100 mmHg for 5 hours resulted
- at 25°C in no damage,
- at 35°C in moderate muscle damage,
- at 40°C in partial epidermal necrosis and moderate muscle damage, and
- at 45°C in full thickness epidermal necrosis, moderate dermal and sub-dermal damage and severe muscle damage.

21

They concluded that these results motivated the conjecture that lower applied temperature could be protective to soft tissue. In a subsequent study [74], temperatures of 25, 27, 30 and 32ºC were applied. These data confirmed that at lower temperature of the skin and the underlying tissues exposed to the increased pressures, there was less severe tissue damage occurring within all the soft tissue layers.

Increased temperature not only results in increased tissue metabolism and oxygen consumption but also in increased perfusion. Patel et al. [58] examined the combined effect of increased temperature and surface pressure on tissue perfusion and deformation. A heater, designed to raise the skin surface temperature locally, was attached to the pressure applicator. Skin displacement was measured by a linear variable differential transformer. A range of pressures, between 3.7 and 73 mmHg (0.5 and 9.7 kPa), were applied at two different temperatures, T=28ºC (no heating) and T= 36ºC. The major conclusions of this study were that there was a significant increase in perfusion, measured by a laser Doppler flowmeter, with increased temperature at surface pressures below 18 mmHg (2.4 kPa), probably due to local auto regulatory mechanisms. There was no increase in perfusion was seen at higher pressures, most likely a result of mechanical occlusion of vessels induced by high surface pressure. In addition, increased temperature caused skin to become stiffer in response to increased surface pressure. At constant applied pressures, heated skin did not deform as much as unheated skin.

2.8 Results and future perspectives

A summary of the main animal model studies is most conveniently summarised in table 2.2. A number of aspects have been considered. For example, some studies have focused on the aetiology of pressure ulcers [16, 20, 22] while others have examined the influence of medicine and nutrition [54, 57] or the effects of temperature [73, 74].

The table also includes details of the applied pressures and period of duration for the different studies. The considerable variation reflects the range of animals used, their size and the test site and precludes a direct interstudy comparison. It also confirms the importance of deriving a parameter, which is independent of geometry, such as local internal stress, which can be calculated using finite element (FE) modelling.

In all previous animal studies histological examination was used for the evaluation of the tissue. This has two main drawbacks. First, tissue histology is a destructive methodology. It therefore precludes follow-up studies to investigate the evolution of tissue damage with time, which is particularly appropriate when studying mechanisms associated with reperfusion damage. In addition, histology is labour-intensive, and thus hampers experiments on a larger scale.

Table 2.2 *Studies performed during the last decade on tissue damage due to mechanical loading. Pressures given in mmHg (7.5 mmHg≡1 kPa)*

(first) author	animal	applied pressure/time	damage	focus on
Swaim [49] (1993)	dog (n=15)	cast for 14 days (0.03N/mm^2)	skin damage	pressure wounds
Salcido [54] (1994)	rat (n=65)	145mmHg/6h, 5daily sessions	damage in all layers	effect of ibuprofen
Hyodo [50] (1995)	pig (n=9)	800mmHg/48h	full-thickness ulcers	Pressure ulcers, spinal cord injury
Kokate [73] (1995)	pig (n=16)	100mmHg/5h	damage in all layers	pressure, temperature
Iaizzo [74] (1995)	pig (n=6)	100mmHg/2, 5 and 10h	damage in all layers	pressure, temperature (cooling)
Goldstein [51] (1998)	pig (n=8)	675mmHg/40min + shear stress, 20 daily sessions	skin breakdown	repetitive mechanical stress
Peirce [19] (2000)	rat (n=52)	50mmHg/10h	skin ulcer (pressure was only applied to skin)	ischaemia, reperfusion
Houwing [23] (2000)	pig (n=6)	375mmHg/2h	damage in muscle and subcutaneous tissue	reperfusion, vitamin E
Sundin [57] (2000)	pig (n=18)	150mmHg/5h	damage in all layers	effect of allopurinol, deferoxamine
Bosboom [28] (2001)	rat (n=5)	1875mmHg/2h	muscle damage	deformation (using MRI)

Magnetic resonance imaging (MRI) is considered a promising alternative, since it is non-destructive and, although inherently expensive, less time consuming. In the study of Bosboom [28] the ability of MRI to assess local muscle damage after prolonged transverse loading was investigated. A pressure of 1875 mmHg (250 kPa) was applied for 2 hours and analysis was performed 24 hours after its completion. Histological examination was used as the gold standard and data was compared with in vivo MR

images. Damage in histological slices was indicated manually from evidence of loss of cross-striation of the muscle fibres and/or the infiltration of inflammatory cells. When a muscle fibre was damaged at least every 30 μm a mark was placed in the centre of the damaged fibre (bottom images, figure 2.6). In the T2-weighted MR images, increased signal intensity reflects tissue damage. Increased signal intensity on T2-weighted MR images can reflect a range of pathologies, including edema, necrosis, inflammation and fatty infiltrations [45]. The two analyses are illustrated for three animals in figure 6. It can be seen that the location of damage in the MR image coincided well with that determined from transverse histological slices.

The hypothesis that prolonged cell deformation is the primary trigger for the onset of tissue damage related to pressure ulcers, was subsequently investigated by comparing the maximum shear strain distributions in the tissue, using FE modelling, and the amount and location of initial tissue damage. The shear strain distribution showed some coincidence with the area of muscle damage but not enough to prove, or reject, the hypothesis at that stage. By modifying the experimental set-up used by Bosboom the present authors will attempt to produce more reproducible tissue damage. Ultimately the aim is to establish a clear understanding on the influence of both tissue deformation and (re)perfusion on the development of pressure ulcers.
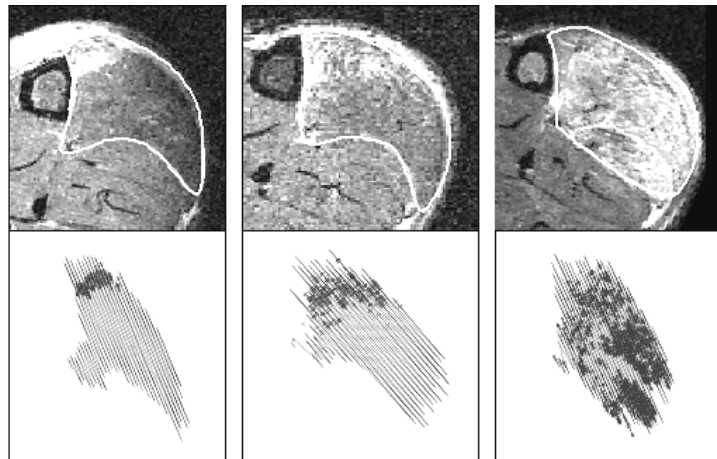
Figure 2.6 *Damage in transverse histological slices (below) and MR images located at the middle of the indenter.*

To be able to simultaneously collect MR data and apply pressure to the muscle, an MR-compatible loading apparatus is being developed. A large variety of imaging techniques has been developed that can be applied to assess structure, function and metabolism of skeletal muscle. Tagging MRI can be used to measure local tissue deformation (necessary for the finite element model), perfusion MRI offers the possibility to measure tissue perfusion and with MR spectroscopy information on the biochemical status of tissue can be obtained.

Chapter 3

A new MR-compatible loading device to study in-vivo muscle damage development in rats due to compressive loading

A. Stekelenburg, C.W.J. Oomens, G. J. Strijkers, L. de Graaf, D.L. Bader, K. Nicolay

3.1 Introduction

Pressure ulcers (decubitus) may be defined as localized areas of degenerated skin and underlying soft tissues, caused by sustained mechanical loads. They represent a serious and increasing health problem to an ever-ageing population. Prevalence figures are very high, ranging between 8% and 23% depending on the severity of wounds included and the subject group under investigation [1, 2, 3]. Prevalence is highest among elderly patients [2, 4] and those with impaired sensations, such as occurs following spinal cord injury [5, 6]. However, a lack of knowledge on the aetiology makes prevention difficult. Previous studies using animal models [20, 21, 22] have shown that pressure ulcers can be initiated either in the superficial skin layers or within deeper tissues, depending largely on the nature of the surface loading. Deep ulcers arise in the muscle layers adjacent to bony prominences and are generally considered to be caused by sustained compression of the tissues [20, 21, 47, 52]. The clinical measures to prevent these deep ulcers are often unsuccessful, leading to a variable prognosis. This is due, in part, to the difficulty in assessing initial pathological changes in the deep tissues with currently available techniques. In addition, it is not known how external loads are transferred to local interstitial stresses and strains and, more importantly, how these loads result in tissue damage. Hypotheses associated with the pathogenesis of pressure ulcers [16] involve localised ischaemia [20, 21], reperfusion injury [19, 23, 75], impaired interstitial fluid flow and lymphatic drainage [24, 25, 26, 27], and sustained deformation of cells [28, 29, 30].

The aforementioned animal studies examining the aetiology of pressure ulcers have employed histological techniques for tissue examination. Histology is well established and accurate but its destructive nature precludes longitudinal studies to investigate the temporal evolution of tissue damage, which is particularly appropriate when examining mechanisms associated with reperfusion damage. In addition, histology is labour-intensive, and thus hampers experiments on a larger scale. Magnetic resonance imaging (MRI) provides advantages over histological evaluation, since it is non-destructive and less time consuming. Indeed it has proven an important non-invasive tool in the detection and characterization of pathologies in the musculoskeletal system [37, 76, 77]. To date, very few studies have employed MRI techniques to examine the evolution of pressure ulcers. MRI has been used to determine pathological tissue changes in patients with spinal cord injury (SCI). In one study a number of male SCI patients, who had current or recent sacral, ischial or peritrochanteric pressure ulcers, were examined with MRI [38]. The technique was able to detect the extent of soft tissue changes, adjacent fluid collection and the involvement of bone. The use of MRI was also evaluated in making clinical decisions when assessing nonhealing pressure ulcers or flap breakdown in a group of SCI patients [39]. The findings revealed that MRI was useful in identifying osteomyelitis, fluid collection, abscesses and sinus tracts that often require surgical revision for successful healing.

MRI can also be used to study the onset of damage in animal models and hence contribute to the understanding of underlying pathways. In a study by Bosboom et al. [40] local muscle damage was assessed after transverse loading for 2 hours with an indenter applied to the tibialis anterior (TA) region of rats. T2-weighted MR images were acquired 24 hours after load removal and compared to histological examination. The spatial distribution of the MRI indices of damage coincided well with that determined from longitudinal histological slices [40].

In order to learn more about the aetiology of pressure ulcers different aspects should be examined. When damage develops after sustained compressive loading, three questions are of importance. 1. What type of damage is found in the muscle tissue? 2. At which location is the tissue damaged? and 3. How does this damage progress with time? MRI can provide information on the spatial and temporal development of damage in muscle tissue and histology can reveal the type of damage. The use of histological examination is indispensable inasmuch as T2-weighted MRI is rather non-specific and will not reveal all types of damage. A combination of both methods was therefore chosen to be able to answer the above questions. To answer these questions, an MR-compatible loading apparatus was developed, which provides the application of pressure to muscle tissue by means of an indenter and simultaneous collection of MR data. This is an important improvement in comparison with the study by Bosboom [28], in which the loading protocol was performed outside the MR scanner. The MR-measurements require that the loading apparatus and all its additional features are MR-compatible, drastically reducing the materials that can be used. The available space is limited by the bore of the magnet, which was 95 mm in the used MR-scanner. Localised data on indentation and damage, which can be obtained from MR-images, is essential for testing the hypothesis involving the sustained deformation of cells. Furthermore, examination of the tissue with T2-weighted MR imaging before, during and after application of load will reveal the moment of damage initiation and the temporal development, which may reveal information on the mechanisms that initiate damage.

3.2 Materials and methods

3.2.1 Animal model

In this study 20-week-old female Brown-Norway rats (n=10) were used weighing between 170 and 200 grams. Rats were housed under standard laboratory conditions (12h light, 12h dark cycles) and maintained on standard laboratory food and water ad libitum. Each rat was anaesthetized for the preparation phase by subcutaneous injection of xylazine (1 μl/g body weight, 2 g/l) and intramuscular injection of ketamine (0.8 μl/g body weight, 100g/l). During the MR measurements, anaesthesia was maintained with isoflurane inhalation (0.4 to 1.0 % isoflurane with N_2O/O_2 mixture (1:1)). Vital signs (pulse and respiratory rate) were monitored and maintained within physiological

values. The rat was placed on a heating pad to maintain body temperature between 35-37ºC. Prior to the loading experiment, the hairs on the left tibialis anterior (TA) region were removed by shaving. The leg was placed in a specially designed mould and plaster cast was applied to obtain a firm fixation in the set-up. The experimental protocol was approved by the Animal Care Committee of the University of Maastricht.

3.2.2 MR-compatible loading device

The loading device consisted of two concentric tubes, the innermost tube housing the animal and the larger outer tube was used to locate the whole arrangement in the MR scanner (figure 3.1). The scanner used was a 6.3 Tesla Varian system, operating at 270 MHz (horizontal bore, inner diameter 95mm) and equipped with a 380 mT/m gradient coil. The anaesthetised animal was placed supine in the loading device (figure 3.1), with its foot positioned in a special holder. The casted leg was fixed by clamping two screws to the cast. In the cast a hole was made for the application of the indenter to the TA. A birdcage radio frequency (RF) coil (inner diameter 4cm, length 6cm, 6 legs) was placed in a fixed position around the limb.
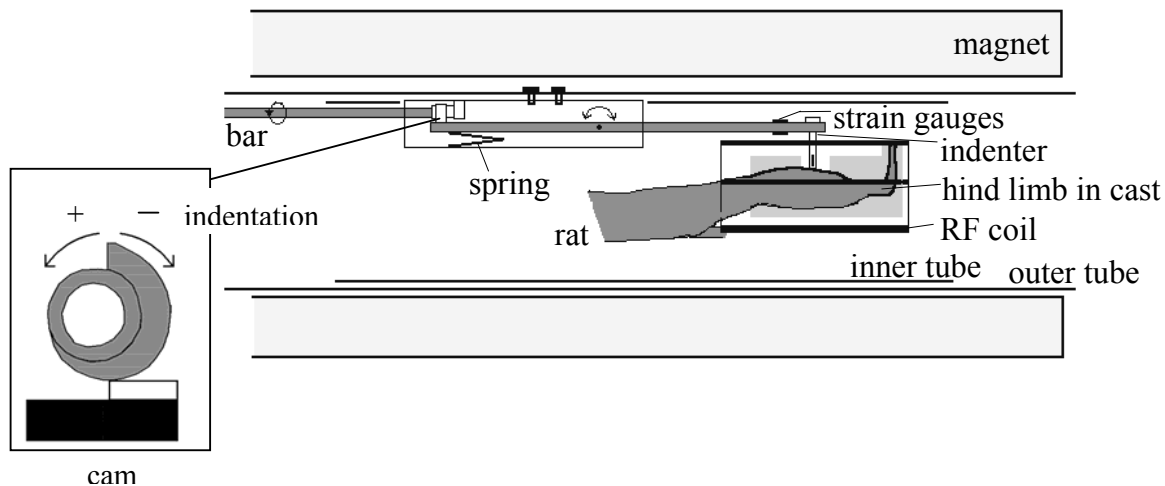
Figure 3.1 *Schematic of the experimental arrangement, indicating the leg of the supine animal fixed in the RF coil. The pressure is applied to the tibialis anterior by an indenter that is positioned through the legs of the coil. By rotating the bar that is attached to the cam, a smaller or larger indentation can be applied (lever).*

A copper RF shield was fixed on the outside of the inner tube. A plastic indenter (diameter 3 mm) was positioned through the legs of the coil halfway between foot and knee perpendicular to the skin overlying the TA. The indenter, which contained a cavity filled with water to ensure visibility in the MR image, was fixed to a loading beam constructed from a glass fibre reinforced polymer (Ertalon 66GF30). Strain gauges (CEA-06-250 UW-350, Vishay Measurements Group) were attached to this

loading beam for measuring the indenter force applied to the TA. The indenter was applied by rotating a bar that was attached to a brass cam, as indicated schematically in figure 3.1. The loading beam was pushed against this cam by a spring, whose stiffness was significantly higher than that of the tissues, thus ensuring a constant indentation.

3.2.3 Force measurement

Before measuring the indenter force applied to the TA-region, the strain gauges were calibrated. To test the potential influence of the magnetic field, force measurements were performed both inside and outside the MR scanner. Calibration measurements were achieved with three different loads, namely 0.3, 0.9 and 2.0 N. These measurements were performed without an animal. The leads of the strain gauges were well shielded against the switching gradient fields, which occur during MR measurements, to prevent damage to the amplifier.

3.2.4 Experimental Protocol

The measurement protocol was divided into five stages. Initially transversal scout images were produced and, where necessary, adjustments made to ensure a prescribed position and angle of the indenter on the TA (TA compressed between indenter and tibia, indentation perpendicular to limb). Before applying the indenter, pre-loading images were taken. A T2-weighted spin echo sequence was used (TE=25ms, TR=4s) to collect 41 consecutive 1 mm thick transverse slices. Each slice had a field of view of $30x30mm^2$, a resolution of 128x128 pixels and was averaged over 2 acquisitions yielding a total scanning time of 17 minutes. Acquisition bandwidth was 55325 Hz. This sequence was followed by a multi-echo sequence (TE= 12-96 ms, 8 echoes, TR=4.5s) to determine a quantitative T2 map of the limb over a scanning time of 20 minutes. To obtain an enhanced contrast to noise ratio (CNR) between normal and damaged tissue, the individual images of the multi-echo sequence were summed. The resulting images are referred to as T2-weighted-sum (T2ws) images. For calculating T2 values, the first four echoes were used. Secondly, following these measurements, the indenter was applied, during which transversal (multi echo sequence) and sagittal and coronal images (single echo sequence) of the leg were recorded. Two loading protocols were used; an indentation of 4.5 mm was applied for 2 hours (n=7), an indentation of 2.9 mm for 4 hours (n=3). Thirdly, immediately after removal of the indenter, the multi echo sequence was repeated up to a maximum of 3 hours. After completion of the measurements the animal was removed from the loading device, the cast was removed and the animal was allowed to recover from anaesthesia and to move freely for the next 20 hours. After this period, the rat was again sedated and the leg put in plaster cast for fixation in the set-up, and the single and multi echo sequences were repeated. The location of the slices during the first scans was retraced the second day by the size and shape of the tibia bone.

3.2.5 Histological analysis

Immediately following the MR measurements at the second day, the animal was sacrificed and perfusion fixated with 4% buffered formalin. The lower limb was cut off and stored in formalin. The TA was excised at least two weeks later, to ensure complete tissue fixation. The muscle was dehydrated in a series of alcohol solutions and embedded in plastic (Technovit 7100, Kulzer). The muscle was cut longitudinally, perpendicular to the direction of load application, or transversal in 5 μm thick sections. The samples were stained with toluidine blue and Gomori's trichrome to visualise both the cross-striated appearance of the muscle fibres and the cell nuclei.

3.3 Results

The developed MR-compatible loading device allowed high quality MR measurements of a rat hind limb before, during and after indentation of the tibialis anterior for 2 or 4 hours. A good fixation of the hind limb, using plaster cast, ensured well-defined consecutive MR measurements for up to 6 hours.

3.3.1 Indentation

The indenter applied to the TA by rotating the bar attached to the cam delivered a constant value of indentation, which could be adjusted up to a maximum value of 4.5 ± 0.1 mm, as determined by the MR images. The absolute value of indentation was constant for all experiments, but the precise location and the direction as well as the size and anatomy of the TA differed slightly between animals. The length of the TA was approximately 25 mm. The size of the TA relative to the size of the indenter is shown in figure 2b and f. Only the cavity in the indenter, which is filled with water, is visible. In figure 3.2b an example is shown of an indentation of 4.5 mm, in figure 3.2f a smaller indentation is shown of 2.9 mm.

3.3.2 Force measurement

Figure 3.3 shows the calibration measurements inside (I) and outside (O) the MR scanner. The set-up was repeatedly slid in and out the bore of the MR scanner with known weights hanging at the loading beam. The black lines show the time span and mean of the signal used for further analysis. The analysis showed that there was no difference in behaviour for sliding into the bore and sliding out of the bore and that the difference in measured force was independent of the applied load. The mean ± standard deviation of the difference in force for all sliding moments was 0.037 ± 0.012 N (n=55). This value was therefore used as a correction force for all subsequent measurements. The indenter was applied slowly over a 3 second period to prevent impact damage. Forces that were measured during large indentation (4.5mm) had peak values between 2 and 3 N (equivalent to a contact stress 283-424 kPa) followed by a relaxation phase. As illustrated in figure 3.4, the indenter force decreased, in this

typical example, from 2.7 to 1.7 N in the first minute, and to 1.1 N (156 kPa) after 60 minutes.
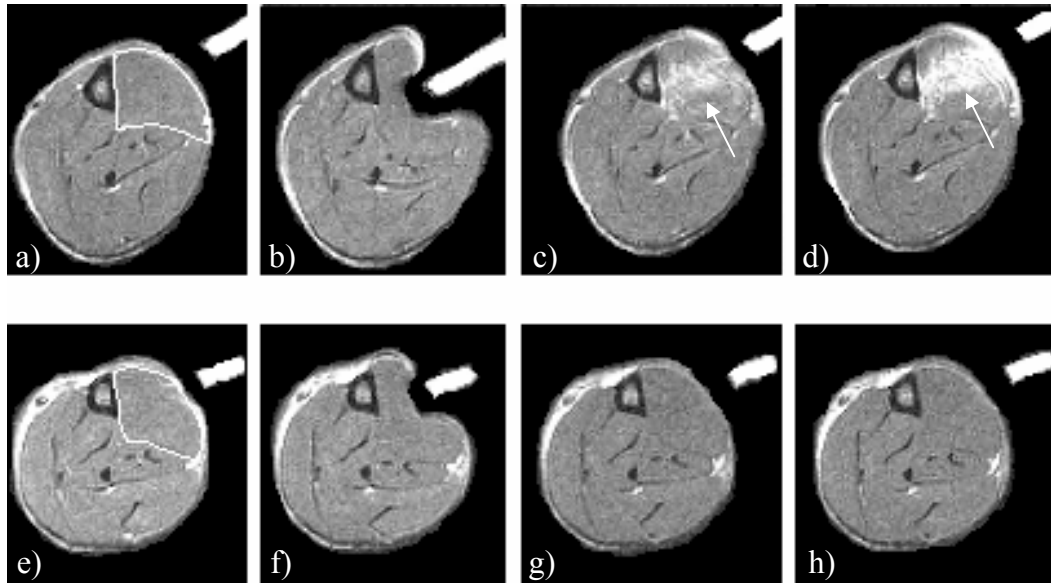
Figure 3.2 *T2-weighted transversal slices of the hind limb underneath the indenter showing a, e) the indenter applied to the skin at the level of the TA (indicated by white line), b, f) indenter applied to the muscle with respectively large (2 hours) and small (4 hours) indentation, c, g) images taken immediately after removal of load and d, h) images taken 30 minutes after unloading. In case of a large indentation (4.5mm) the signal intensity was increased in the tibialis anterior region following indenter release (arrow). In case of the small indentation (2.9mm) the signal intensity remained unchanged.*

3.3.3 Damage

Two series of T2-weighted-sum MR images collected before, during and after indentation are shown in figure 3.2. In figure 3.2a-d images are shown of an experiment in which a large indentation (4.5 mm) was applied to the TA region. Figure 3.2b shows the image taken just before unloading, which revealed no signal increase in the loaded area. This was found in all experiments. It is evident that after the loading period of two hours, the signal intensity was higher in the loaded regions of the tibialis anterior (arrow) compared with the images taken prior to loading.

From the images taken prior to loading a threshold value was determined defined by mean ± 2SD. The percentage affected area, defined by percentage pixels in TA with signal intensity > threshold, varied between 60 and 76 %. In 5 out of 7 experiments, this region with signal increase expanded in the first half hour, as shown in figure 3.2c and d, while in the other 2 experiments the affected region remained constant. From the

multi echo sequence the T2 values of the muscle tissue were determined. This revealed a significant increase in T2 in the affected region from 19.6 ± 3.7 ms before, to 30.9 ± 4.1 ms at 30 minutes after indenter release. In figure 3.2e-h images are shown of an experiment with a small indentation (2.9 mm). This indentation applied for 4 hours did not result in any signal increase in the TA region as shown in figure 3.2g and h.
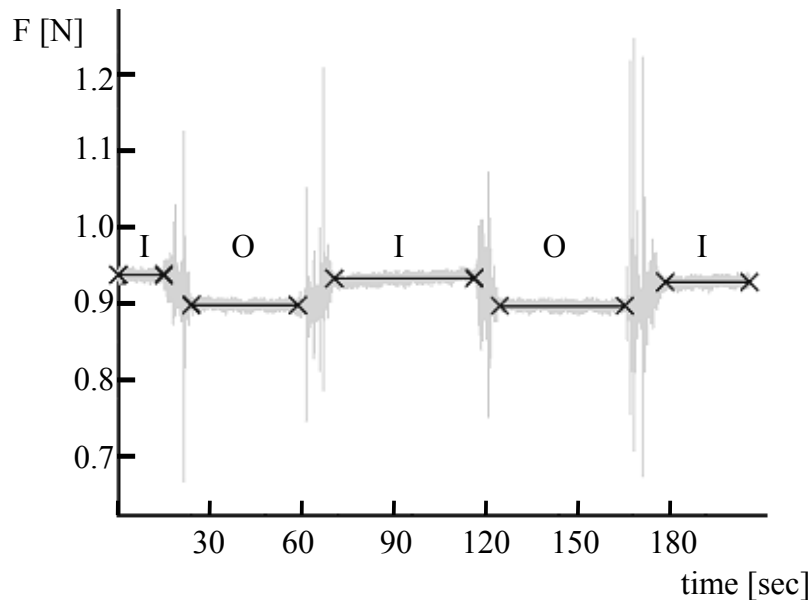
Figure 3.3 *Force measurements inside (I) and outside (O) the MR scanner. The set-up was repeatedly slid in and out the bore of the MR scanner with known weights hanging at the loading beam. The black lines show the time span and mean of the signal used for analysis.*

Three transverse slices through the lower limb are indicated in figure 3.5a, with the location of the indenter. The corresponding T2ws-images are shown at 15min, 2 hours and 20 hours after unloading (figure 3.5b). The images of the slice directly under the indenter (middle row of figure 3.5b) revealed a diffuse area with increased signal intensity taken immediately after load removal. This diffuse area became more localised extending from skin to bone when recorded 2 and 20 hours after loading (arrow). In other experiments, however, the decrease in affected area was less marked after 2 and 20 hours. In the slice above the indenter (top row) there was a negligible change in signal intensity immediately after load removal, although by 2 hours a small, localised area was visible in the TA region (arrowhead). In the slice under the indenter (bottom row) some increase in signal intensity was visible in the image taken immediately after load removal, but this did not persist in the images taken at 2 and 20 hours. Close examination of the images of all experiments revealed that the location and size of the regions with higher signal intensity largely depended on the precise location, direction and degree of indentation
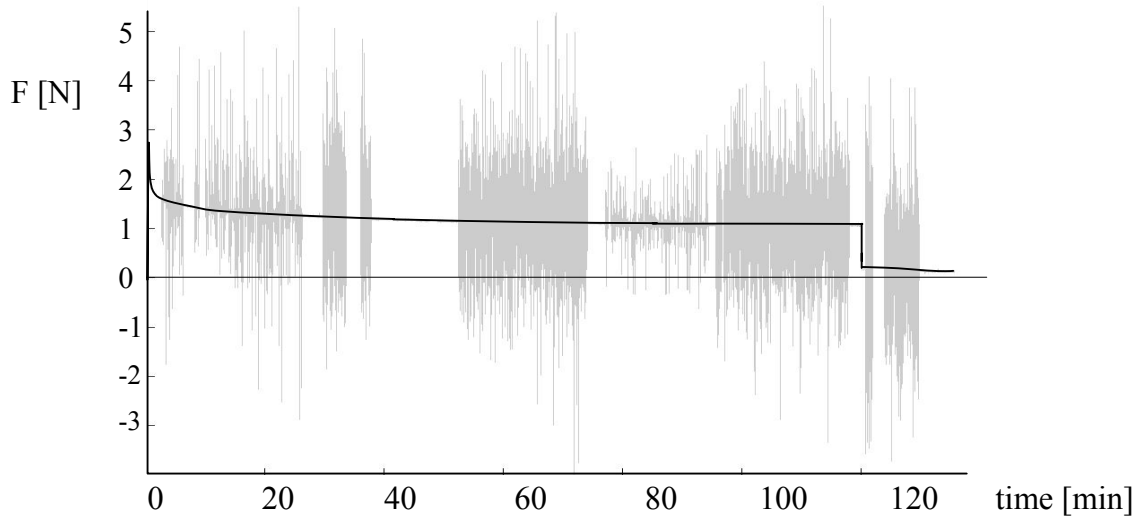
Figure 3.4 *Indenter force measured during a 2-hours loading period (4.5mm indentation), showing the viscoelastic behaviour of muscle tissue. After the relaxation phase a value of approximately 1.1N (156 kPa) is reached. Raw data is shown in grey, the high-frequency fluctuations were caused by MR-measurements (switching gradient fields) that were performed during the loading period.*

a)   b) during loading   15 min   2 hours   20 hours
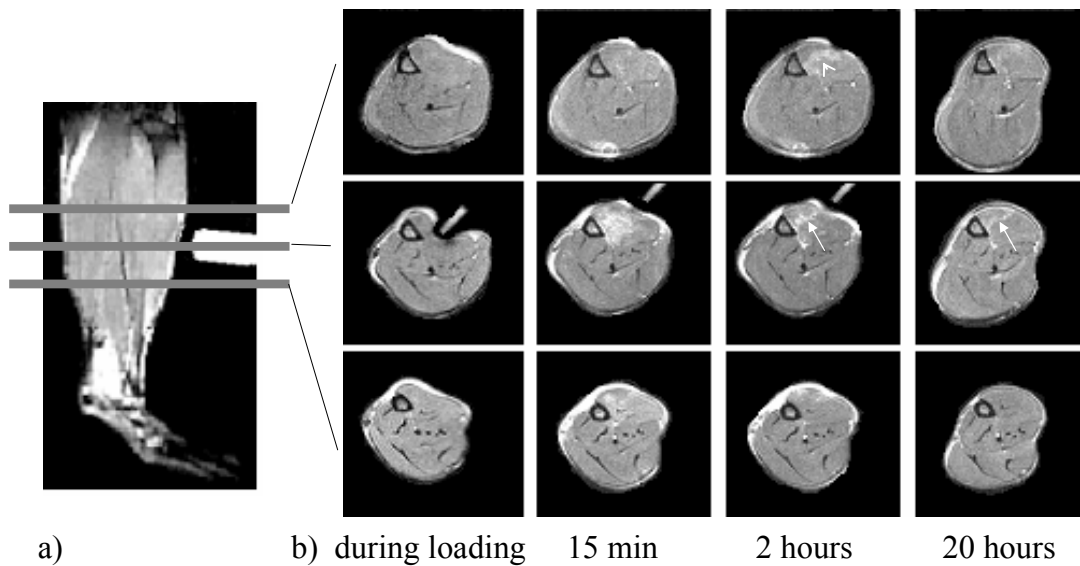
Figure 3.5 a) S*agittal slice of the lower limb showing the position of the indenter relative to the TA. b) Transversal T2-weighted images at three different positions, as indicated in left image. The extent of indentation is shown in the first column, while images taken 15 min, 2 hours and 20 hours after unloading are shown on the right side. The different shape of the leg in the last column was caused by differences in casting between the first and second day. The high values at the outer layer of the leg are caused by the skin layer.*

3.3.4 Histology

A longitudinal slice of the TA, fixated 20 hours after a 4.5 mm indentation for 2 hours, stained with Gomori's trichrome is shown in figure 3.6a. Loss of cross-striation in parts of muscle fibres and infiltration of polymorphonuclear leukocytes (PMNs) and monocytes is visible. The infiltration of PMNs and monocytes reveals an extensive inflammatory reaction. A transverse slice of the damaged TA is shown in figure 3.6b. Normal muscle fibres appear dark after staining with Gomori's trichrome, whereas light-stained fibres are damaged. The damaged region showed a patchy appearance suggesting only partial damage to the whole muscle.
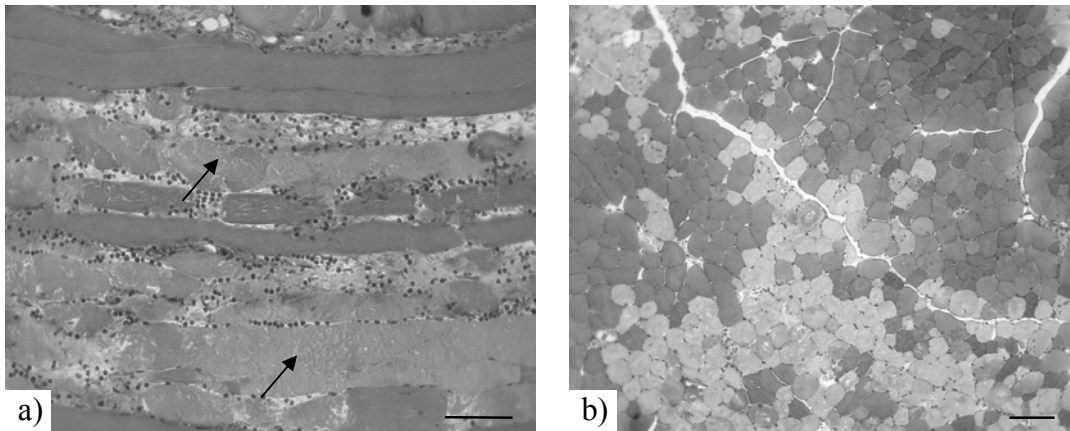
Figure 3.6 *a) Longitudinal histological slice (stained with Gomori's trichrome) showing loss of cross-striation (arrow) and extensive infiltration of polymorphonuclear leukocytes and monocytes (dark dots). b) Transverse slice showing an intermixture of damaged (necrotic) fibres (light) and undamaged fibres (dark). Muscle tissue was fixated at 24 hours following a 4.5 mm indentation for 2 hours. Bar represents 100μm.*

3.4 Discussion

An MR-compatible loading device was developed to permit the simultaneous application of pressure to the tibialis anterior of rats and collection of MR-data. The position of the indenter and the indentation of the TA region could be visualized for each experiment. The indenter force was measured using strain gauges attached to the loading beam, and damage to the tissue was measured using T2-weighted MR imaging.

Force measurements showed a small constant increase in force when measured inside the MR scanner compared to values measured outside the scanner. The difference was caused by the high magnetic susceptibility of the material used for the loading beam (Ertalon 66GF30). By using the correction factor, the indenter force could be estimated correctly during indenter application. The loading beam showed some visco-elastic behaviour, which led to a small underestimation of the applied pressure (within 5%).

Affected regions within the soft tissues could clearly be distinguished on the T2-weighted images (figure 2 and 5). Increased signal intensities were observed directly after unloading and after a period of 20 hours. Abnormal signal intensity within damaged skeletal muscle is frequently encountered with MR imaging and potential causes are diverse [37]. The pathological features associated with pressure ulcers [21, 47, 78] that may affect muscle proton density and relaxation times are inflammation, oedema, necrosis, haemorrhage, fibrosis, and fatty infiltration. Inflammation, oedema and also haemorrhage usually lead to an increased proton density, caused by increased intracellular and extracellular free water. This will result in an increase in T1 and T2 because free water has longer relaxation times. In a recently published study by Linder-Ganz and Gefen [79] the role of free water was also discussed. An increase in stiffness was found in compression-injured muscle in a rat model of pressure ulcers. The increased stiffness was hypothesized to be caused by free water, which increased the swelling pressure in the tissue.

One disadvantage of using T2 as a damage indicator is that it's non-specific, as described above. Besides, not all changes to the tissues can be measured by T2-weighted MRI. Partly caused by the limitation in resolution (in this study 234x234 µm, slice thickness 1mm), which precludes detecting e.g. single cell death. In addition, damage to tissue, which does not immediately lead to changes in amount or properties of water will obviously not be detected. E.g. large strains applied to the membranes of muscle fibres during loading, could lead to damage to the membranes [80], but this might only become apparent after unloading when large osmotic shifts of water occur due to the membrane damage. This is important to bear in mind, while if disregarded, this would lead to wrong conclusions e.g. that damage only started after unloading. Histological examination of the muscle tissue, fixated 20 hours following a 4.5 mm indentation for 2 hours, showed loss of cross-striation in localised areas of the TA. In addition, infiltration of polymorphonuclear leukocytes and monocytes was observed, which indicates an inflammatory response. The necrotic tissue showed a patchy appearance, with a mixture of damaged and undamaged fibres. Only parts of muscle fibres were revealed to be damaged, a state known as segmental necrosis, which is also observed in other muscle pathologies [81].

In the study by Bosboom [28] the damaged areas varied between 0 and 70%. This large range was probably partly caused by differences in applied indentation, while only the pressure could be measured. In the current study the affected area immediately after unloading varied between 60 and 76 %, showing a much larger similarity. It was, however, observed that the precise amount and direction of indentation had a large influence on damage location and development. Again emphasizing the importance of measuring the actual indentation and not only the applied surface pressure.

Large indentations, equivalent to surface pressures of 150 kPa, applied for 2 hours were necessary to produce distinctive damage in the muscle tissue. These loads are relatively high compared to those used in other animal models to create muscle damage. Husain

[47] noted microscopic changes in the muscles in rats when pressures as low as 14 kPa were applied for 2 hours. Kosiak [21] did not find any marked damage in rat muscle (involvement of more than 10 per cent of muscle examined) with an applied pressure of 32 kPa for 2 hours, but did observe individual damaged fibres. The damage observed in the current study involved, however, large necrotic regions, and is therefore of a different order than in the mentioned studies. An addition explanation might be in differences in skin between different breeds of rats used in the studies, albino rats versus Brown Norway rats in the present study, the latter having a relatively strong skin. The large differences remain, however, striking.

It remains difficult to compare data between studies, particularly when considering that it is the internal conditions, as opposed to external loading, which determines the initiation of tissue damage. This is one of the main advantages of MR-study, where the actual indentation of the muscle can be visualized. The difference between internal and external conditions can be demonstrated by finite element (FE) modeling. Oomens [82] showed, using a FE model of a supported buttock, that stress distribution inside the tissues were higher than the interface stresses, and the highest stress was found in the muscle layer. An interface stress of 120 kPa resulted in von-Mises stress in the muscle layer of 180 kPa. Linder-Ganz and Gefen [79] showed even larger increases. FE models of pelvis, shoulders, heels and head, all body parts vulnerable to pressure ulcers, were developed. It was shown that peak stresses in deep muscles under the bony prominences of the human pelvis and shoulders were significantly higher than peak contact stresses. A peak contact pressure of 11 kPa resulted in maximal von-Mises stresses of 290 and 150 kPa in the longissimus and gluteus muscle, respectively. These studies clearly demonstrate the limited value of comparing interface pressures between different models.

The large deformations used in this study are considered to be physiologically realistic. Indeed in a human MRI study, the total compression of the soft tissue composite above a bony prominence was estimated to be 30% and 50% for normal and paraplegic subjects, respectively [83]. These values were determined with supine individuals and it might be expected that deformations could be enhanced in appropriate tissues in seated individuals.

This MR-compatible loading device also offers the potential of using other MR-techniques in the same model. For example, by using MR tagging, 3D maps of the displacement due to indentation can be measured, from which 3D strain maps can be calculated. These can be used for testing the hypothesis that the sustained deformation of cells plays a key role in damage initiation. One of the competing hypotheses [23] suggests that local ischaemia of the tissue, and subsequent reperfusion damage by oxygen free radicals, is an important trigger for the development of pressure ulcers. By using contrast-enhanced MRI perfusion in the muscle during and following indentation can be measured [84] to obtain information on ischaemic regions and connection to damage initiation.

In summary, the developed MR-compatible loading device provides the possibility to measure non-invasively skeletal muscle status and indentation. By using T2-weighted imaging damage initiation and development can be measured. The different factors that may play a role in the onset of muscle damage can be studied in this model, which can be expected to lead to a better understanding of the factors that contribute to pressure ulcer development.

Acknowledgements

Chapter 4

Compression-induced deep tissue injury examined with magnetic resonance imaging and histology

A. Stekelenburg, C.W.J. Oomens, G. J. Strijkers, K.Nicolay, D.L. Bader

4.1 Introduction

Pressure ulcers are areas of soft tissue breakdown that result from sustained mechanical loading of skin and underlying tissues. They can interfere with quality of life, activities of daily living, and rehabilitation and, in some cases, may prove life threatening. Pressure ulcers can develop either superficially or deep within the tissues, depending on the nature of the surface loading and the tissue integrity [15, 16]. The superficial type forms within the skin, with maceration and detachment of superficial skin layers. If allowed to progress the damage may form an ulcer, which is easily detected. By contrast, deep ulcers arise in muscle layers covering bony prominences and are mainly caused by sustained compression of the tissues. These ulcers develop at a faster rate than superficial ulcers and yield more extensive ulceration with an uncertain prognosis. The underlying mechanisms that lead to these deep ulcers are not fully understood. The focus of the present study is therefore on deep pressure ulcers, which necessarily involve deep tissue injury, recently defined as "A pressure-related injury to subcutaneous tissues under intact skin" [NPUAP, 2005]. This definition instantly reveals one of the major problems associated with their early detection.

One of the populations susceptible to the development of deep pressure ulcers are spinal cord injury (SCI) subjects [5, 6]. As an example, the study by Garber and Rintala [6] reported an incidence rate of 39% in a three-year period. A significant proportion of these were stage IV ulcers [12], two-thirds of which were associated with the pelvic region. Particular risk factors for SCI subjects include limited activity and mobility levels, and sensory deficit.

In order to learn more about the underlying mechanisms leading to pressure ulcers different animal models have been used over many decades. Several theories have been proposed. The most commonly adhered theory is that compression of the tissues causes occlusion of capillary blood flow, resulting in local ischaemia and a depletion of the supply of vital nutrients to the cells [20, 22, 85]. More recently, reperfusion following an ischaemic period has been suggested as an additional factor in damage development [23]. A further theory focuses on the role of the interstitium between cells. This theory assumes that mechanical loading results in a disturbance in the metabolic equilibrium around cells [26, 27]. The prolonged deformation of cells, per se, has also been proposed to play a major role in the onset of tissue damage [28, 29, 30, 86].

In association with the latter hypothesis, the larger deformations found in muscle tissues of SCI subjects might be an additional risk factor for this subject group [83, 87]. In a human MRI study, the total compression of the soft tissue composite above a bony prominence was estimated to be 30% for normal subjects compared to 50% for a SCI subject with flaccid paralysis [83]. These values, determined with supine individuals, might be enhanced in appropriate tissues in seated individuals. Indeed such deformations can be associated with significantly increased interface pressures in SCI

subjects with flaccid paraplegics compared to other groups, such as the elderly and spastic paraplegics [87].

There has been considerable research associated with muscle damage. Most of this research has involved exercise-induced damage [88, 89], muscle diseases [90] and ischaemia/ reperfusion injury [91, 92]. By contrast, only a few studies have examined muscle damage directly related to pressure ulcers. These latter studies have generally used histology to assess muscle damage in the form of loss of cross striation and infiltration of inflammatory cells [28, 52, 79]. A more detailed examination of the histopathology, however, might reveal information that is vital to the understanding of the primary damage mechanism. In addition, information on the spatial and temporal development of damage in muscle tissue *in vivo* can be provided by magnetic resonance (MR) imaging, which is a non-destructive technique [37, 76].

Bosboom et al. [28] developed an animal model in which the tibialis anterior (TA) of Brown Norway rats was compressed by means of an indenter. Muscle tissue was examined after 24 hours using both histological analysis and magnetic resonance (MR) imaging. It was shown that affected tissue localized by T2-weighted MR imaging correlated well with damaged areas determined by histological examination. This model was recently improved by building an MR-compatible loading device [chapter 3, 93], which provided the possibility of simultaneous application of pressure to the TA and measurement of tissue status by means of MRI.

Our hypothesis is that initial damage to the muscle fibres is induced mechanically by local excessive deformation and subsequent disruption of muscle fibres. This damage is followed by a cascade of processes as the tissue homeostasis is disturbed. Based on the notion that the initial muscle damage might reveal the proposed mechanical damage, the focus of the present study was to examine the early damage in muscle tissue after compressive loading. Therefore, T2-weighted MRI was performed both during loading and up to 20 hours after unloading and histological examination was performed at early time points after unloading. These measurements were combined in order to elucidate the damage mechanisms leading to deep pressure ulcers.

4.2 Material and methods

4.2.1 Animal model
In this study 20-week-old female Brown-Norway rats were used weighing between 170 and 200 grams. They were housed under standard laboratory conditions (12h light, 12h dark cycles) and maintained on standard laboratory food and water ad libitum. Each rat was anaesthetized for the preparation phase by subcutaneous injection of xylazine (1 µl/g body weight, 2 g/l) and intramuscular injection of ketamine (0.8 µl/g body weight, 100g/l). During the MR measurements, anaesthesia was maintained with isoflurane

inhalation (0.4 to 1.0 % isoflurane with N_2O/O_2 mixture (1:1)). Vital signs (pulse and respiratory rate) were monitored and maintained within physiological values. Each rat was placed on a heating pad to maintain body temperature between 35-37ºC. Prior to the loading experiment, the hairs on the left tibialis anterior (TA) region were removed by shaving. The leg was placed in a specially designed mould and plaster cast was applied to obtain a firm fixation in the set-up. The preparation phase took approximately 45 minutes. The experimental protocol was approved by the Animal Care Committee of the University of Maastricht.

4.2.2 MR-compatible loading device

The experimental set-up is described in detail in chapter 3 [93]. To review briefly, the loading device consisted of two concentric tubes, the inner of which houses the animal while the outer tube was used to position the whole arrangement in the MR scanner. The scanner was a 6.3 Tesla Varian system, operating at 270 MHz (horizontal bore, diameter of 95 mm) with a 380 mT/m gradient coil. The anaesthetized animal was placed supine in the loading device (figure 4.1), with its foot positioned in a special holder in which the casted leg was fixed. In the cast a hole was made for the application of a rounded plastic indenter, of 3 mm diameter, to the TA region (figure 4.1b). A birdcage radio frequency coil was placed in a fixed position around the limb. The indenter was fixed to a glass fiber reinforce polymer (Ertalon 66GF30) loading beam to which strain gauges were attached to enable force measurements during indentation. An indentation was applied by rotating the bar that is attached to a cam, as shown in figure 4.1a. Figure 4.1c shows a transversal MR image of the lower limb underneath the indenter during indentation.

4.2.3 Experimental Protocol

Animals (n=10) were divided into three groups (designated I-III). The loading protocol was the same for all groups, while the moment of perfusion fixation was different.

The measurement protocol involved five separate phases, as indicated in figure 4.2. Initially transversal scout images (sc) were produced and, where necessary, adjustments made to ensure that the TA was compressed between the indenter and tibia and the indentation was perpendicular to the surface of the limb. Before applying the indenter, a T2-map ($T2_p$) was measured using a multi-echo sequence over a scanning time of 20 minutes. Thereafter an indentation of 4.5 mm was applied, at a rate of 1.5 mm/s to avoid impact damage, which was maintained for 2 hours. During indentation sagittal and coronal images and a T2-map ($T2_L$) of the leg were recorded. Thirdly, immediately after removal of the indenter, a series of T2-measurements was started ($T2_{1-8}$). For group I animals (n=3), two measurements were performed in a one hour period after which the animal was sacrificed for histological examination. For group II animals (n=4) up to eight consecutive measurements were performed and, at 4 hours, the animals were sacrificed. After completion of the measurements, group III animals

(n=3) were removed from the loading device, their cast was removed and they were allowed to recover from anaesthesia and to move freely for the next 16 hours. After this period, the animal was again sedated and the leg fixed in the set-up. A single T2-measurement (T2$_9$) was performed after which the animal was sacrificed (figure 4.2).
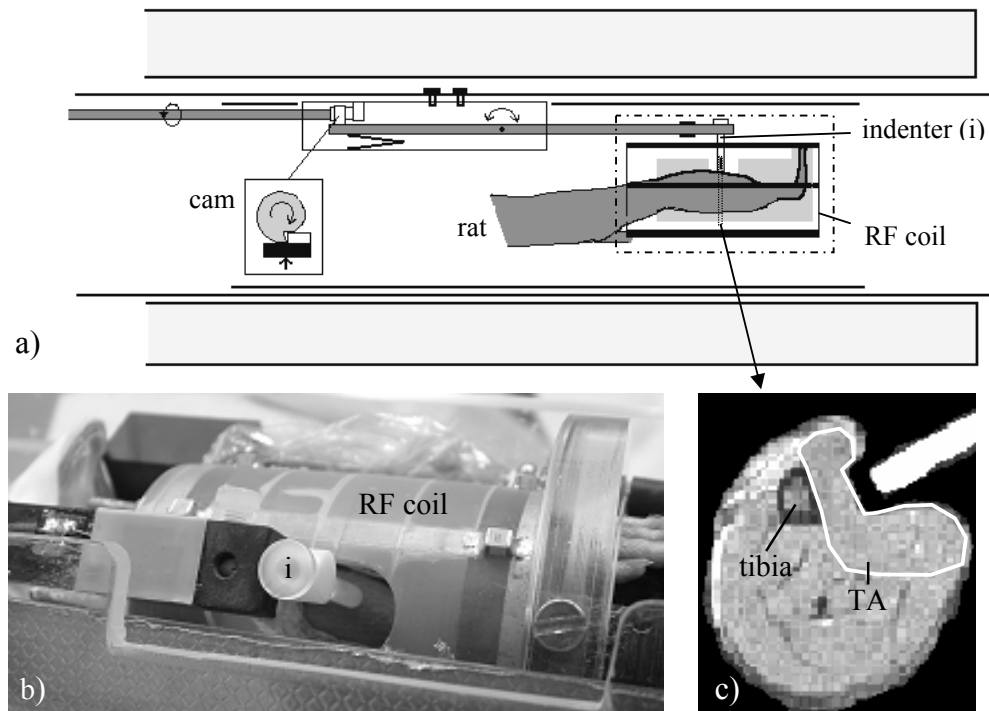
Figure 4.1 *a) Schematic of MR-compatible loading device. Animal is lying supine in the set-up with its leg fixed in the RF coil. b) A photograph of an expanded view of the loading device in which pressure is applied to the tibialis anterior by an indenter (i) that is positioned through the legs of the RF coil. c) Transversal MR image showing the TA (indicated by white line) compressed between tibia and indenter. The indenter was filled with water to ensure visibility on the MR- image.*

4.2.4 MRI Parameters

A multi-echo spin echo sequence was used to obtain T2-maps. Signal intensities (SI) of the echoes were fitted to the equation SI= A + B exp (-t/T2), to determine T2 values. Imaging parameters were: slice thickness = 1mm, field of view FOV= 25x25mm^2, matrix size = 128x128 pixels, number of signal averages NSA = 2, echo time TE = 12 - 96 ms, number of echoes = 8, repetition time TR=4.5 s. Number of slices = 41, centered on the longitudinal axis of the indenter. Total scanning time was 20 minutes.

A T2-weighted spin echo sequence was used to collect 31 slices in the sagittal and coronal direction, perpendicular to the indenter direction. Imaging parameters were:

slice thickness = 1mm, FOV = 60x30 mm^2, matrix size 128x128 pixels, NSA = 2, TE = 25 ms, TR = 4s. Total scanning time was 17 minutes.
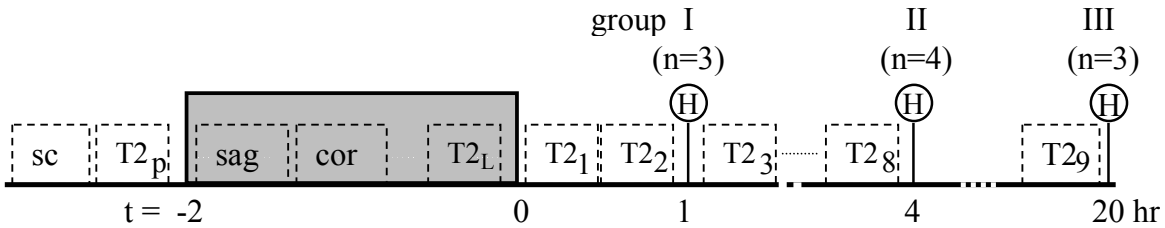
Figure 4.2 *Time schedule of MR measurements and sacrifice for histological examination. Shaded rectangle represents loading period. sc: scout images, T2: T2-map, sag/cor: sagittal and coronal images, H: histological analysis, subscript p: pre-loading, L: during loading, 1-9: number of measurement after unloading, t=0 is defined as moment of unloading.*

4.2.5 MR data analysis

To obtain an enhanced contrast to noise ratio (CNR) between normal and affected tissue, the individual images of the multi-echo sequence were summed. The resulting images are referred to as T2-weighted-sum (T2ws) images. On the T2ws images that were collected pre loading ($T2_p$), the TA region was manually defined, which excluded both the skin and fat layer. In this area a mean T2 value was calculated, and a threshold value defined as equal to the mean + 2 SD. This threshold was applied to all images up to $T2_8$ (figure 4.2). The affected area was then defined as the percentage number of pixels with signal intensity above the threshold value Spatial and temporal development of affected regions was evaluated in volumes consisting of 2 adjacent 1mm thick slices. Three volumes were used for evaluation: underneath the indenter and at 3 mm proximal and distal to the indenter. For the calculation of temporal development of damage, only those experiments were included in which 8 consecutive T2-maps had been collected (n=4). Data are presented as mean ± SE. For images of group III animals taken on the second day, slices were retraced according to the size and shape of the tibia bone.

4.2.6 Histological analysis

Immediately following the last MR measurement, each animal was sacrificed and perfusion fixated with 4% buffered formalin. The lower limb was cut off and stored in formalin. The TA was excised at least two weeks later, to ensure complete tissue fixation. The muscle was dehydrated in a series of alcohol solutions and embedded in plastic (Technovit 7100, Kulzer). The muscle was cut longitudinally, perpendicular to the direction of load application, or in the transversal direction in 5 μm thick sections. The samples were stained with Gomori's trichrome to visualize both the cross-striated appearance of the muscle fibres and the cell nuclei.

4.3 Results

4.3.1 MRI

Figure 4.3 illustrates transversal T2ws images of the lower limb underneath the indenter recorded before, during and after loading. Images are shown for two typical experiments. The images (figure 4.3b and e) taken during loading ($T2_L$) were collected just before load removal and revealed no systematic changes in signal intensity in the loaded region. In the slices distal to the indenter position, some signal increase was observed during loading. Figure 4.3c and f show the images, which were taken directly after unloading ($T2_1$) and clearly demonstrate a marked signal increase in the TA region in a localized area extending from skin down to the tibial bone. There was considerable similarity between all experiments in locations of the areas exhibiting an increased signal intensity.
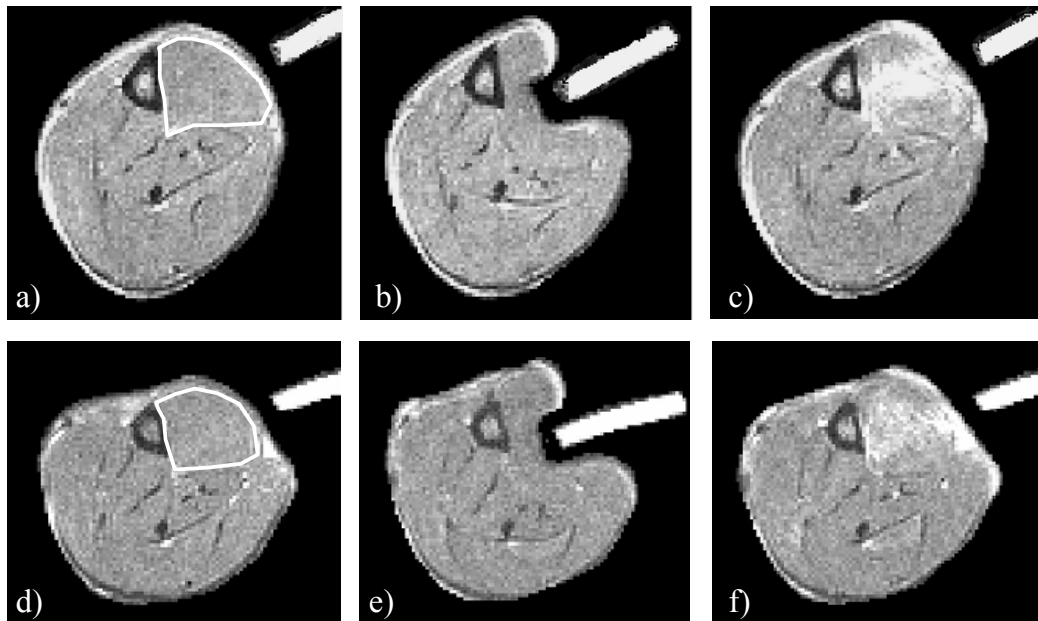
Figure 4.3 *Transversal T2-weighted-sum images underneath the indenter for 2 typical experiments. The first column shows the images taken before loading ($T2_p$), the second column the images taken during loading ($T2_L$) and the last column the images taken immediately after unloading ($T2_1$). TA is indicated by the white line in first images.*

A typical temporal distribution of T2-values in the TA region underneath the indenter is shown in figure 4.4. The T2 distribution before loading appeared to be symmetrical with a mean value of 20.3 ± 2.7 ms (figure 4.4a) and a threshold value of 25.7 ms, which is indicated by the vertical line. Pixels with a T2 above this value are considered to be indicative of muscle damage. The distributions associated with the post loading periods were clearly skewed towards higher T2 values. Thus the median T2 values

increased to 26.8 and 30.0 ms at 15 and 90 minutes after unloading, respectively. Thereafter there was a decrease to a value of 27.9 ms corresponding to 190 minutes after load removal.
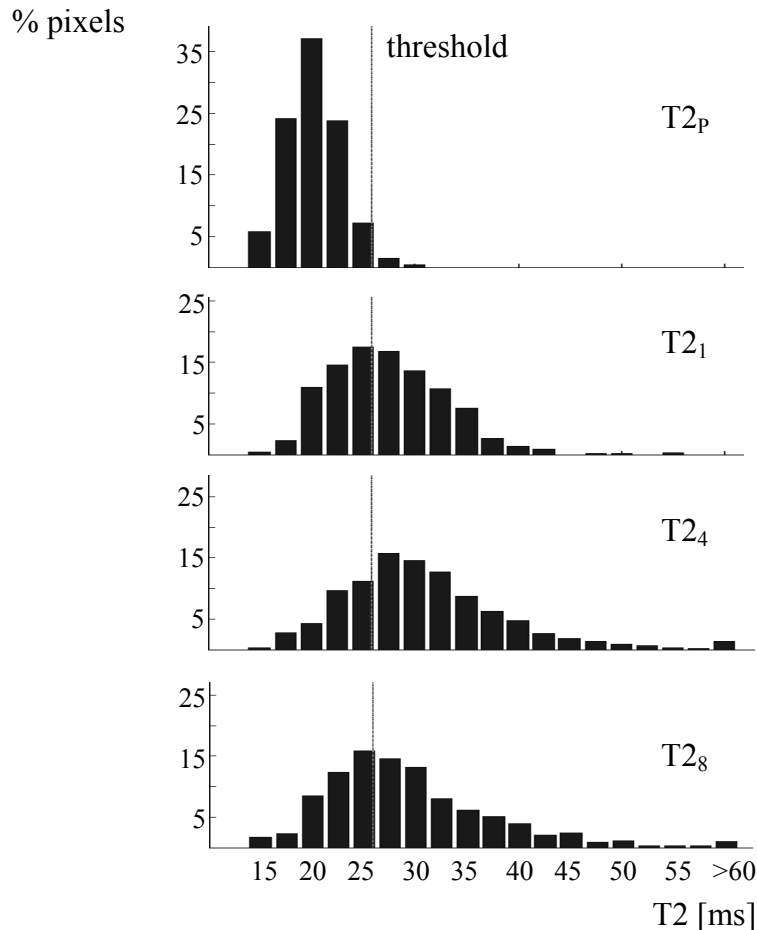
Figure 4.4 *Distribution of T2-values in TA underneath the indenter. a) Before loading the distribution is symmetrical with a mean value of 20.3 ± 2.7 ms. Threshold value (mean + 2 SD) is indicated by vertical line. After load removal a skewed distribution towards higher T2 values was found with a median of b) 26.8 ms at 15 minutes, c) 30.0 ms at 90 minutes, and d) 27.9 ms at 190 minutes after load removal.*

The trends in temporal response are more closely illustrated in figure 4.5. The percentages number of pixels with a T2 above the threshold value are shown for 15 to 190 minutes after load removal. Trends are illustrated for three volumes (figure 4.5a), underneath the indenter and at 3 mm proximal and 3 mm distal to the indenter position. It should be noted that the largest percentage affected volume was found underneath the indenter (volume 2 in figure 4.5a). This volume slightly increased in the first 90 minutes to 60% after which it started to decrease. In the volumes at 3 mm distance from the indenter, the affected percentages were lower. Two different trends were observed. In the slices proximal to the indenter, a small affected volume was present directly after

unloading, which increased in the first 90 minutes from 11% to 33%. Thereafter it tended to decrease. In the slices distal to the indenter the percentage number of affected pixels was 39% at 15 minutes, which decreased to 25% in the first hour after unloading. Thereafter a small decrease in affected volume was evident.
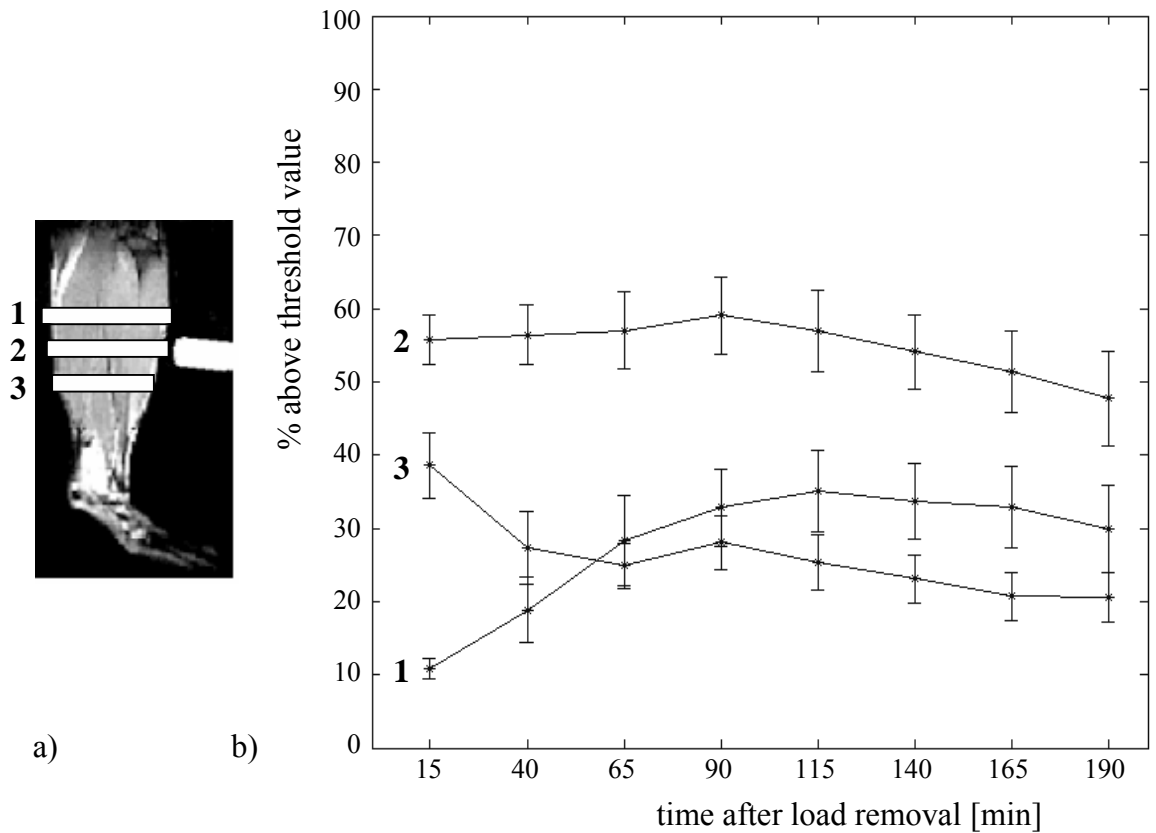
Figure 4.5 *Temporal and spatial distribution of affected tissue characterized by a significantly prolonged T2. a) Sagittal slice of lower limb with three volumes selected for analysis; proximal to (1), underneath (2) and distal to (3) the indenter. b) Percentage number of pixels in selected volume above threshold value as a function of time. Percentages are indicated as mean ± SE (n=4).*

The T2-maps underneath the indenter recorded before ($T2_p$) and during loading ($T2_L$), and 190 minutes ($T2_8$) and 20 hours ($T2_9$) after unloading are shown in figure 4.6. The regions in the TA with enhanced signal intensity exhibited a similar distribution at 20 hours when compared to 190 minutes after unloading for all three experiments (group III animals). The high T2 values evident at the edges (figure 4.6b and c) were caused by water accumulation in the skin layer.
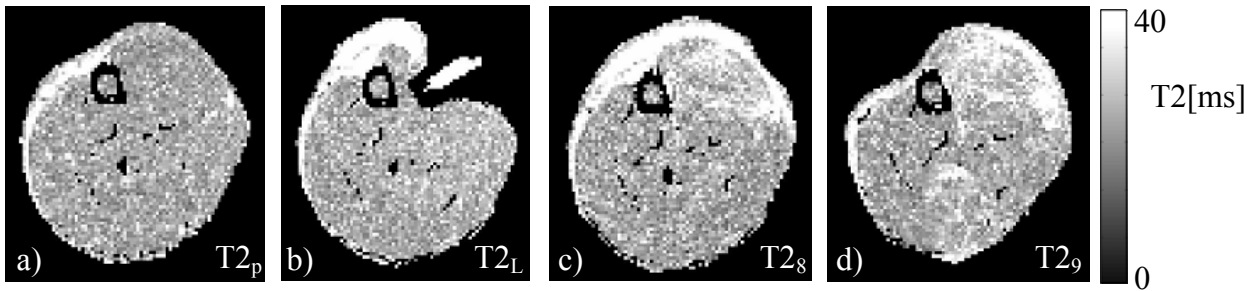
Figure 4.6 *T2-maps of lower limb underneath the indenter taken a) before and b) during loading, and at c) 190 minutes and d) 20 hours after unloading. The different shape of the leg in image d) is caused by small differences in casting between the first and second day.*

4.3.2 Histology

Longitudinal slices taken from muscle fixated 60 minutes after load removal (group I animals) are illustrated in figures 4.7a and b. Two regions are shown taken from the mid portion of the muscle, where the muscle was compressed by the indenter. A large area was evident with a complete absence of the normal cross-striated pattern of skeletal muscle, indicating a disorganization of the internal structure of muscle fibres. The filaments were 'snapped' and clustered together, leaving empty spaces within the fibres. The morphology of individual fibres indicated both necrotic regions and normal appearance separated by segmental contraction. In those, slightly darker stained, parts of the fibre the diameter was clearly increased (figure 4.7a, short arrows). At the interface between hypercontracted and undamaged fibres, longitudinal tears were observed (figure 4.7b, arrows). Adjacent to the necrotic region, the membrane of the fibres had a wavy-like appearance and the interstitial spaces were widened. The histological slices of muscles from group II animals fixated four hours after load removal (figure 4.7c and d) showed necrotic areas with similar structural damage to the muscle fibres. In some fibres the contractile material was slightly less clustered together. At the edges of the necrotic region early infiltration of polymorphonuclear cells (PMNs) was observed (figure 4.7c, arrows). In some parts of the muscle, there was an alternating pattern of damaged and undamaged fibres. Normal cross-striated fibres were found adjacent to completely disrupted fibres (figure 4.7d). The membranes of the disrupted fibres seemed largely intact, with only minor evidence of fragmentation. After 20 hours of load removal (figure 4.7e and f) the cellular debris was more diffusely distributed within the fibres, occupying the empty spaces observed in the first hours after load removal. This cellular material was stained lighter compared to the undamaged filaments. It is interesting to note that despite the extensive regions of necrosis, the individual fibres could clearly be distinguished. An extensive infiltration of PMNs and monocytes was observed, revealing a pronounced inflammatory response. These inflammatory cells aggregated in areas of the interstitium of the muscles and invaded a proportion of muscle fibres.
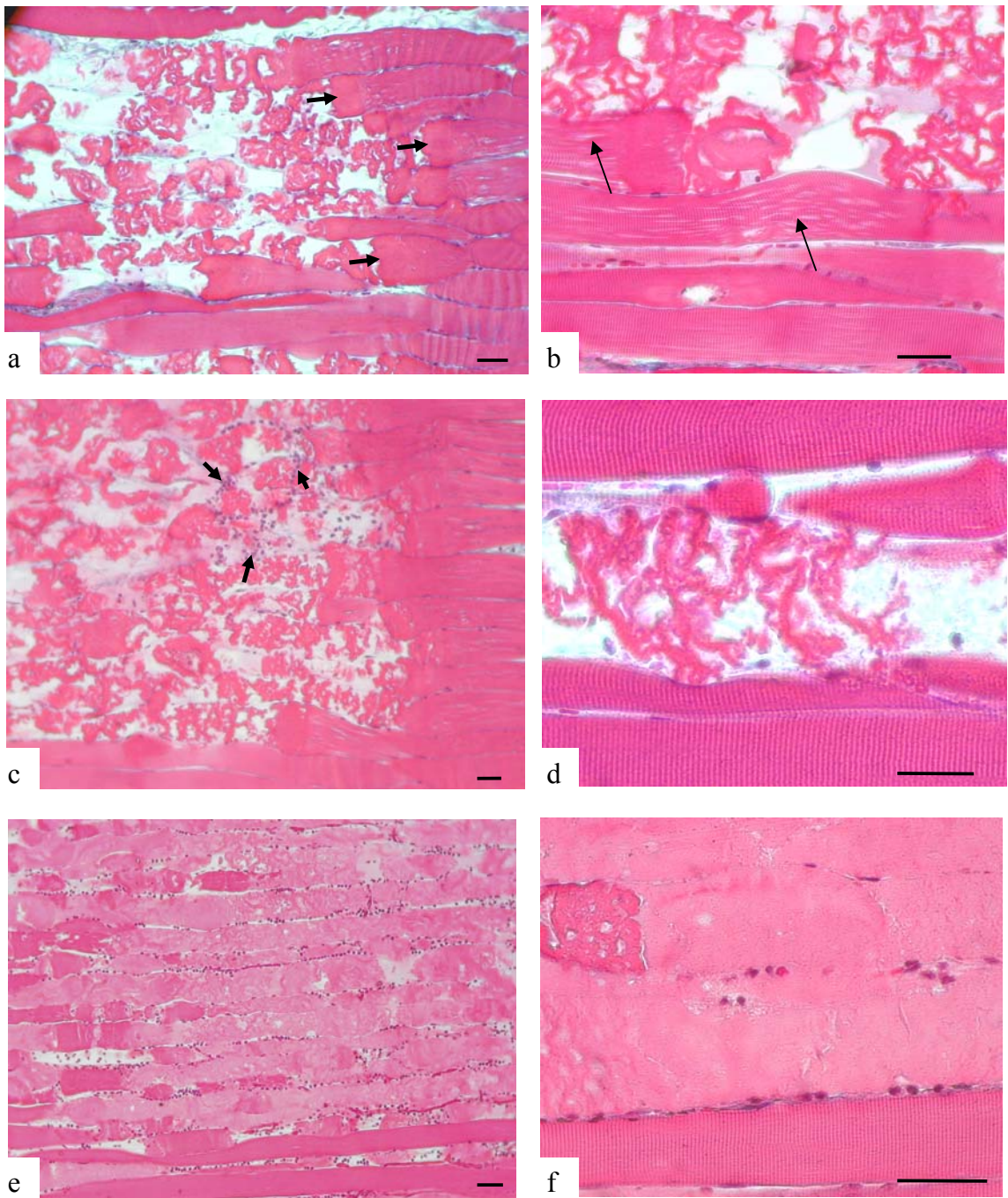
Figure 4.7 *Longitudinal histological slices, taken from the mid portion of TA, stained with Gomori's trichrome. Muscle fixated 1 hour (group I, a-b), 4 hours (group II, c-d) or 20 hours (group III, e-f) after removal of load. The muscle fixated 1 hour after load removal showed a complete disorganization of the internal structure of the muscle fibres. After 4 hours (c-d), early signs of inflammation were visible by infiltration of polymorphonuclear leukocytes (figure c, arrows). After 20 hours (e-f) an extensive infiltration of PMNs and monocytes is visible. Bar represents 50 μm.*

Transversal histological slices of muscle fixated 20 hours after load removal are illustrated in figure 4.8. These slices more clearly demonstrate the distribution of size and shape of the muscle fibres. In undamaged regions fibres were angular in shape and show a uniform intensity of staining. The injured region showed damage ranging from slightly different staining intensity and rounded appearance of fibres (indicated by arrows, figure 4.8c) to necrotic, pale-stained, fibres (figure 4.8a). An extensive infiltration of PMNs and monocytes was also observed in these slices. Some fibres showed phagocytotic infiltration (indicated by arrow, figure 4.8b). It is also evident that these large fibres compressed surrounding fibres, indicated by asterisks in figure 4.8b. Overall, the distribution of necrotic fibres within the fascicles did not reveal a systematic pattern.
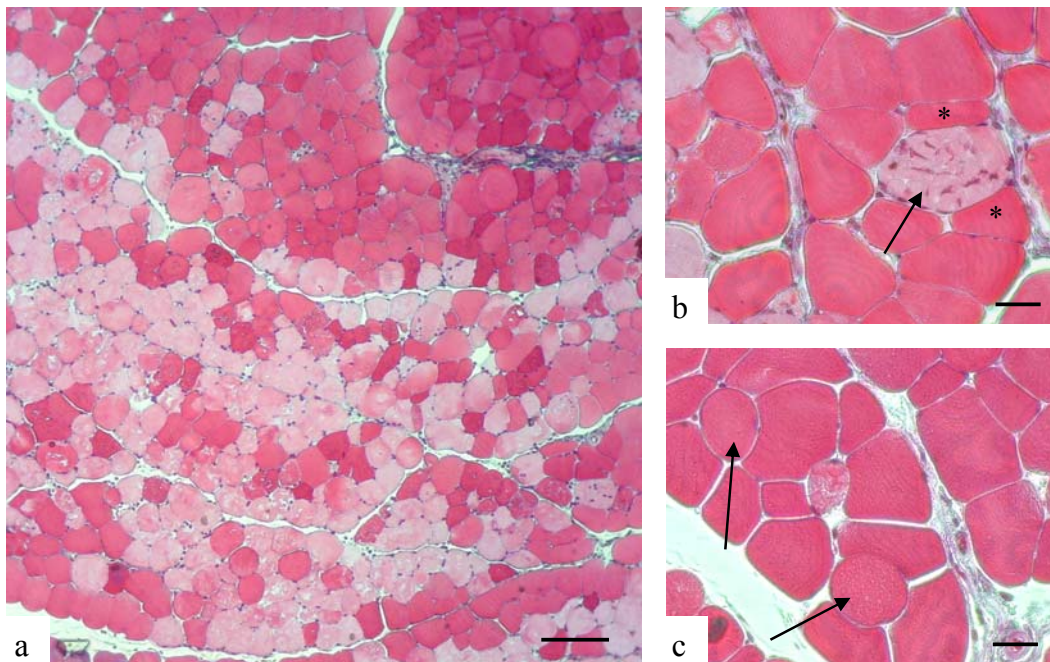
Figure 4.8 Transversal slices of TA stained with Gomori's trichrome from muscle fixated 20 hours after unloading. a) A mixture of damaged (necrotic) fibres (light) and undamaged fibres (dark). The infiltration of PMNs and monocytes (dark dots) revealed an extensive inflammatory reaction. The mononuclear cells aggregated in localised areas of the interstitium of the muscles and in some muscle fibres (figure b, arrow). The large fibre compressed surrounding fibres (figure b,*). Round swollen cells, with normal staining intensity, lie scattered within the cross-sections (figure c, arrows). Bar represents a) 200μm, and b, c) 50μm.

4.4 Discussion

In the present study muscle damage after compressive loading was examined with T2-weighted MR imaging in combination with histological examination. Affected regions within the muscle tissue could clearly be distinguished on T2-weighted images. In

addition, the subsequent temporal development of damage could be monitored. Histological examination at early time points after unloading revealed the initial damage to the muscle fibres.

The correlation between these two techniques is not straightforward as changes in T2 can reflect a range of pathologies [45]. Bosboom et al. [28] examined the correlation between the increase in T2 and histological damage in rat skeletal muscle tissue at one time point. An extensive and labour-intensive method was used to correlate damage in histological slices to high intensities in T2-weighted MR images, both determined 24 hours after load removal. Damage in the histological slices was indicated manually from evidence of loss of cross-striation of the muscle fibres and/or infiltration of inflammatory cells. Damage in MR-slices was determined by applying a threshold level to the images. The correlation found between the damaged areas as quantified using MRI and histology, 24 hours after load removal, was very high ($r^2 = 0.93$). In the present work, the histological damage observed 20 hours after load removal appeared similar to that described in the previous [28]. It may therefore be inferred that the increase in T2 at 20 hours after unloading, as was observed in the present study, was a direct results of the change in appearance of the muscle fibres, as found in the histological slices (figure 4.7e and f and figure 4.8).

The correlation between T2 increase and changes in tissue integrity at earlier time points after load removal is, however, more complex in nature. In the histological slices taken 1 and 4 hours after load removal several changes were observed. Primarily, in the area underneath the indenter large necrotic regions were observed with condensed contractile material clustered together within the fibres. Adjacent to this necrotic region, there was a less systematic picture. Areas containing both necrotic fibres and fibres exhibiting different stages of damage including longitudinal tears, wavy-like membranes, probably with changed permeability, widened interstitial spaces and hypercontracted zones. These factors will probably all contribute to an increase in T2. It is important to note that the T2 value in a MRI pixel is a mean value of a region containing approximately 20 fibres with a length of 1 mm, equivalent to the thickness of the MR slice. Thus the resolution of MRI is considerably lower than that provided by histology. Therefore in the present study only a qualitative correlation was performed.

In this study large indentations, equivalent to surface pressures of approximately 150 kPa, were applied, simulating the indentation of muscle tissue by bony prominences [82, 83]. Underneath the indenter no systematic changes in signal intensity were observed during loading. Although this finding suggests that no large changes in water balance occurred in the loading phase, it does not indicate whether the tissue was affected when exposed to large deformations, since T2 does not reflect all changes to tissue and the resolution is limited. Directly after unloading a large area with increased T2 values was present, tending to decrease in size after 2 hours. A striking difference was observed between slices proximal and distal to the indenter position (figure 4.5). In the slices proximal to the indenter, T2 values started to increase after unloading. The

affected volume increased in the first hour after which it slowly decreased. In the slices distal to the indenter, however, higher T2 values were already observed during and directly after load removal. However, the affected area decreased in the first hours. The deformations in both these regions are necessarily small. Therefore a possible explanation for the different responses is the perfusion status of the tissue. The perfusion in the tissue distal to the indenter was presumably blocked by the large indentation, while in the slices proximal to the indenter the perfusion was minimally affected during loading. The difference in amount of affected volume largely disappeared in the first hour, implying that the effect of ischaemia, as indicated by an increase in T2, was reversible within the muscle tissue.

The large deformations used in this study are considered to be relevant, especially for SCI subjects. It is known that muscle tissue properties change after spinal cord injury. In a review by Scelsi [94], the pathological changes were summarised, and included muscle fibre type transformation, with type I fibre change to type II, muscle atrophy, changes in fibre size, and alterations in myofibrillar apparatus. Studies on an experimental spinal cord transection showed changes in rat skeletal muscle, with almost complete type I to type II fibre transformation after 1 year [95]. The use of such an animal model might be valuable in studying the vulnerability of SCI subjects. Several pressure ulcer related studies involving paraplegic animals have been performed [20, 46, 50]. Results were however contradictory, caused, in part, by differences in time between spinal cord transection and experiments, which seemed to represent a critical factor.

The large deformations underneath the indenter result in large strains on the muscle fibres. These high strains on individual muscle fibres resulting from compressive loading may be similar to those reported associated with exercise. The two common hypotheses [89] to explain exercise-induced damage are metabolic overload and mechanical factors, the latter of which may have direct relevance to the current study. Indeed, Lieber and Fridén [96] demonstrated in an *in-vivo* model that muscle damage after eccentric contraction was a function of active muscle strain as opposed to muscle force. The possible analogy between the characteristics of damage after compression and exercise may be examined by reproducing a histological schematic of damage after eccentric exercise (figure 4.9b), indicating a muscle fibre with segmental damage surrounded by normal fibres [97]. Feature include hypercontraction zones, bilateral to the necrotic zone, which displace and compress adjacent fibres, while in the region of the lesion, these normal fibres taper along the damaged and narrow fibre, all of which are illustrated in figure 4.9b. These features in damaged fibres were also found in the present histology after compressive loading as illustrated in figure 4.9a, suggesting a similar mechanical damage mechanism.

Different studies on the effect of stretching muscles [96, 98, 99] have shown the importance of strain on muscle fibres as an initial damage mechanism. Local strains might be correlated to damage location by using MR tagging experiments of local

tissue deformation, involving separate repetitive indentation phases. Another approach to estimate strains during indentation is to develop a dedicated finite element model to examine the spatial relationship between damage and predicted strains. Both methods will be adopted in future studies.

In summary, the proposed relevance of large deformation of muscle cells in the development of deep tissue injury was supported by the location of damage indicated by T2-weighted MRI and a resemblance in histological appearance between exercise-induced and compression-induced muscle damage. Based on the difference in the response of muscle tissue observed distal and proximal the indenter, which was most likely an effect of perfusion, the increase in T2 revealed tissue changes due to ischaemia alone. These tissue changes will most probably accelerate and/or increase the damage development during and after compressive loading
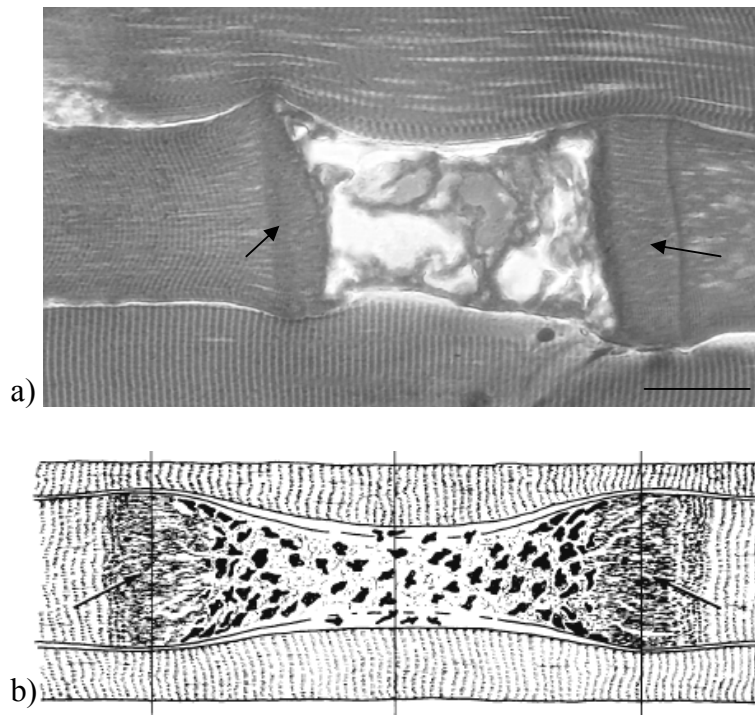
Figure 4.9 *Segmental damage to muscle fibre. a) Longitudinal slice of muscle fixated 1 hour after 2 hours of compressive loading, stained with Gomori's trichrome. Hypercontraction zones (arrow) are bilateral to the necrotic zone. Bar represents 50μm   b) Schematic drawing of longitudinal section of muscle after eccentric exercise showing the different zones, normal - hypercontraction (arrow) - necrotic - hypercontraction - normal, in a fibre with segmental damage. Adapted from Fridén and Lieber [97].*

Acknowledgements

We gratefully acknowledge Jo Habets for his help with the animal experiments and Prof. Verheyen from the University of Maastricht and Prof. Lammens from Radboud University Nijmegen Medical Centre for their help with the interpretation of the histological slices.

Chapter 5

The relative contributions of deformation and ischaemia to deep tissue injury

5.1 Introduction

Pressure ulcers are areas of soft tissue breakdown that result from sustained mechanical loading of skin and underlying tissues. They can develop either at the skin layer and progress towards deeper layers, or progress from underlying tissues towards the skin [15, 29]. The latter ulcers develop at a faster rate than superficial ulcers and yield more extensive ulceration with an uncertain prognosis. The underlying mechanisms that lead to these deep ulcers are not fully understood. Several mechanisms have been proposed to explain muscle damage after compressive loading. The most popular theory is that compression causes a severe reduction of the capillary blood flow, resulting in local ischaemia [20, 22, 85]. This theory can explain the differential sensitivity of skin and muscle tissue, since muscle tissue is metabolically more active than skin and is thus potentially more susceptible to ischaemic stress [20, 100]. More recently, reperfusion following an ischaemic period has been proposed as an additional factor in damage development [23]. A further hypothesis focuses on the role of the interstitium between cells, and proposes that mechanical loading results in a disturbance in the metabolic equilibrium in the vicinity of cells [26, 27]. The prolonged compression-induced deformation of cells, per se, has also been proposed to play an important role in the onset of soft tissue damage [29, 30].

Most of the current knowledge on the aetiology of pressure ulcers has been provided by animal models [20, 21, 47]. These studies have mainly focused on the effects of both the magnitude and duration of loading and its nature, in particular, continuous versus intermittent loading. However, unravelling the complex interactions between the mechanisms that lead to local cell damage is a difficult task. In discriminating between the different factors, the use of *in-vitro* models provides a useful complementary approach. *In-vitro* models are currently being used to study the relationship between muscle cell deformation and cell damage in response to compressive strains [101]. For example, experiments with tissue engineered skeletal muscle tissues were used to examine the effect of strain on muscle cells, in the absence of ischaemia [86]. A significant increase in cell death was observed at clinically relevant strains within 1-2 hours. Furthermore, it was shown that higher strains led to earlier initiation of damage. However, to extrapolate these results to the clinical situation, related *in-vivo* experiments using animal models are needed. An *in-vivo* approach provides the opportunity to discriminate between the effects of pure ischaemia on muscle tissue and the effects of tissue compression, including ischaemia, large cell deformation and possible disturbance of the metabolic equilibrium.

The objective of the present *in-vivo* animal study was to distinguish between the different factors that contribute to muscle tissue damage related to deep pressure ulcers that develop after compressive loading. This was accomplished by using two separate loading protocols incorporating uniaxial loading, resulting in compression of the tissue, and ischaemic-induced loading. By using these two different protocol it can be

examined whether or not there is difference in response of tissue as a result of pure ischaemia compared to a situation of deformation and ischaemia. The animal model developed by Bosboom et al. [28] and recently modified by the authors [93] was used. The effect of both loading protocols on muscle tissue was evaluated using T2-weighted MRI, contrast-enhanced MRI and histological analysis.

5.2 Materials and methods

5.2.1 Animal model

In this study 20-week-old female Brown-Norway rats (n=6) were used weighing between 170 and 200 grams. Rats were housed under standard laboratory conditions (12h light, 12h dark cycles) and maintained on standard laboratory food and water ad libitum. Each rat was anaesthetized for the preparation phase by subcutaneous injection of xylazine (1 µl/g body weight, 2 g/l) and intramuscular injection of ketamine (0.8 µl/g body weight, 100g/l). During the MR measurements, anaesthesia was maintained with isoflurane inhalation (0.4 to 1.0 % isoflurane with N_2O/O_2 mixture (1:1)). Vital signs (pulse and respiratory rate) were monitored and maintained within physiological values. The rat was placed on a heating pad to maintain body temperature between 35-37ºC. Prior to the loading protocols, the hairs on the left tibialis anterior (TA) region were removed by shaving. The leg was placed in a specially designed mould and plaster cast was applied to obtain a firm fixation in the set-up. For administration of the MRI contrast-agent a catheter (Portex, outer diameter 0.61mm) was inserted in the jugular vein. The experimental protocol was approved by the Animal Care Committee of the University of Maastricht.

5.2.2 MR-compatible device

The experimental set-up is described in detail in chapter 3 [93]. To review briefly, the device consisted of two concentric tubes. The inner tube houses the animal and the outer tube was used to position the whole arrangement in a 6.3 Tesla MR scanner (Varian system), operating at 270 MHz (horizontal bore, diameter 95 mm) with a 380 mT/m gradient coil. The anaesthetised animal was placed supine in the device, with its foot positioned in a special holder in which the casted leg was fixed. A birdcage radio frequency coil was placed in a fixed position around the limb. A hole was made in the cast, which enabled application of a plastic indenter to the TA region. The indenter was fixed to a glass fibre reinforced polymer (Ertalon 66GF30) loading beam to which strain gauges were attached to enable force measurements during loading. The loading beam could be attached to the outer tube of the set-up. The indenter was applied by rotating the bar that was attached to a cam.

5.2.3 Loading protocols

Two distinct loading protocols were used:

1. Uniaxial loading (n=3) was applied to the tibialis anterior (TA) region by means of an indenter. The indenter (diameter 3 mm) was curved at its edges to minimize high stresses. An indentation of 4.5 mm was applied slowly, at a rate of 1.5 mm/s, to avoid impact damage, and after 2 hours the indenter was removed. These experiments are referred to as indenter-experiments.

2. Ischaemic loading (n=3) was applied to the TA by an inflatable tourniquet which was positioned above the knee of the animal. The tourniquet was inflated instantaneously up to 140 kPa and after 2 hours the pressure was released. These experiments were performed using the above described loading device without the indenter, and are referred to as tourniquet-experiments.

5.2.4 MR measurements

Two different MR measurements were used for both loading protocols. Each series of measurements will be discussed separately.

T2-measurements

Changes in the transverse relaxation time T2 are generally accepted as a measure of tissue damage [45]. To obtain T2-maps of the lower limb a multi-echo spin echo sequence was used. Signal intensities of successive echoes were fitted, on a pixel-to-pixel basis, to the equation

$$SI = A + B \exp (-t/T2) \tag{5.1}$$

to determine T2 values. Imaging parameters were: slice thickness = 1 mm, field of view (FOV) = 25x25 mm^2, matrix size = 128x128 pixels, number of signal averages (NSA) = 2, echo time (TE) = 12 - 48 ms, number of echoes = 4, repetition time (TR) = 4.5 s. Number of slices = 41, in the case of the indenter-experiment centred on the longitudinal axis of the indenter.

In the indenter-experiment a T2-weighted spin echo sequence was also used to collect 31 slices in the sagittal direction. These measurements were performed to determine the angle of indentation relative to the TA. Imaging parameters were: slice thickness = 1mm, FOV 60x30 mm^2, matrix size 128 x 128 pixels, NSA = 2, TE= 25 ms, TR = 4s.

Contrast-enhanced MRI

There are basically two methods for obtaining information on tissue perfusion using MRI. The first uses an injection of an exogenous tracer or contrast agent, while in the second method endogenous water protons are used as tracers in the arterial compartment. The former contrast-enhanced MRI has the advantage of a high signal-to-

noise ratio, and is therefore suitable for the estimation of perfusion status in resting muscle with a good spatial resolution [84].

Based on a previous procedure [84], a T1-weighted gradient spoiled gradient echo multi slice sequence was used to obtain a perfusion index (PI) map in three selected transverse 1-mm thick slices. For the indenter-experiment, one slice was selected at the height of the indenter, the other two slices selected 3 mm distal and proximal to the indenter position, respectively. For the tourniquet-experiment, slices were selected at equivalent positions through the TA. After 20 baseline image acquisitions a bolus of Gd-DTPA, Magnevist (Schering AG Berlin, Germany), at a dose of 0.2 mmol/kg was administered via a catheter in the jugular vein. Imaging acquisition was continued for 6.5 minutes with a time resolution of 5 seconds/slice. Imaging parameters were: slice thickness = 1 mm, FOV = 25x25 mm^2, matrix size 64x64 pixels, NSA=2, TE = 2.5ms, TR = 35 ms.

Different methods have been described to determine a perfusion index (PI) from the signal enhancement after injection of a contrast agent, including maximal signal intensity, upslope of the bolus, mean transit time and integrated curve area [84, 102, 103]. It has recently been shown that the relative signal intensity difference (ΔSI_{rel}) with respect to a reference signal at the same location is a valid measure for perfusion status [102]. This method is less sensitive to noise compared to, for example, the upslope of the curve, and was therefore used in the present study. ΔSI_{rel} was defined by

$$\Delta SI_{rel} = \frac{SI_{max} - SI_0}{SI_0} * 100\% = PI, \qquad (5.2)$$

SI_0 represents the averaged value of 10 baseline values, measured before the injection of the contrast agent, and SI_{max} is the average value of 10 measurements at maximal signal increase. A typical pattern of signal intensity before and after the injection of the contrast agent is shown in figure 5.1, which also indicates estimated values of SI_0 and SI_{max}. This method was used on a pixel-by-pixel basis to determine a PI-map.

The temporal resolution of sequential PI measurements is in the range of 60 minutes because of the relatively slow clearance of the contrast agent [84]. In the present study, successive PI measurements were separated by approximately 90 minutes. Pilot studies showed that T2-measurements were not affected by the contrast agent when conducted at least 30 minutes after the injection.

5.2.5 MR data analysis

To obtain an enhanced contrast to noise ratio (CNR) between normal and damaged tissues based on differences in T2, the individual images of the multi-echo sequence were summed. The resulting images are referred to as T2-weighted-sum (T2ws) images. For quantification of the changes in T2 values in the indenter-experiments, three regions-of-interest (ROI) were selected. These are indicated in figure 5.2, which

shows a transverse slice of the lower limb. ROI 1 was chosen within the compressed area, as determined from the T2ws images taken during loading. ROI 2 was selected outside the compressed region, but inside the region with hypo-perfusion, as determined from the corresponding PI map during indentation, and ROI 3 served as a control region (figure 5.2). Each ROI incorporated approximately 60 pixels.
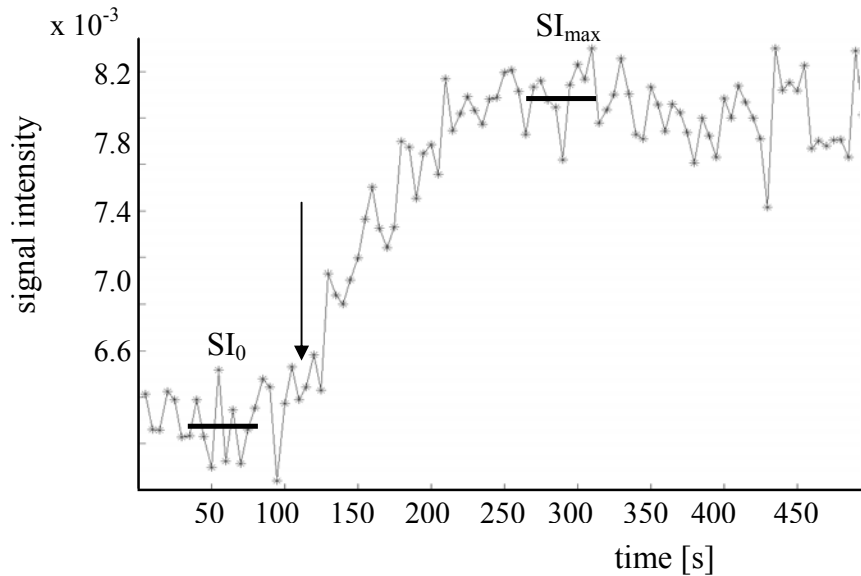
Figure 5.1 *Time-course of signal intensity in region of TA before and after injection of Gd-DTPA. The arrow indicates time point of the Gd-DTPA injection. SI_0 and SI_{max} represent values before injection and at maximal signal intensity.*

During the indenter-experiments, ROI 1 was compressed, and thus T2 values could only be estimated in both ROI 2 and 3. In the tourniquet experiments T2 values were estimated in ROI 1, to enable comparison between the effects of both loading protocols in the same region. For each experiment, T2 values were normalized to the pre-loading value. This normalization was used since the measured T2 is sensitive to the position in the RF coil and precise MR settings, which were slightly different for each experiment, and to minimize inter-animal variations. Values were presented as mean ± standard error (SE). Statistical differences were examined using a two-tailed unpaired Student's t-test, with a significance level of 5%.
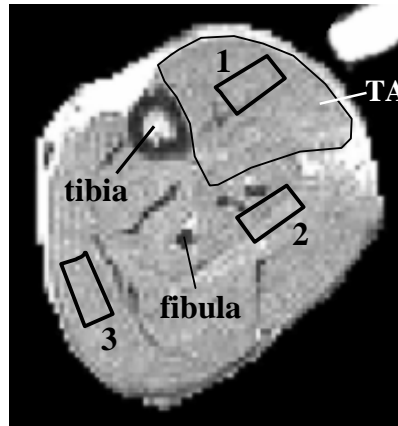
Figure 5.2 *Regions of interest outlined on a T2ws image for calculation of T2 values: 1) ROI 1, compressed area during loading, 2) ROI 2, ouside the compressed region, but inside the region with hypo-perfusion, as determined from the corresponding PI map during indentation, and 3) ROI 3, control region. TA is indicated by black line.*

5.2.6 Experimental protocol

The experimental protocol involved several distinct phases. The preparation phase consisted of sedation of the animal, insertion of catheter in jugular vein, casting, and fixation of the animal in the set-up. This phase took approximately 60 minutes. The following phases included MR-measurements, for which the time schedules are depicted for both loading protocols in figure 5.3. The first injection was given to measure the perfusion index map before loading (PI_P) and 30 minutes after the injection a T2-map ($T2_P$) was measured. Following these pre-loading measurements, the load was applied for 2 hours (shaded area in figure 5.3), during which a PI-map and T2-maps were measured as indicated. A sagittal image was recorded in the indenter-experiment to determine the direction of indentation. Immediately following unloading, a PI-map (PI_1) was measured followed by a series of T2-measurements ($T2_{1-5}$). In the tourniquet-experiment an extra perfusion measurement (PI_2) was performed to confirm the restoration of normal blood flow. In the final phase, 4 hours after load removal, the animal was sacrificed for histological examination (H).

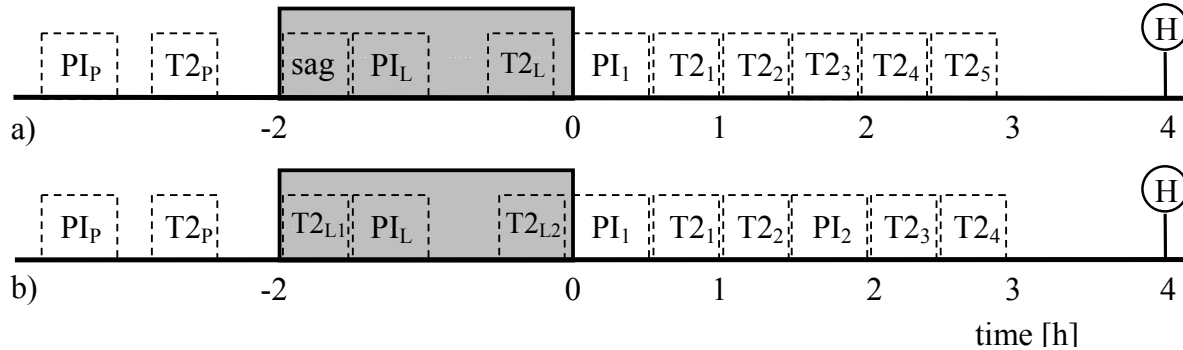Figure 5.3 *Measurement protocol for a) indenter-experiment and b) tourniquet-experiment. Shaded rectangle represents loading period for indenter or tourniquet application. Meaning of symbols: PI: perfusion index map, T2: T2-map, H: histological analysis, sag: sagittal T2-weighted images, subscript P: pre loading, L: during loading, 1-5: number of measurement after unloading, t=0 is defined as the moment of unloading.*

5.2.7 Histological analysis

Immediately following the MR measurements, the sacrificed animal was perfusion fixated with 4% buffered formalin. The lower limbs were cut off and stored in formalin. Both TAs were excised, at least two weeks later, to ensure complete tissue fixation. The unloaded muscle was used for control samples. The mid portion of the muscle was dehydrated in a series of alcohol solutions and embedded in plastic (Technovit 7100, Kulzer). The muscle was cut in 5 μm thick transversal slices and individual samples were stained with toluidine blue.

5.3 Results

5.3.1 MRI

Figure 5.4 shows the perfusion index (PI) maps (a-c), determined from the relative signal increase after Gd-DTPA injection, and the T2ws images (d-f), determined from the multi-echo sequence, for a typical indenter-experiment measured before and during indenter application and after its release. Figure 5.4a shows a normal pre-loading PI-map that is indicative of a homogeneous perfusion index. The PI-map taken during loading (PI_L) showed a large region with low PI values, while after unloading the PI values (PI_1) were high in this region. If the scale of figure 5.4c1 is expanded twofold, it is evident that the highest PI values were found in the previously compressed region (figure 5.4c2).

Figure 5.4 *Perfusion index (PI) maps (a-c) and T2-weighted-sum images (d-f) of the lower limb for a typical indenter-experiment. Top row illustrates PI maps a) before and b) during indentation, and c) 5 minutes after indenter release. The PI-map in figure c1) is shown with the same colour scale as in figure a) and b). For improved visualization of the distribution of PI in the TA, figure c2) illustrates the PI map of c1) with enlarged scale. Bottom row shows T2ws images d) before and d) during loading, and f) 40 min after unloading. TA is indicated in figure d) by the black line.*

T2ws-images measured during loading ($T2_L$) showed some signal increase in the region near the indenter (figure 5.4e). A much more pronounced increase in signal intensity, however, was observed after indenter release ($T2_1$), in an area extending from skin to the tibia bone (figure 5.4f). It should be noted that this region with high signal intensities was located at approximately the same position as the region with high PI-values, as shown in figure 5.4c2.

Figure 5.5 shows PI-maps measured during indentation in three slices through the lower limb. The positions of the slices relative to the indenter are indicated in the sagittal image on the left. The PI-maps measured in the slices underneath (figure 5.5b) and distal to the indenter (figure 5.5c) showed low PI values in the TA region, while the PI-map proximal to the indenter showed no evidence for hypo-perfusion. In the TA region the PI values were even slightly increased.
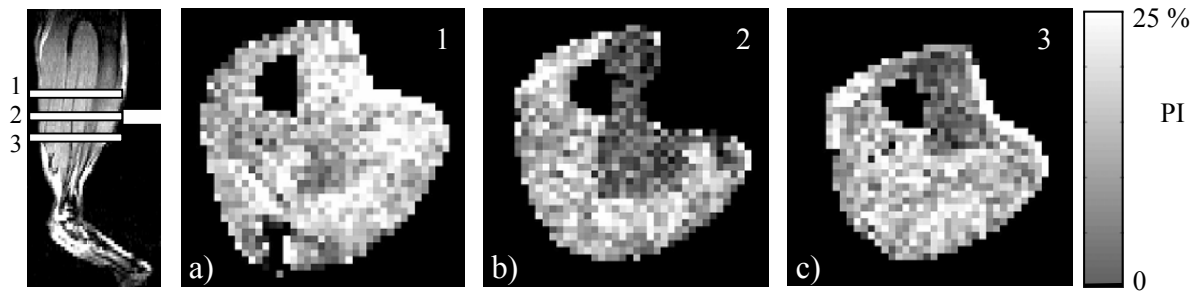
Figure 5.5 *PI maps measured during indentation in three slices of lower limb: a) 3 mm proximal to the indenter position (slice 1), b) underneath the indenter (slice 2), and c) 3 mm distal to indenter position (slice3).*

The PI-maps and T2ws images for a typical tourniquet-experiment are shown in figure 5.6. It is evident that during inflation of the tourniquet (PI_L), the perfusion was strongly reduced in the lower limb. After 2 hours the tourniquet was deflated, which initially led to high PI values in the leg (PI_1) associated with a reactive hyperaemia response. These PI values were restored to normal within 90 minutes (PI_2). T2ws-images taken during inflation ($T2_L$) showed some global increase in signal intensity, but these values returned to preloaded-values within 2 hours.
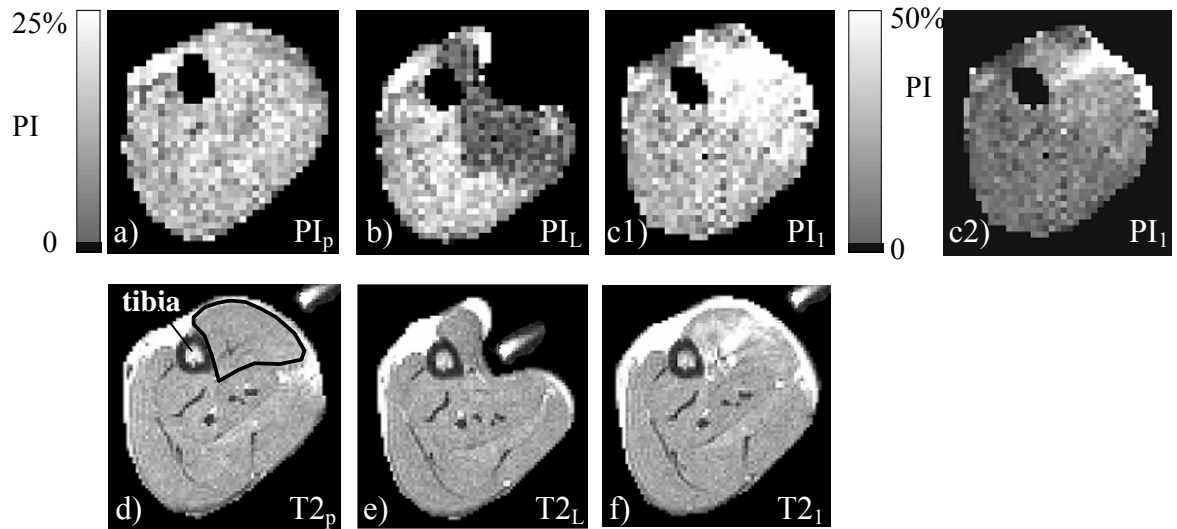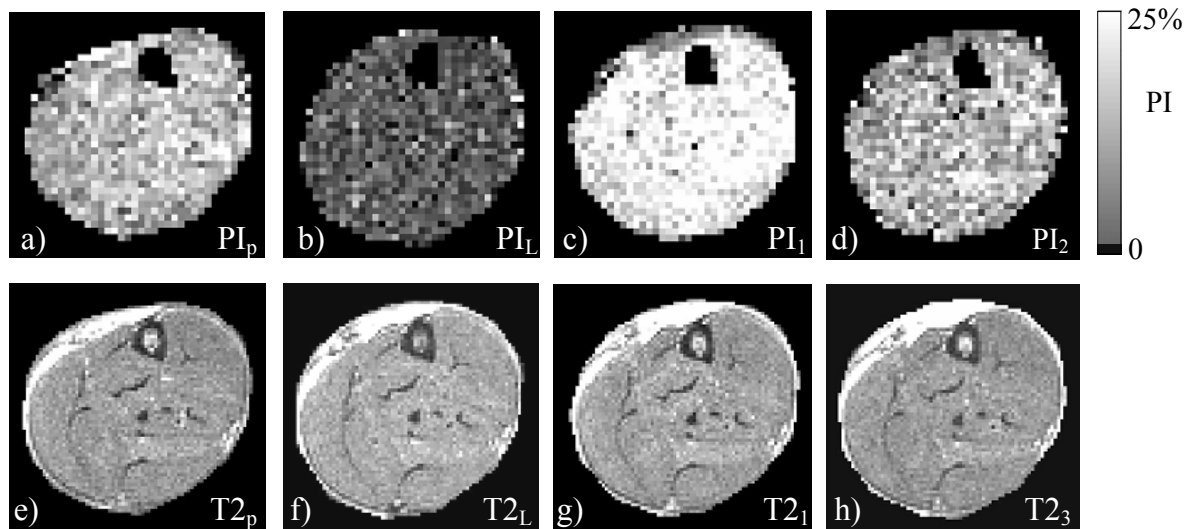

Figure 5.6 *Perfusion index (PI) maps (a-d) and T2-weighted-sum images (e-h) of lower limb for a typical tourniquet-experiment. Top row shows PI maps a) before and b) during application of tourniquet and c) 5 minutes and d) 90 minutes after deflation of tourniquet. Bottom row shows T2ws images measured e) before and f) during tourniquet and g) 40 and h) 115 min after deflation of tourniquet.*

Figure 5.7 illustrates the normalized T2 values determined from the indenter-experiments (open symbols) and tourniquet-experiments (closed symbols). Mean T2 value measured in the TA region before loading was 21.4 ± 0.3 ms (n=6). In the indenter experiments, T2 values during loading could only be calculated in ROI 2 and 3. It was noted that there was a small shift of tissue in ROI 2 during indentation. T2 values were significantly increased in the compressed area (ROI 1) after unloading ($p < 0.001$). In ROI 2 the T2 values were significantly increased ($p < 0.05$) during the ischaemic period, but were restored to pre-loading values within 40 minutes after unloading. There were no significant changes in T2 values in ROI 3 throughout the indenter experiments. T2-values in the tourniquet-experiments (ROI 1) showed a small decrease after 20 minutes of ischaemia, but a significant increase ($p < 0.05$) after 95 minutes of ischaemia. T2-values were restored to pre-loading values within 40 minutes after deflation of the tourniquet.
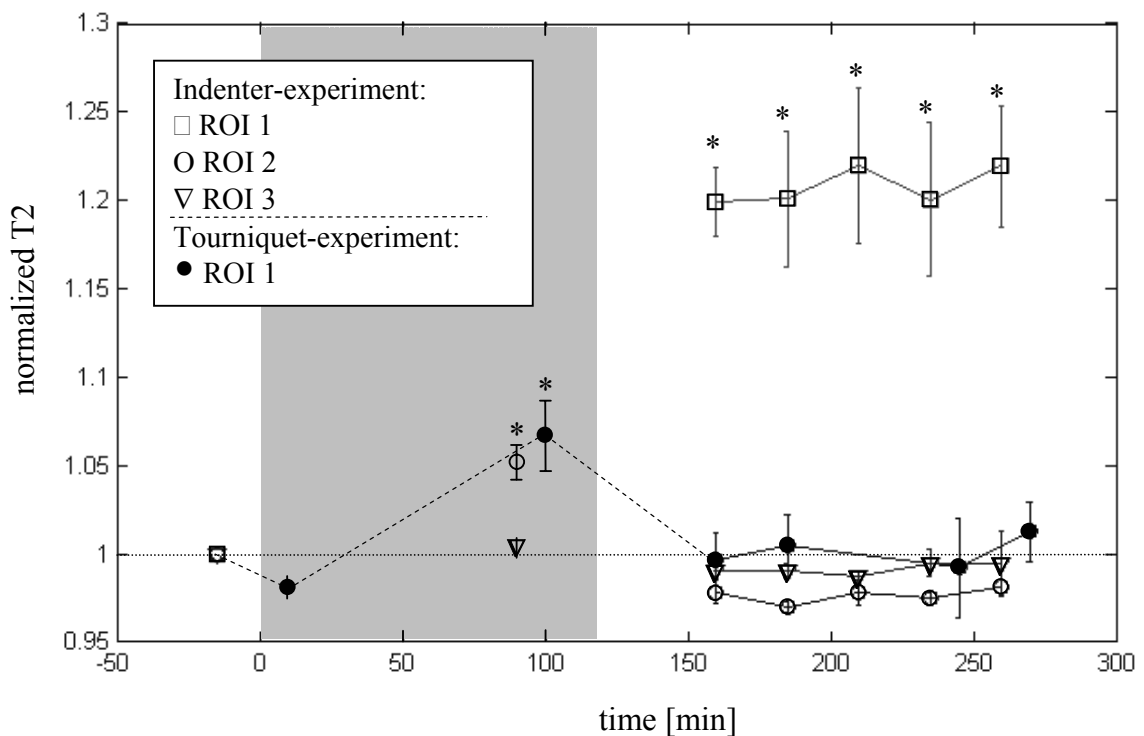
Figure 5.7 *Time course of normalized T2 values before and during loading and after unloading for indenter (open symbols) and tourniquet (closed symbols) experiments. Loading period is indicated by shaded rectangle. ROIs are indicated in figure 5.2. During indenter application, no values could be calculated in ROI 1, due to compression of the tissue. Trends are indicated by dashed lines. Values are presented as mean $\pm$ SE (n=3). * denotes statistical significance ($p < 0.05$) relative to initial value.*

5.3.2 Histological findings

Figure 5.8 shows transversal histological slices of muscle tissue from the TA (ROI 1) from both indenter and tourniquet experiments. Figure 5.8a shows a control slice, in which the normal rectangular shape of muscle fibres with small interstitial spaces is visible. Slices of the compressed muscle tissue showed large necrotic regions. Figure 5.8b shows necrotic fibres with disorganization of the internal structure. Slices of muscle tissue from the tourniquet experiments showed some regions with increased interstitial space and somewhat rounder shaped fibres (figure 5.8c), although the major part of the TA had a normal histological appearance. No necrotic fibres were found.
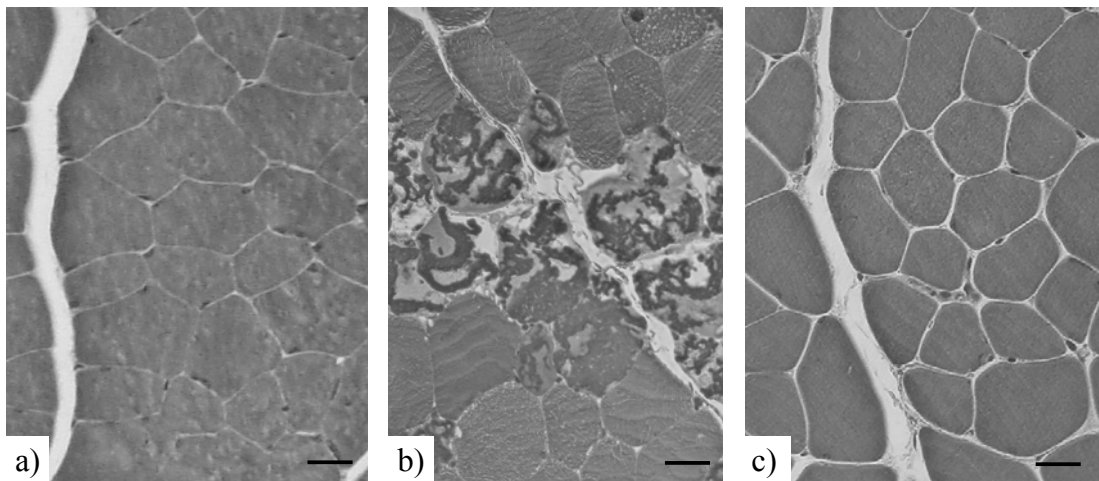
Figure 5.8 *Transversal histological slices of TA stained with toluidine blue. a) Control, b) indenter-experiment: 2 hours of compression followed by 4 hours of reperfusion, and c) tourniquet-experiment: 2 hours ischaemia followed by 4 hours of reperfusion. Bar represents 50 μm.*

5.4 Discussion

Ischaemia and deformation are both factors that play a role in deep tissue injury following compressive loading. In the present study, two loading protocols, designed to distinguish between these two factors, were applied to the lower limb of Brown Norway rats. An inflatable tourniquet positioned above the knee of the animal was applied for ischaemic loading, while uniaxial loading was applied to the TA region by means of an indenter to study the combined effect of ischaemia and deformation. Both protocols were applied for 2 hours. Spatial as well as temporal information on the tissue perfusion was obtained by using contrast-enhanced MRI. Changes in tissue properties, both during and after loading, were measured with T2-weighted MRI. Both MR-measurements were performed consecutively for up to 6 hours in both loading experiments (figure 5.3).

The method of using contrast-enhanced MRI to measure the perfusion status in resting muscle was first reported by Luo et al [84]. The method is based on the fact that following an intravenous injection of a bolus of Gd-DTPA, the initial accumulation and distribution of the agent in tissues is largely dependent on tissue perfusion. The previous study showed that the maximum uptake rate of the contrast agent provided a valid parametric measure for tissue perfusion. Furthermore, it was demonstrated that this MRI-based perfusion index correlated well with radionuclide-labeled microsphere blood flow measurements [84]. In the present study the relative signal intensity difference was used, since this method is less sensitive to noise. The obtained signal-to-noise (SNR) ratio in the present study was lower compared to the study of Luo et al. [84], which was a direct result of the decrease in selected slice thickness, from 3mm to 1mm in this study. Although this method does not estimate a quantitative perfusion value [103], it provides sufficient spatial resolution to distinguish regions with normal perfusion, hypo-perfusion and reactive hyperaemia. The temporal resolution was limited to 90 minutes, due to the relatively slow clearance of the contrast agent, but was sufficient to measure a relative perfusion index before, during and after loading.

The PI-map taken during loading (PI_L) showed an extensive region with low PI values. This clearly indicates hypo-perfusion, probably due to the fact that a large vessel, adjacent to the tibia bone, was blocked by the compression. This finding was observed in all three experiments. In the compressed region, in association with the high T2 values, very high PI values were found after unloading (figure 5.4c). It is suggested that these high PI values are a combined result of a reactive hyperaemic response and a possible leakage of the contrast agent into the damaged region, since capillaries were likely damaged. This proposal might be further examined by administration of Evans Blue Dye, which is a widely used method to study blood vessel and cellular membrane permeability [104].

A marked difference was found in the effect on T2 after 2 hours of compression versus pure ischaemia. In the indenter-experiments, T2 values in the compressed region were significantly increased after unloading (figure 5.7). Increased T2-values after compression were correlated to necrotic regions and regions with different stages of muscle fibre damage, as shown by histology examination. The histological appearance of damaged muscle tissue after compression is extensively described in chapter 4. Ischaemic loading led to a small initial decrease followed by a significant increase in T2 during loading (figure 5.7). After deflation of the tourniquet, the T2 values returned to normal within 40 minutes. An initial decrease in MR signal intensity after occlusion of blood flow has previously been reported [105], but was mainly found in T2* values, and was associated with the blood oxygen level dependent (BOLD) effect. In addition to the effects of molecular interactions, T2* values include the effect of inhomogeneities in the magnetic field. Although the multi echo sequence measures T2, the BOLD effect could also be responsible for the observed T2 decrease, since deoxygenation leads to a decrease of both T2 and T2*. The observed increase in T2 after 90 minutes of ischaemia can be explained by osmotic shifts of water caused by an

accumulation of waste products of anaerobic metabolism. Indeed, it was shown in a human study by Ostman et al. [106] that 90 minutes of ischaemia leads to an accumulation of lactate. These increased lactate levels indicated accumulation of products of anaerobic metabolism, which was initiated by severe hypoxia caused by tourniquet inflation. An associated decrease in intracellular pH after occlusion of blood flow has been shown by several studies [107, 108]. Appell et al. [109] demonstrated that relatively short periods (15 to 90 minutes) of ischaemia, without reperfusion, already cause pathological alterations, particularly affecting metabolically important organelles. The T2 values that were increased during ischaemic loading returned to pre-loading values within 40 minutes after deflation of the tourniquet, indicating a rapid restoration of the normal water balance.

In previous experiments (chapter 4) it was shown that in slices 3 mm distal to the indenter, a different T2 response was observed, compared to slices 3 mm proximal to the indenter. The observed difference was proposed to be caused by differences in perfusion status during loading. An example of these measurements is shown in figure 5.9, which depicts T2ws images collected before and during loading, and 15 and 65 minutes after unloading. The figure clearly demonstrates that in the slice proximal to the indenter, the area with increased T2 is comparatively small 15 minutes after loading, but increases thereafter (figure 5.9c and d). Conversely, in the slice distal to the indenter, immediately after unloading a large area is visible with increased T2 values, which decreases thereafter (figure 5.9g and h). The PI measurements at 3 mm distance from the indenter in the present study demonstrated a hypo-perfusion region distal to the indenter, although no such region was evident proximal to the indenter. This indeed suggests that the observed differences can be explained in terms of their relative status of perfusion

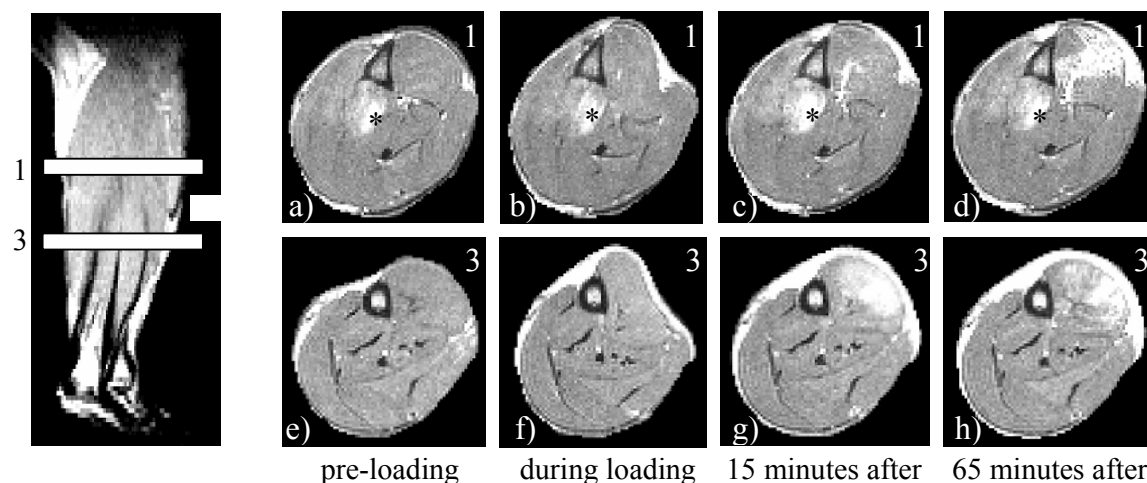pre-loading   during loading   15 minutes after   65 minutes after

Figure 5.9 *Slices 3 mm proximal (top row, a-d) and distal (bottom row, e-h) to indenter position before and during indentation, and 15 and 65 minutes after its release. * indicates wrap around artefact (backfolding).*

The combined effect of compression and ischaemia on muscle tissue has previously been studied by examining tissue both beneath and distal to a tourniquet [110, 111]. These studies were performed to define "safe" durations of tourniquet application in surgery of the extremities. A specially designed curved tourniquet was applied to the hindlimb of a rabbit, and was used to produce a uniform distribution of tissue pressure upon cuff inflation. It was found that histological abnormalities were more severe in compressed thigh muscles than in ischaemic leg muscles. In the compressed muscles, considerable intra-individual and inter-individual variability in damage was noted. This might be explained by the present hypothesis concerning the importance of local deformation. Two hours of distal ischaemia induced minor histological abnormalities, which was also observed in the present study.

Compared to other tissues, like cardiac and cerebral tissues, resting skeletal muscle has been described to be relatively resistant to ischaemia because the maintenance of its metabolic capacity is assumed to cease only after five to seven hours [112, 113]. It is, however, known that the rate of metabolic processes is increased if e.g. twitch stimulation is imposed during ischaemia and reperfusion [114]. This increases the rate of energy depletion and, accelerates the damage processes associated. If instead large deformations are imposed during ischaemia and there is already muscle damage by the large strains on the fibres, then the metabolic demand might also be raised. Accordingly, 2 hours, as applied in the present study, might be sufficient to cause metabolic stress, which will have an aggravating effect.

Based on the recovery of T2-values to pre-loading values following deflation of the tourniquet, no damaging effect of reperfusion was observed after the 2 hours ischaemic period. In the indenter-experiment, the effect of reperfusion was more difficult to determine. It can, however, be predicted that, if initial damage is initiated during loading of the muscle tissue, the reperfusion phase might cause additional damage.

In summary, the present study demonstrated that compressive loading for 2 hours led to irreversible damage to the muscle tissue, while ischaemic loading resulted in reversible tissue changes. This implies that large deformation, superimposed on the ischaemia, provided the main trigger for irreversible muscle damage.

Acknowledgements

70

Chapter 6

Correlating local strain fields to damage location in a model of deep tissue injury

6. 1 Introduction

Pressure ulcers can arise when a prolonged mechanical load is applied to soft biological tissues, for example when subjects are bedridden or wheelchair bound for a prolonged period. Pressure ulcers may also occur in situations where orthoses and prostheses are used to support soft tissues. It is known that muscle tissue is more sensitive to mechanical loading than skin [100], and that damage often starts near bony prominences. In addition, muscle tissue degeneration starts at the cellular level [21, 29, 100]. The clinical measures to prevent deep pressure ulcers, which initiate within deeper tissues, are often unsuccessful, leading to a variable prognosis. This is due, in part, to the difficulty in assessing initial pathological changes in the deep tissues.

It is clear that for the successful prevention and treatment of deep pressure ulcers it is necessary to gain an improved knowledge of the events associated with their aetiology. A more complete understanding of the relationship between load and location and severity of tissue damage needs to be established. This will provide design criteria for optimal pressure relief strategies and may lead to measures that can enhance both tissue resistance and repair.

An animal model was developed [28, 93] in which an indenter is applied to the tibialis anterior of Brown Norway rats to study the effect of compressive loading on muscle tissue. In previous experiments, as described in chapter 3 and 4, the ability of T2-weighted MRI was demonstrated for measuring tissue status *in vivo* during and after loading, with a suitable temporal and spatial resolution. Experiments in chapter 5 showed a large region with hypo-perfusion during loading, but only a small localised region with increased T2-values in the subsequent unloaded phase. The location of the damage suggested an influence of deformation in its initiation. From both human observations and cell model studies it has become clear that cells are very sensitive to deformation but relatively resistant to high hydrostatic pressure [28]. Various studies examing the effects of stretching muscles [96, 98, 99] have shown the importance of strain on muscle fibres as an initial damage mechanism. Therefore in the present study the correlation between location of damage and local strain fields was studied.

To determine the local strain fields in the tissue during external loading two approaches can be used. The first involves MR tagging, which is a non-invasive technique for measuring three-dimensional motion and deformation, mostly used in the field of cardiac biomechanics [115]. Tags represent regions of tissue whose longitudinal magnetisation has been altered before imaging, so that for approximately 1 sec they temporary appear dark in subsequent magnetic resonance images. The tags move with the underlying tissue and serve as easily identifiable landmarks within the tissue. From the displacements of tag lines due to indentation, local tissue deformation and related strain distributions can be calculated. The developed MR-compatible loading device, as described in chapter 3, offers the possibility to perform MR tagging experiments in the same model as was used to determine the location of damage after compressive

loading. The tagging experiments, however, require separate repetitive indenter applications in a rapid manner. This protocol per se causes damage and swelling to the tissues. Therefore, these tagging studies could not be incorporated in the experiments in which damage is measured during and after a 2 hr loading period (chapter 3, 4, 5), which involved the indenter to be applied slowly to prevent impact damage. The alternative approach is to develop a dedicated finite element (FE) model. Such a model can be used to calculate local strain fields during loading, for each individual experiment. The MR tagging experiments can be used to validate these calculated strain fields. Subsequently, the locations of high strain, as calculated by the FE model, can be correlated to locations of damage obtained from T2-weighted MR images.

The present chapter describes both approaches: the MR tagging experiments and the first steps towards the development of the dedicated FE model. The former served two purposes:
1. Tagging experiments with a small indentation, approximately 2.2 mm, were used to validate the strain fields obtained in the numerical simulation with the strain fields calculated from the tagging data. These indentation values were chosen to match with the current 'capacity' of the finite element simulation.
2. Tagging experiments with a large indentation, approximately 4.3 mm, were used to globally compare location of damage, measured by T2-weighted MRI, to local strain fields determined from the tagging data. This comparison was made with experiments using different animals.

6.2 Material and methods

6.2.1 Animal model

The same animal model (n=4) was used as in previous experiments, described in chapters 3.2.1, 4.2.1 and 5.2.1. The experimental protocol was approved by the Animal Care Committee of the University of Maastricht.

6.2.2 MR-compatible loading device

The MR-compatible loading device has been described in chapters 3.2.2, 4.2.2 and 5.2.2. For the tagging experiments the indenter had to be applied in a controlled, repetitive and rapid manner. Therefore, a motor (Maxon DC motor 135700, USA) was coupled to the cam (position of cam is depicted in figure 3.1) by a polycarbonate rod at least 2 metres long. This was used to rotate the cam that applied the indenter. The motor had to be positioned at a large distance from the magnet because of interference with the high magnetic fields of the MRI scanner. A photograph of the experimental arrangement is shown in figure 6.1.
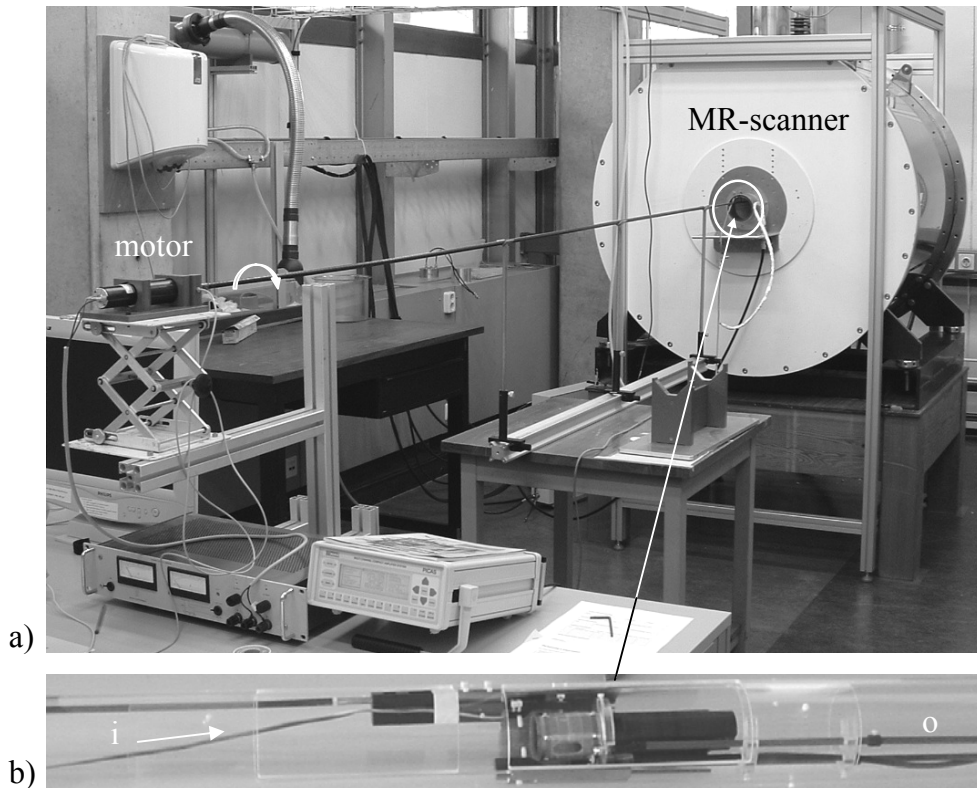
Figure 6.1 *Photograph of experimental arrangement. a) Set-up for tagging experiment. An extended bar was used to rotate the cam, which applied the indenter to the TA region of the rat. b) MR-compatible loading device consisting of two tubes; the inner tube (i) housing the animal, the larger outer tube (o) to locate arrangement in MR scanner.*

6.2.3 Experimental protocol

Initially transversal scout images (TR = 3s, TE = 25ms, slice thickness = 1mm, FOV=30x30 mm^2, 64x64 pixels) were recorded and, where necessary, adjustments were made to ensure a prescribed position and angle of the indenter on the TA (TA compressed between indenter and tibia, indentation perpendicular to limb). Seven transversal slices were selected centered on the position of the indenter. Tag lines were applied in the two orthogonal directions, with two C-SPAMM acquisitions [116] for each direction, with a phase difference of 180° (requiring 4 measurements per slice). Thus, the indenter was applied 28 times in total to obtain all images. The entire experiment, including preparation phase and positioning of the indenter, took approximately 3 hours. Custom software written in LabVIEW (National Instruments, USA) was used to apply the indenter in a controlled and repetitive manner. The motor rotated the bar with a constant frequency of 0.25 Hz. The recorded force signal and the corresponding positions of the cam, for one rotation, are shown in figure 6.2. The high-

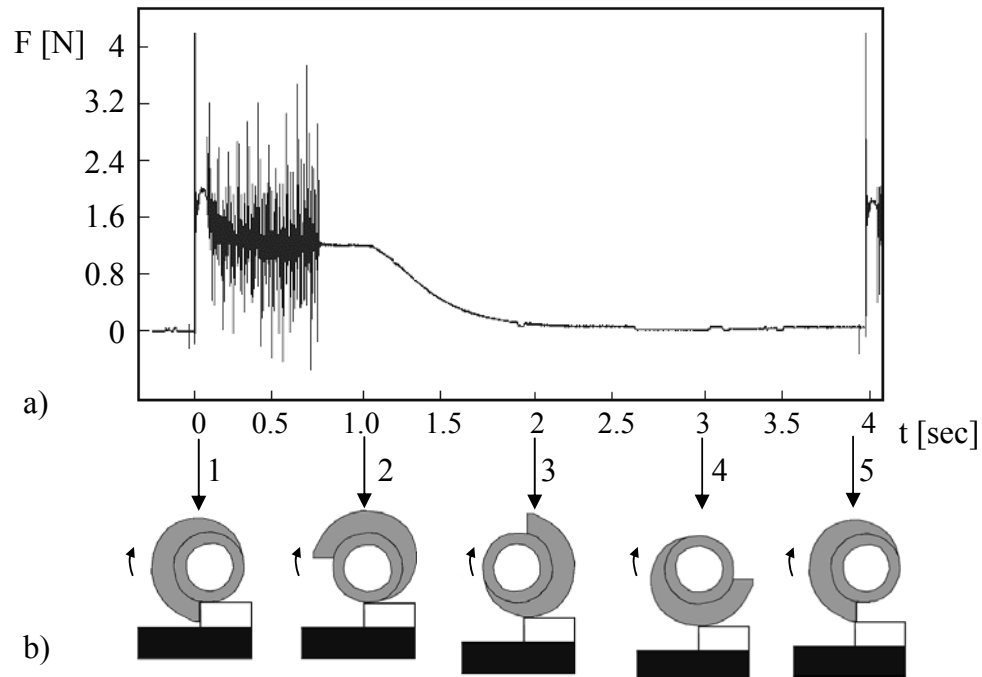frequency fluctuations in period 1-2 were caused by MR-measurements (due to switching gradient fields).

Figure 6.2 *a) Force signal measured by strain gauges and b) representative positions of the cam, which was rotated by the motor. 1) Moment of indenter application, 2) start of gradual unloading of indenter, 3) partially unloaded, 4) indenter fully unloaded and 5) moment just before indenter application. High-frequency fluctuations during period 1-2 were caused by MR-measurements due to switching gradient fields.*

The force signal was used to verify the timing of the experiment as indicated in figure 6.3. By using a metal sensor and a screw attached to the bar, a trigger was given to the MRI scanner once every cycle. This pulse, arrow 1 in figure 6.3, was used to start the MR protocol. At a pre-determined period after this pulse the tagging grid was applied to the tissue (arrow 2), after which the indenter was applied defined at time zero (arrow 3). Subsequently, the deformed tagging grid was measured within 0.8 seconds, after which the indenter was gradually unloaded by means of the rotating cam. This protocol was repeated four times to obtain the required data for one slice.

6.2.4 Loading protocols

Two loading protocols were used. A small indentation of 2.2 mm was applied (n=2) to allow a comparison to the numerical model, and a large indentation of 4.3 mm was used (n=2) to allow a comparison with damage locations obtained with T2-weighted MR imaging in separate experiments.
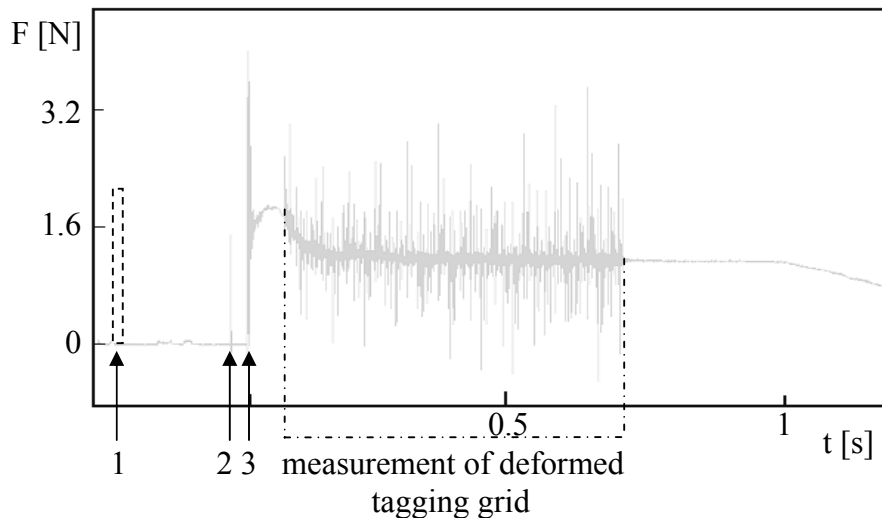
1. signal from axis
2. application of tagging grid
3. application of indenter

Figure 6.3 *Time schedule for one tagging measurement. Signal from strain gauges, indicated by grey line, was used to verify the timing of the pulses and measurements.*

6.2.5 Imaging protocol

Tagged transversal images were taken before and immediately after applying the indenter. This made it possible to use the tagging grid lines deformation to determine both the tissue displacement and associated deformation. To determine displacement during indentation in one direction, a 1D tagging grid was applied perpendicular to that direction by using complementary spatial modulation of magnetisation (C-SPAMM) [116]. From pilot experiments it was estimated that a minimum line spacing of 3.3 mm should be used for displacements in the transverse direction in order to distinguish the lines in a deformed state. The tagging grid was applied with a Gaussian RF-pulse of 200 µs with a flip angle of 45°, a gradient strength of 30 mT/m and an effective gradient duration of 150 µs. This resulted in a grid line spacing of 14 pixels or 3.3 mm. A gradient-spoiled fast field echo sequence was used to image the tagging grid, with TR = 10 ms, TE = 2.5 ms, and a flip angle of 30°. Slices were 1 mm thick and had a field of view of 30x30 mm^2. The matrix consisted of 128x64 points and was zero-filled to 128x128 points. The read-out direction was chosen orthogonal to the tagging direction. In that case the frequency peaks, in which the displacement information is stored, are contained in the central k-space lines, where the signal is maximal. Centric k-space sampling was used to minimize signal attenuation by T1 relaxation.

6.2.6 Deformation

The type of mechanical damage and hence the definition of mechanical parameters, which is best related to tissue damage still remains uncertain. However, there is evidence that cells are very sensitive to deformation [29]. The maximum shear strain in the material is a good measure of the deformation and has the advantage that it can be directly determined from MRI tagging data. Therefore, this parameter was used in both the validation of the FE model and the correlation to damage location. The validation was performed in the 2D slice underneath the indenter. It was assumed that strain was only evident in planes parallel and perpendicular to the slice, with no associated shear strains in the third direction.

6.2.7 Processing of the MR tagging data

The applied method for quantification of the tag displacements was the HARmonic Phase (HARP) analysis, based on the method described by Osman et al. [117]. First the two images of the SPAMM acquisitions were subtracted from each other to increase signal to noise ratio and, at the same time, remove the dc intensity offset. The resulting C-SPAMM image was subjected to 2D Fourier transformation and the resulting k-space data was multiplied by a band pass filter to isolate the C-SPAMM convoluted image information. The bandwidth of the filter was set to 19 pixels in k-space. After an inverse Fourier transformation of the filtered data, HARP images were obtained by calculation of the phase in each pixel. Finally, phase unwrapping was used, in which the phase on a line of pixels was accumulated so that all pixels acquired a unique phase. This procedure was repeated with the tag lines applied in the other direction, such that all image pixels had a unique phase in both directions, which enabled the tracking of these points in 2D space.

From the displacement fields the Green-Lagrange strains were estimated using the gradient deformation method proposed by Geers et al. [118]. To review briefly, this method estimates the deformation tensor **F** at a certain point from the displacements of neighbouring points. Nine neighbouring pixels were used for each pixel in the image to calculate **F.** With the deformation tensor in a point known, and **I** the unity tensor, the Green-Lagrange strains followed from

$$\mathbf{E} = \tfrac{1}{2}\,(\mathbf{F}^c \cdot \mathbf{F} - \mathbf{I}). \tag{6.1}$$

The maximum shear strain τ in the 2D slice could be calculated from

$$\tau = \tfrac{1}{2}\,(\lambda_1 - \lambda_2), \tag{6.2}$$

with the principal strains λ_1 and λ_2 representing the eigenvalues of the Green–Lagrange strain tensor. For this it is assumed that in the slice underneath the indenter the strain in the direction perpendicular to the 2D surface is also a principle strain.

6.2.8 Finite element (FE) model

From the transversal MR image underneath the indenter (figure 6.4a), the contours of the leg and tibia bone, as well as the indenter position and angle were detected. Matlab's PDE Tool was used to fill the contour with a 2D triangular mesh (figure 6.4b). The tibial bone was modelled as a hole, while the fibular bone was neglected in the model.
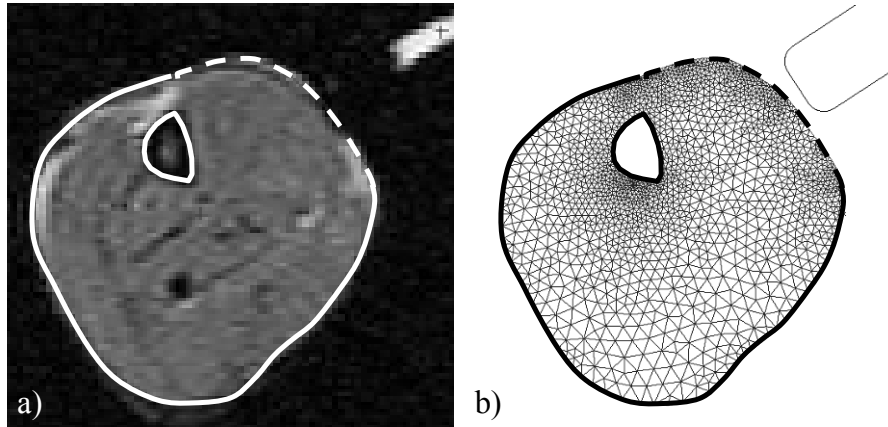

Figure 6.4 *a) Transversal MR image of lower limb underneath the indenter, and b) corresponding mesh. In the computational model, nodes on the solid contour were fixed in all directions and nodes on the dashed contour were free to move.*

This mesh was subsequently converted to an extended quadratic triangular mesh. The numerical code was programmed in the finite element package Sepran [119], and the model was solved with a HSL solver [120]. All soft tissues in the leg were modelled as a single material with incompressible non-linear Neo-Hookean behavior, described by

$$\sigma = -p\mathbf{I} + G\,(\mathbf{B\text{-}I}), \tag{6.3}$$

where σ is the Cauchy stress, G the shear modulus, and $\mathbf{B}$ the Finger tensor, defined as $\mathbf{F\cdot F}^c$, with $\mathbf{F}$ the deformation tensor. In the numerical model of the 2D slice a plane stress situation was chosen. The nodes on the solid contour, as indicated in figure 6.4b, were fixed in all directions to simulate the restrictions applied by the plaster, in which the leg was cast, and the tight fascia, by which the TA is surrounded. Contact between the rigid indenter and the deformable muscle along the dashed contour near the TA region was modelled with frictionless quadratic line contact elements. The Green-Lagrange strains, and associated maximum shear strain τ, were calculated from the deformation tensor for each node as provided by the finite element program. With the assumed plane stress situation, the maximum shear strain could be calculated from the two in-plane principal strains.

6.3 Results

6.3.1 MR Tagging measurements

Tag lines were applied in two directions in the transversal slices. Figure 6.5 shows the images of the slice underneath the indenter before (top row) and during loading (bottom row). The tag directions were approximately perpendicular (figure 6.5b and e) and parallel (figure 6.5c and f) to the indentation direction. The applied indentation in this experiment was 2.2 mm. The contours of the undeformed and deformed leg are indicated by the dashed white lines.
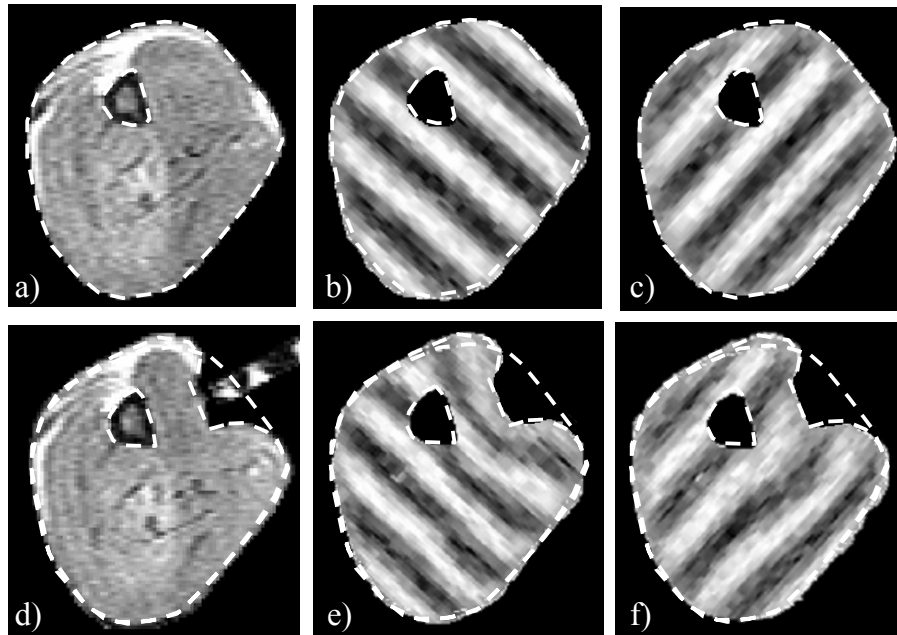
Figure 6.5 *Tagging grid applied in two directions. Top row shows images before application and bottom row after application of the indenter. Anatomical images a) before and d) during loading, and CSPAMM images with tags lines b, e) perpendicular and c, f) parallel to indentation direction. Dashed lines indicate deformed and undeformed contours.*

The indentation and maximum shear strain distributions were calculated from the deformation of the tag lines, and are indicated in figure 6.6b and c, respectively. By plotting the deformed contour on the calculated values for indentation (figure 6.6b) it could be confirmed visually that the indented region calculated from the tagging experiment agreed with the observed indentation. The maximum shear strain distribution (figure 6.6c) showed two regions with high shear strain values. The largest region extended from the skin towards the tibia bone with a peak value of 0.64, and a

small region was found superficially, with a peak value of 0.6. The second experiment showed similar results.
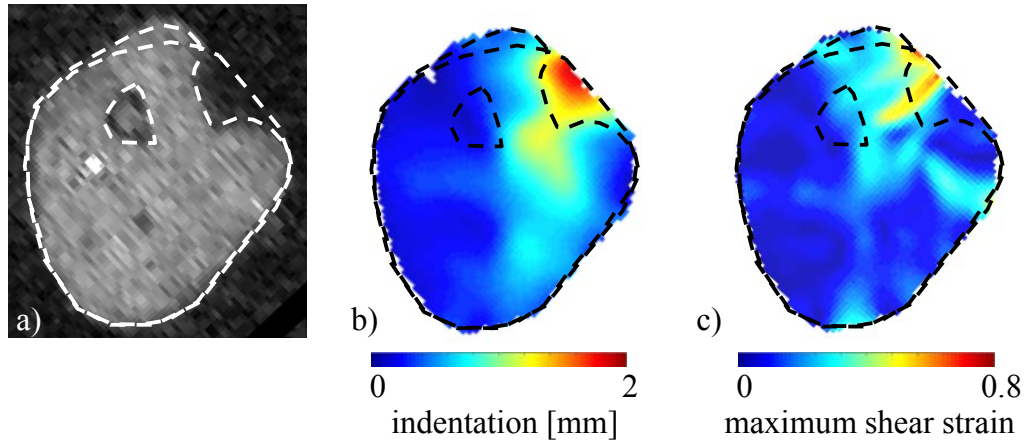
Figure 6.6 Indentation and maximum shear strain calculated from tagging data for experiment with 2.2mm. a) Scout image with dashed lines indicating contours of undeformed and deformed leg, b) indentation calculated from displacement of tag lines, and c) maximum shear strain calculated from Green Lagrange strains.

6.3.2 Numerical simulation

The contours of the leg and bone obtained from the MR image before loading (figure 6.5a) were used to create a 2D mesh. The deformed mesh is shown in figure 6.7a. The dashed black lines indicate the deformed contour calculated by the FE model.
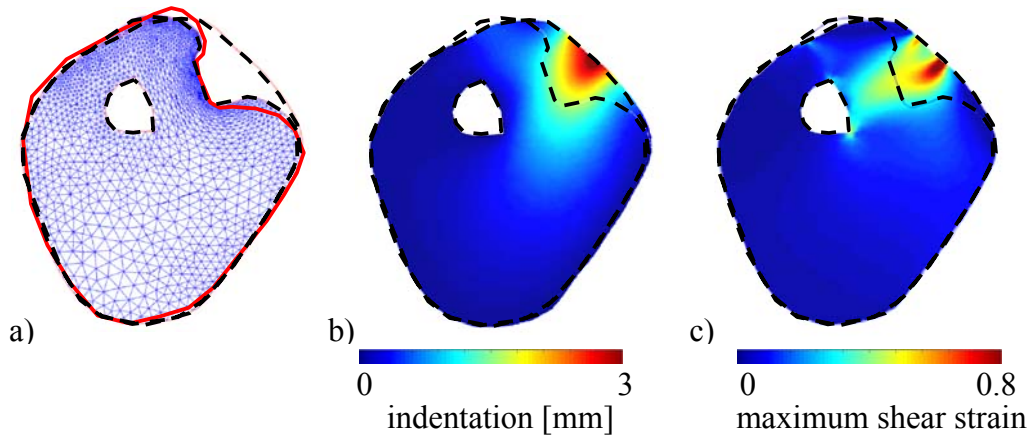
Figure 6.7 Indentation and maximum shear strain calculated with FE model. a) Deformed mesh, b) indentation, and c) maximum shear strain calculated with numerical simulation. Dashed black lines indicate contours calculated by FE model, solid red line in a) reflects contour obtained from MR image taken during loading.

The calculated indentation is shown in figure 6.7b and the distribution of maximum shear strain in figure 6.7c. The maximum shear strain distribution showed two regions with high shear strain values. A small region with a peak value of 0.6 and a large region with peak values exceeding 0.8 and, in some cases, reaching 1.0. The two regions coincided with the edges of the indenter in the deformed mesh.

### 6.3.3 Comparison FE model / tagging measurement

For comparison of the deformations predicted by the FE simulation with the deformation measured in the tagging experiment, the deformed contour obtained from the MR image (solid red line, figure 6.7a) was superimposed on the deformed mesh. This shows that the predicted global deformation by the numerical model corresponded well with the actual deformation, although a number of small differences can be observed. The depth of indentation applied in the numerical model was based on the agreement with the deformed contours determined from the MR image. The calculated indentation in the FE model was larger compared to the values calculated from the tagging data. However, a close similarity was found in the distribution of maximum shear strains. Both distributions showed two regions with high values corresponding to the two edges of the indenter. The absolute values of maximum shear strain were, however, higher in the numerical model compared to the values calculated from the tagging data.

6.3.4 Comparison tagging measurement / damage location

A tagging experiment with an indentation of 4.3 mm was performed to compare the spatial pattern of maximum shear strain to locations of damage as deduced from increased T2 values. Figures 6.8a and b indicate the applied indentation in the tagging experiment. The calculated maximum shear strain distribution is depicted in figure 6.8c. A region with high strain values was found which extended from skin towards the tibial bone, with peak values of the order of 1.0. The results of two experiments, described in chapter 4 and 5, are shown in the middle and bottom rows of figure 6.8, in which an approximately similar indentation was applied as in the tagging experiment. Figure 6.8f and i show the resulting area with increased signal intensity after a loading period of 2 hours. Figure 6.8f shows a highly localised region with increased T2 values extending from the skin towards the tibial bone, while in the second experiment (bottom row) a more diffuse hyper-intense area was found. However, in both experiments the damaged region showed a high resemblance with the region of high shear strain values as indicated in figure 6.8c.
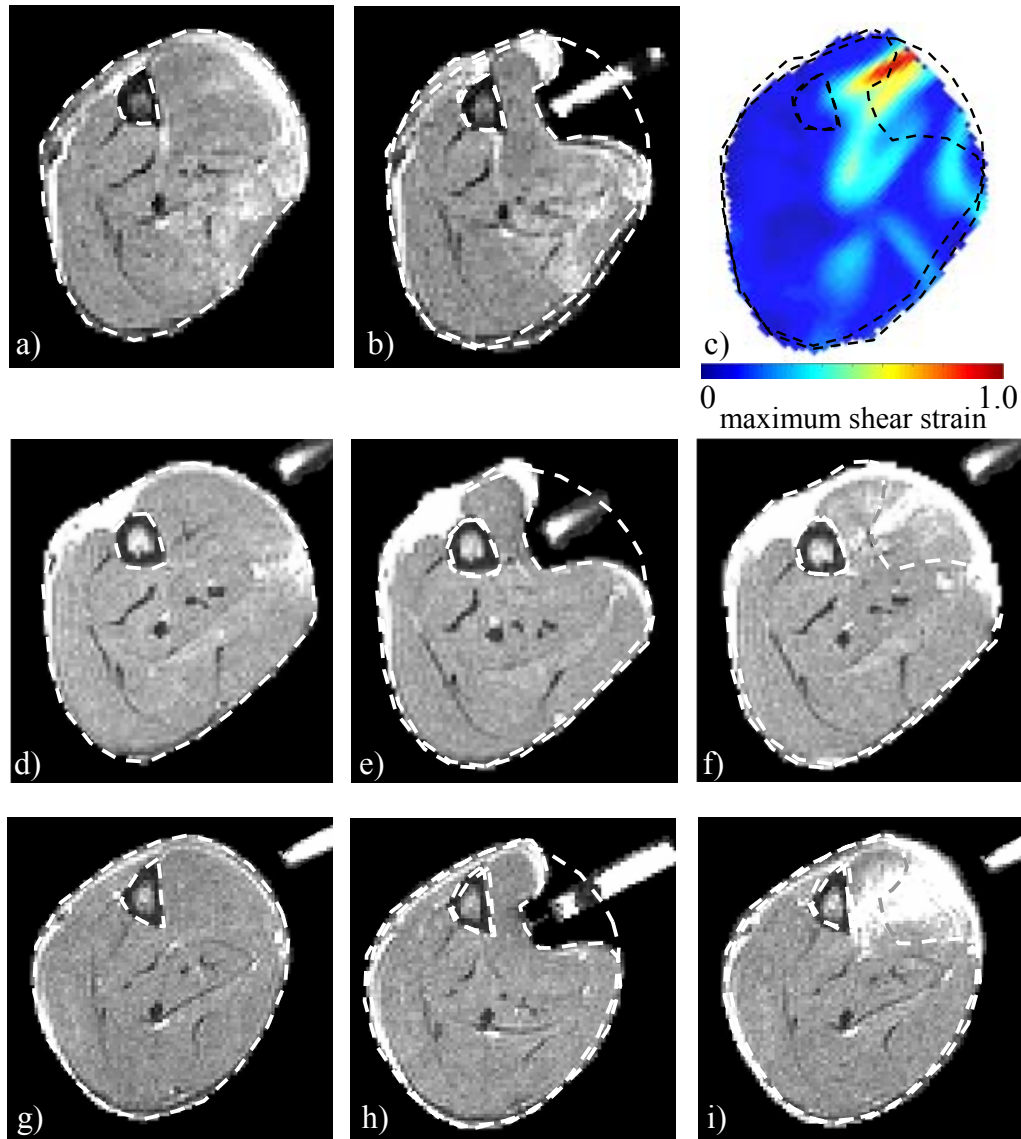
Figure 6.8 *Comparison of regions with high shear strain and location of damage indicated by an increase in T2. a-c) Top row shows tagging experiment with indentation of 4.3 mm with c) calculated maximum shear strain. d-f) Middle and g-i) bottom row show 2 experiments with comparable indentation and f, i) location of high T2 values in TA region 65 minutes after unloading. Dashed lines indicate deformed and undeformed contours.*

6.4 Discussion

The objective of this study was two-fold. First, the validation of the strains determined by a dedicated numerical model with strain fields obtained from MR tagging data. Secondly, the correlation between local strain fields and location of damage after

compressive loading. Both the validation and the correlation with damage location were performed in a 2D slice underneath the indenter. The local strain fields calculated by the FE model showed an apparent correlation with the distribution calculated from the measured tagging data, although the absolute values were slightly different. The location of damage determined with T2-weighted MRI was found in regions which showed high values of maximum shear strain in tagging experiments with similar indentation.

The MR tagging experiments required repetitive indenter applications in a rapid manner. This caused inevitable damage to and swelling of the tissue. In addition, after a certain number of indenter applications, the tissue did not fully 'recover' within 4 seconds. Accordingly there was some residual deformation when the tagging grid was applied. This resulted in lower calculated indentation compared to the first indentation, the contour of which was used for the validation of the FE model and for comparison to location of damage. This was particularly the case for the large indentation, which severely damaged the muscle. The accuracy of the data analysis procedure was not tested in this study, which is particularly required for the large indentations. A validation study might include the use of a gel phantom with known characteristics [121, 122] or simulated digital images [123].

The numerical model has several limitations. First of all, a 2D model was used for, in reality, a 3D problem. Several test problems were performed with a 3D model, but this model led to convergence problems at the large indentations that were applied in the experiments. An analysis of these problems revealed very high distortions of elements close to the indenter, which were responsible for the numerical problems and would have to be resolved by remeshing. As such a procedure is unfeasible for a 3D-model, at the present time, a 2D-model was chosen for analysis. Several simulations were performed at small deformations where 3D-models were compared with plain strain and plain stress models. From these simulations and the comparison with the experiments it became clear that because there were deformations in the axial direction in the muscle, the plain stress model was closest to the 3D situation, if compared with the plain strain situation. This led to a qualitatively good comparison between the measured tagging strains and displacements and those found in the simulations, although the strains and displacements in the latter were higher (figure 6.6 and 6.7). This finding was in part, due to the nature of the material laws used to model the soft tissues. In addition, the measured indentation from the tagging data was lower which was caused by inaccuracies in the determination of the displacement of tissue from the tagging data, as described above.

Comparing the deformed contours obtained from the MR images with those predicted by the FE model, some small differences were observed (figure 6.7a). These can partly be explained by the fact that in the FE model no separate skin layer was present. Indeed in the tagging experiments, swelling was observed in the skin layer due to the repeated indentations. Furthermore, as an approximation to the non-linear viscoelastic behaviour

[124] of muscle tissue, a non- linear Neo-Hookean material law was implemented. All the soft tissues in the leg were modelled as a single material, which neglected the presence of both fascia and membranes between muscles. It was observed in the MR images taken during loading that the deformations were largely restricted to the TA region. This indicates that the leg was indeed firmly fixed and that the tight fascia around the TA prevented large deformation of adjacent muscles. Therefore the boundary conditions were chosen such that only the line elements on the TA surface were allowed to move.

An apparent correlation was found between the location of high shear strains, determined from tagging data, and the location of damage, indicated by an increase in T2 (figure 6.8). Separate experiments had to be used, as the tagging protocol involved repeated indentations which were damaging to the tissue. All loading protocols were, however, performed inside the MR scanner, and therefore the precise indentation in each experiment was categorised. As a result, experiments with similar indentation could be selected for valid comparison. The regions with high shear strain values were found near to the edges of the indenter during loading, coincident with high levels of tissue distortion. The fact that the location of damage correlated with these regions confirmed the importance of strain in the initiation of damage.

The ultimate goal of this phase of the work is to make a direct correlation between strain values and damage, and to determine objective damage thresholds. Currently, the major obstacle is that the FE model cannot accommodate the large deformation used in the experiments. A remeshing procedure, which is currently being developed, might prove the solution for this problem. This method is largely restricted to 2D, preventing the development of a more realistic 3D model. However, if a valid model can be developed, the present dedicated FE model might prove to be a valuable tool in defining objective damage thresholds. In addition, it can be used to easily test the influence of variations in parameters such as changing material properties, without the need of additional animal experiments.

Acknowledgements

Chapter 7

General Discussion

7.1 Introductory remarks

Pressure ulcers are localised areas of degenerated skin and/or underlying soft tissues, caused by sustained mechanical loads. They can be initiated either at the skin layer and progress towards deeper layers, or progress from the underlying tissues towards the skin. The former are easily detectable, and adequate treatment measures can be taken with time. By contrast, by the time a deep pressure ulcer becomes visible at the skin layer, effective clinical intervention may prove problematic and prognosis is variable. The focus of the present thesis was therefore on these deep pressure ulcers. The underlying mechanisms leading to deep tissue injury following compressive loading are not well understood. Hypotheses associated with the pathogenesis of pressure ulcers involve localised ischaemia [20, 21, 22, 85], reperfusion injury [23], impaired interstitial fluid flow and lymphatic drainage [24, 25, 26, 27], and sustained deformation of cells [28, 29, 30].

Research on deep pressure ulcers has largely been hampered by a lack of non-invasive techniques to examine initial pathological changes in deep tissues. In addition, it is not known how external applied loads are transferred to local internal stresses and strains, which are most relevant for tissue breakdown and, more importantly, how these loads result in tissue damage. In the present thesis the mechanisms associated with deep tissue injury were examined. An animal model was used to determine *in vivo* tissue responses due to compressive loading. It was hypothesised that the temporal and spatial identification of initial muscle damage might reveal the underlying damage mechanisms. Therefore, it was considered essential to evaluate the tissue status during and immediately after loading, with both a high spatial and temporal resolution. In order to distinguish between different factors that contribute to muscle damage several loading protocols, including ischaemic versus compressive loading, were used. To study the relevance of the sustained deformation of cells, the results of selected animal experiments were combined with MR tagging measurements. In addition, the preliminary stages of a dedicated finite element (FE) model were developed to provide information on the local mechanical conditions in the tissues during loading.

In the following sections the animal model (section 7.2) and the experimental analysis (section 7.3) are discussed. The results of the experiments are summarised and discussed in section 7.4, after which the clinical relevance of this research (section 7.5) and recommendations for future research (section 7.6) are provided.

7.2 Animal model

The use of a rat model in studying muscle damage related to deep pressure ulcers is well established based on the similarities in skeletal muscle structure between humans and rats [chapter 2]. The animal model used was developed by Bosboom et al. [28] and

modified in the present study [chapter 3, 93]. In the former study, an interface pressure of 250 kPa was applied for 2 hours to the tibialis anterior (TA) region of Brown Norway rats. Muscle tissue was evaluated 24 hours after unloading by means of a combination of T2-weighted MRI and histology. The ability of T2-weighted MRI to detect muscle damage 24 hours after load removal, and the correlation to histological damage was demonstrated [28]. In the different experiments, damaged areas varied considerably between 0 and 70 % due, in part, to differences in applied indentation since only the applied pressure could be measured. Therefore, in the present study an MR-compatible loading device was designed and built, which allowed visualisation of the precise indentation for each experiment. This modification was critical, considering the importance of local mechanical conditions. The angle and position of the indenter could, to a certain degree, be varied in the experimental system, which allowed the indenter to be applied in a reproducible manner. In addition, the applied surface force could be measured by means of strain gauges that were attached to the loading beam. Furthermore, the MR-compatible loading device allowed simultaneous application of indentation and collection of MR-data. This offered the opportunity to measure the time of damage initiation and the subsequent temporal development of damage based upon an increase in T2. The loading device also enabled the use of different MR-techniques, such as contrast-enhanced MRI to obtain information of the perfusion status, and tagging MRI to measure deformation of the tissue during indentation.

In the experiments described in chapter 3, two loading protocols were employed. A large indentation was applied for 2 hours and a small indentation was applied for 4 hours. Only the large indentation led to damage after unloading, based on increase in T2 and histological features. The large indentation was therefore chosen for the subsequent experiments to study the damage mechanisms and contributions of several factors. The applied loads were relatively high compared to those used in other animal models to create muscle damage [chapter 2]. The applied indentation led to large deformations which are, however, considered to be physiologically realistic representing a worst-case situation on patients sitting on hard surfaces [125]. In a human MRI study, the total compression of the soft tissue composite above a bony prominence was estimated to correspond to equivalent strains of 30% and 50% for normal and paraplegic subjects, respectively [83]. These values were determined with supine individuals. It might be predicted that deformations will be enhanced in appropriate tissues in seated individuals.

The loading geometry is such that the muscle tissue is compressed against the tibial bone. However, it must be accepted that the nature of the indenter, in terms of its curvature and stiffness is also equivalent to a bony prominence. This arrangement highlights both the importance of the internal mechanical state and the limited value of surface pressures. Indeed, several authors have reported on the variable relationship between surface pressure and internal, or interstitial, pressures, which is a function of internal geometry including the proximity of bony prominences [126, 127].

It should be emphasised that the goal of the loading protocol was not to cause deep pressure ulcers per se, but to induce modest muscle damage after compressive loading for two hours, which enables studying the underlying mechanisms.

7.3 Experimental analyses

In the present thesis a range of MRI methodologies were used to study the mechanisms leading to deep tissue injury. These included T2-weighted MRI, contrast-enhanced MRI and tagging MRI, as summarised in table 7.1

Table 7.1 *A critical analysis of MRI methods used in the thesis*

MR method	Parameter of interest	Comments	Complementary methods
T2-weighted MRI (chapter 3,4,5,6)	Tissue changes and damage, indicated by increase in T2	- good spatial resolution - follow development in time - non-specific	histological analysis
Contrast-enhanced MRI (chapter 5)	Perfusion status, indicated by signal increase after injection of Gd-DTPA	- good spatial resolution - temporal resolution restricted to 1 hr - semi-quantitative method	
Tagging MRI (chapter 6)	Deformation and associated strain fields, determined from displacement of tag lines	- requires separate experiments - repetitive indentations in rapid manner cause substantial damage	finite element (FE) model

An increase in the transverse relaxation time T2 is generally accepted as a measure of tissue damage [45]. Affected regions within the soft tissues could clearly be distinguished on T2-weighted images [chapter 3 and 4]. This method for evaluating tissue status benefits from its non-invasive and non-destructive character, thus enabling the monitoring of tissue damage development in an unhindered manner. Indeed to the author's knowledge, the experiments described in chapter 3 and 4 represent the first to describe the temporal development of damage after compressive loading. However, one limitation of using T2 as a damage indicator is that it is non-specific. Therefore, the specific pathological features associated with pressure ulcers [21, 47, 78] can not be resolved by the use of T2-maps alone. These features include inflammation, oedema, necrosis, haemorrhage, fibrosis, and fatty infiltration. Another limitation is that not all tissue changes can be measured by T2-weighted MRI. This is partly because of a limited spatial resolution which, in the present study involves 234x234 μm^2 and a slice

thickness of 1mm. In addition, damage to tissue does not necessarily lead to an immediate change in the amount or properties of protons in water molecules, which can therefore be measured by T2-weighted MRI.

Information of perfusion status before, during and after loading was obtained using contrast-enhanced MRI. In the experiments, described in chapter 5, a bolus of Gd-DTPA was administered and from the increase in signal intensity a relative perfusion index (PI) was calculated. The obtained spatial resolution (500x500 μm^2, slice thickness 1 mm) was sufficient to distinguish regions with normal perfusion, hypo-perfusion and reactive hyperaemia. In a gradient echo multi slice sequence the number of slices influences the time of acquisition, in contrast to a spin echo multi slice sequence, in which a long repetition time (TR) is required, which allows multi-slice measurements. The number of slices chosen in the present study was 3, which determined the time resolution per image to 5 seconds.

The PI measurements could be incorporated in the same protocol as the damage experiments. Therefore, information on perfusion status during and after loading could be combined with damage location and development measured by T2-weighted MRI in the same experiment. The temporal resolution of the contrast-enhanced MR measurements was limited to 60 minutes, due to relatively slow clearance of the contrast-agent, but was sufficient to measure a relative perfusion index before, during and after loading.

Tagging MRI was used in chapter 6 to determine the local deformation of the tissue during loading. The tagging experiments required repetitive indentation applied in a rapid manner to obtain 2D displacement maps and associated strain distributions. This caused damage to and swelling of the tissue. In addition, after a certain number of indenter applications, the tissue did not fully 'recover' within 4 seconds. As a consequence there was some residual deformation when the tagging grid was applied, resulting in an underestimation of the indentation at single application. This was especially the case for the large indentation, which severely damaged the muscle. The approach was designed to address specific requirements. First, the tagging experiments were used for the validation of a dedicated finite element model, which is currently being developed in the host laboratory to correlate location of damage to local mechanical conditions. An apparent correlation was found between the maximum shear strain distribution calculated from the displacements of the tagging grid and the distribution predicted by the numerical simulation, although the absolute values did show some differences. The validation could only be performed at small indentations, as at indentation depths larger than 3 mm convergence problems occurred in the simulation due to distorted elements. Secondly, tagging experiments with similar indentation as used in the damage-experiments were performed, which allowed a global comparison between locations of maximum shear strain, calculated from the displacement of tag lines, with locations of damage measured with T2-weighted MRI.

7.4 Characteristics of deep tissue injury

Deep tissue injury arises in the muscle layers adjacent to bony prominences due to sustained loading. External loading results in a heterogeneous internal mechanical state, leading to large local deformations. Our hypothesis proposes that the initial damage to the muscle fibres at those locations is induced mechanically by local excessive deformation and subsequent disruption of muscle fibres [29, 86]. In chapter 4, the importance of deformation was examined by assessing the status of muscle tissue during and directly after loading using T2-weighted MRI. Histological examination was performed one, four or twenty hours after unloading. During loading no systematic signal changes were observed, while immediately after unloading signal intensities increased significantly (figure 4.3). The affected region involved a localised area extending from skin down to the tibial bone, which tended to decrease in size after 2 hours. Histological analysis after one and four hours after unloading revealed large necrotic regions with condensed contractile material clustered together (figure 4.7). Hypercontraction zones were found bilateral to the necrotic zone. The histological appearance of compression-induced damage showed similarities to that of exercise-induced damage (figure 4.9), possibly indicating a similar damage mechanism. An analogy between compression and exercise might be found in the high strains imposed on individual muscle fibres, leading to their disruption. Twenty hours after unloading an extensive infiltration of PMNs and monocytes was observed, revealing a pronounced inflammatory response.

In the T2-weighted images of the lower limb, a striking difference was observed in the temporal development of affected areas between slices proximal and distal to the indenter position (figure 4.5 and 5.9). In slices proximal to the indenter, the area with increased T2 was small directly after unloading and increased in the first hour. Conversely, in slices distal to the indenter, immediately after unloading a large area was visible with increased T2 values, which subsequently decreased in the first hour. The observed differences were proposed to be caused by differences in perfusion status during loading, which was subsequently examined with contrast-enhanced MRI [chapter 5]. From the signal increase after an injection of a bolus of Gd-DTPA, a perfusion index was calculated on a pixel-to-pixel basis. The perfusion status was measured in three slices, underneath the indenter and in slices 3 mm proximal and distal to the indenter position. The PI measurements demonstrated a hypo-perfusion region 3 mm distal to the indenter and no such region proximal to the indenter. This indeed suggests that the observed differences in T2 response distal and proximal to the indenter can be explained on the basis of differences in perfusion status. In addition, in distinguishing between the effects of pure ischaemia versus compression, which includes large cell deformation, ischaemia and possible disturbance of the metabolic equilibrium, a second loading protocol was used in chapter 5. Instead of applying the indenter, a tourniquet was applied above the knee of the rat, which induced ischaemic loading to the TA. A marked difference was found in the effect on T2 after 2 hours of ischaemia versus compression (figure 5.7). Pure ischaemic loading led to a small initial

decrease followed by a significant increase in T2 during loading. After deflation of the tourniquet, however, the T2 values returned to pre-loading values within 40 minutes. In the indenter-experiments the changes in T2 were not reversible and remained elevated up to 20 hours after unloading. This was also observed in the histological analysis. For example, muscle slices taken from underneath the indenter showed large necrotic regions, while tissue of the TA of the ischaemic limb only showed minor histological abnormalities (figure 5.8).

The importance of deformation on damage initiation was further studied in chapter 6 by calculation of the local strain fields during loading from MR tagging data, and comparing the locations of high strain to locations of damage. Although the local strain fields were calculated in separate experiments, a co-localisation of high strains and areas of damage could be demonstrated.

In summary, the effect of 2 hours of pure ischaemia on the T2 of muscle tissue was demonstrated to be reversible within 40 minutes, which was confirmed by the histological examination showing only minor abnormalities. Compression of the tissue for 2 hours did lead to persistent increased T2 values up to 20 hours and necrotic regions as indicated by histology. This implied that the deformation, superimposed on the ischaemia, was a major trigger for the initiation of damage. However, the increase in T2 during ischaemic loading did reveal tissue changes due to ischaemia alone. These tissue changes will most probably accelerate and/or increase the damage development during and after compressive loading. The importance of deformation was further confirmed by the correlation between regions of high shear strain calculated from tagging MR data and damage location. These findings can be summarized in figure 7.1 which shows the location of damage after 2 hours of compressive loading (figure 7.1a), the ischaemic region during loading (figure 7.1b) and the estimated distributions of maximum shear strains (figure 7.1c), the latter being calculated from a separate MR tagging experiment with an approximately similar value of indentation.

7.5 Clinical relevance

 The research presented in this thesis is part of a larger decubitus research programme being pursued at the Eindhoven University of Technology. One of the goals of this research is the early detection and evaluation of deep pressure ulcers, and subsequent development of a clinically useable monitoring system. Therefore a hierarchical research approach has been adopted [16] in which the effects of loading are studied at different, yet complementary, model systems with increasing complexity and length scales and incorporating one or more functional tissue units. Experimental studies are combined with computational models to elucidate the underlying mechanisms. The additional incorporation of animal experiments within the programme has enabled the

assessment of the relative roles of deformation, tissue (re)perfusion and lymph flow, as well as the interaction between tissue layers in bulk tissue.

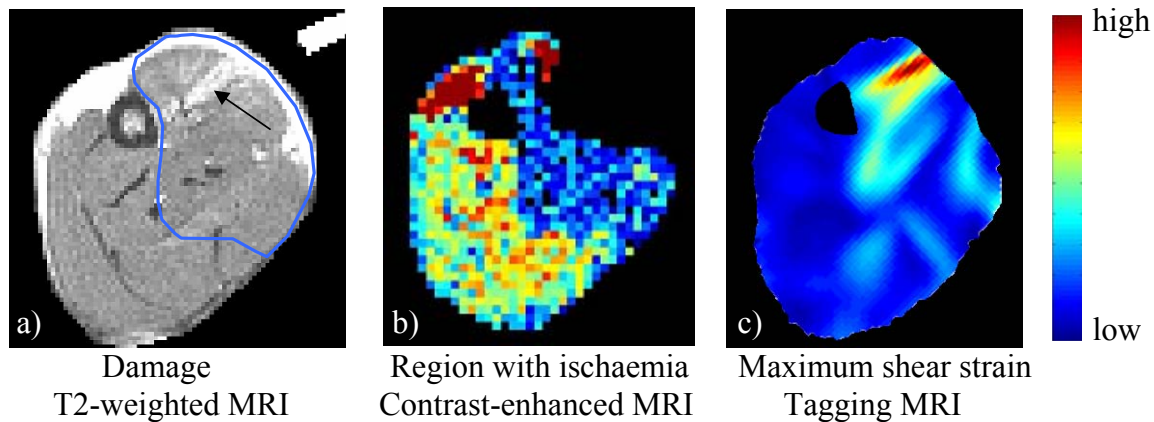|		
a)	b)	c)
Damage	Region with ischaemia	Maximum shear strain
T2-weighted MRI	Contrast-enhanced MRI	Tagging MRI

Figure 7.1 *A summary of the findings of the MR measurements in the slice underneath the indenter. a) Location of damage after unloading indicated by increase in T2 (arrow). The blue line indicates the area that appeared to be ischaemic during loading, as measured by contrast-enhanced MRI. b) Perfusion index (PI)-map during loading determined from signal increase after Gd-DPTA injection. c) Distribution of maximum shear strain during loading, as calculated from MR tagging measurements. This was measured in a separate experiment, with indentation values similar to that in a) and b).*

The current study has provided evidence for the ability of T2-weighted MRI to detect the initiation of muscle damage and subsequent development. In addition, the relative importance of deformation, in addition to ischaemia, in damage initiation was demonstrated. Deformation is clearly related to tissue properties and thus, for example, decreased muscle stiffness will be associated with enhanced tissue deformation [59]. The fact that patients can stay free of ulcers for a long time but suddenly, in a very short time, develop an ulcer, may be related to changing tissue properties caused by disease or trauma. The relevance of properties of muscle tissue may also be illustrated by the increased susceptibility in SCI subjects with flaccid paralysis compared to those with spastic paralysis [128, 129]. This clinical finding has been explained by the fact that the physical characteristics of the soft tissues under load in the SCI subject with spastic paralysis are considered to be similar to the normal subject, as the presence of spasm maintains muscle bulk and blood flow even though useful functional movements are absent [128]. The proposed positive effect of electrical stimulation for flaccid muscle tissues in reducing the risk of pressure ulcers [130] is also related to the importance of tissue properties, and therefore to deformation at both tissue and cellular levels.

If a valid dedicated FE model can be developed in the future it can be used to define objective damage thresholds, and these can be used in design criteria for supporting surfaces. In addition, a parametric approach can be adopted to vary parameters in the

model, such as mechanical stiffness, without the need of additional animal experiments. Thus the model could simulate different tissue properties of spinal cord injured subjects and thus predict conditions which can lead to increased susceptibility of this group.

In principle it is possible to measure location and size of damaged muscle areas by means of MR techniques, with high resolution scanners using the T2-weighted parameter. By means of molecular imaging techniques it may even be possible to get more detailed identification on the nature of the damage in tissues. It is well accepted that MR-imaging will not be available or even practical for use with all patients at risk. Thus a pre-screening method is required, incorporating the identification of physical markers and early damage markers, which can be measured in, for example, blood. These markers can be used as a pre-screening indicator for subsequent MR scanning.

7.6 Recommendations

Some important questions remained unanswered. In particular, the degree of muscle damage during loading needed to be ascertained. Related to this was the examination of the effect of load removal, associated with reperfusion, on damage development. In the T2-weighted images taken during loading no large signal changes were observed. However, large strains applied to the membranes of muscle fibres during loading, might have caused damage to the membranes [80], but this might only become apparent after unloading when large osmotic shifts of water occur directly due to the membrane damage. This is important to bear in mind, since if disregarded, this would lead to possible wrong conclusions e.g. that damage only started after unloading, which might overestimate the role of reperfusion damage.

Another important factor in the mechanical hypothesis is time. The question remains as to whether the proposed strain-induced damage already occurred at early time points during loading. This can be examined by choosing different loading periods with similar indentations. Subsequent to that, it might be proposed that the period of ischaemia at a constant deformation, determines the degree of damage that develops after unloading. Test protocols could be developed accordingly. The effects of such proposals can be illustrated in figure 7.2, which represents a schematic of damage development, associated with strain and ischaemia. The contribution of strain is proposed to increase only slightly with time based on the changes in properties observed in damaged tissues [131]. The arrow in figure 7.2 indicates that damage increases with increasing strain [86]. A more influential factor, however, that contributes to the temporal increase in damage is proposed to be ischaemia. This is based on the known damaging effects of prolonged periods of ischaemia [132]. It is proposed that these additional effects of ischaemia will start to occur following the initial damage to fibres caused by large strains. An estimated value of one hour is proposed, based on the observation of signal increase in T2-weighted images during ischaemic loading (figure 5.7). A similar schematic might be proposed during the

unloading phase. For this, however, a damage function associated with reperfusion and a remodelling term would have to be introduced.
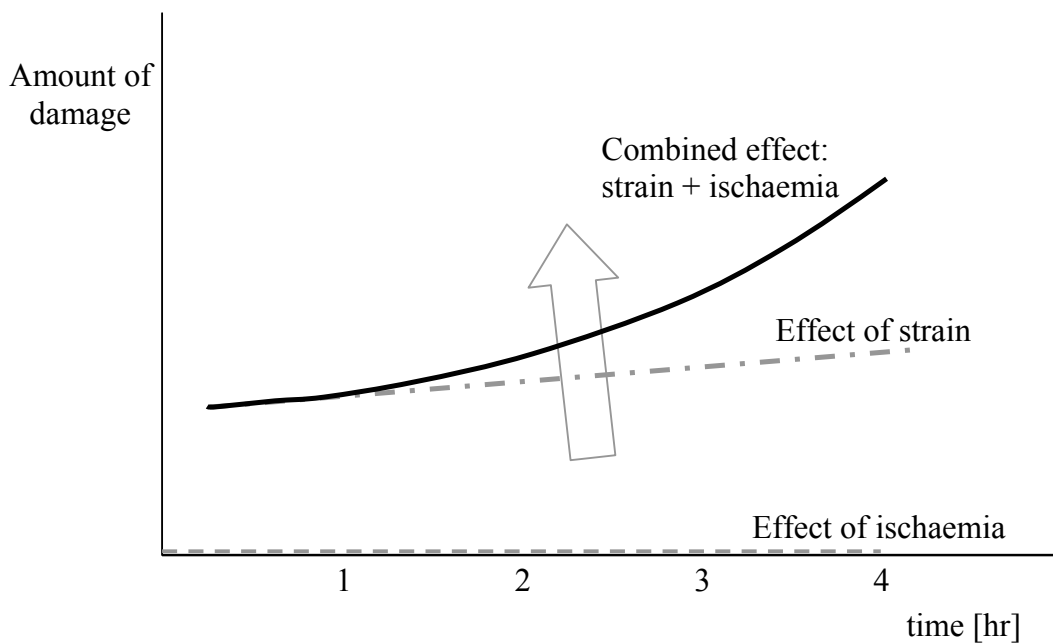

Figure 7.2 *Proposed schematic representation of damage during the loading phase, with individual contribution of strain and ischaemia.*

An important consideration not addressed in the present thesis was the effect of intermittent loading. In a clinical setting, many patients utilise periods of pressure relief in between periods of sustained loading. Intermittent loading has been demonstrated to be more damaging, compared to continuous loading, a finding which might be related to reperfusion damage associated with, for example, the release of oxygen free radicals [65, 66]. Different loading protocols can be designed to examine these effects using the developed MRI methods.

For testing the presence of early damage markers in blood, the MR-measurements should be repeated to include the collection of blood samples at selected time intervals. Indeed, a number of markers have been reported in the literature as suitable markers for muscle damage [133, 134]. The most promising markers are: myoglobin (Mb), fatty acid binding protein (FABP), creatine kinase (CK) and nitric oxide. In particular the low molecular weight proteins, FABP and Mb, are attractive candidate markers, as they rapidly enter the circulation and can be measured within one hour of damage initiation. Indeed assays are available, which are sensitive enough to measure very small signs of damage. As an example, from the ratio of FABP to Mb it can be uniquely determined that the damage is associated with skeletal muscle damage as opposed to heart muscle [135]. Thus experiments could be designed to correlate changes in the MR images to those measured with biochemical markers. This might lead to the development of a

unique relationship between temporal profiles of these marker concentrations and damage evolution.

It must be recognised that each of these technologies should be designed to be appropriate for use in the clinical situation. A temporal change in the levels of relevant markers should be used as an indication for applying a more detailed analysis in a MR scanner prior to the introduction of appropriate intervention strategies. Such MRI methodologies could include, in addition to T2-weighted MRI, magnetic resonance elastography (MRE) [136]. It was demonstrated by Linder-Ganz and Gefen [79] that tissue properties change due to damage. MRE is a relatively new diagnostic method for detecting changes in the mechanical properties of tissues. It can be applied to a variety of tissues, and is based on the visualisation of propagating acoustic strain waves. To date, the technique has been successful in the detection of tumors, which are observable as stiff solid mass regions in the MRE images. Another MR measurement that might be used to detect muscle damage is diffusion weighted imaging (DWI) [137] and diffusion tensor imaging (DTI) [138, 139]. Diffusion of water in biological tissue is composed of the random motion of water in the intra- and extracellular compartments as well as exchange processes. DWI can yield important information about the condition of healthy and pathological tissues.

The large deformations used in this study were considered to be relevant, especially for SCI subjects. However, it is known that muscle tissue properties change after spinal cord injury. In a review by Scelsi [140], the pathological changes were summarised, and included muscle fibre type transformation, with type I fibre change to type II, muscle atrophy, changes in fibre size, and alterations in myofibrillar apparatus. Studies on an experimental spinal cord transection showed changes in rat skeletal muscle, with almost complete type I to type II fibre transformation after 1 year [141]. The use of such an animal model might be valuable in studying the vulnerability of SCI subjects. Several pressure ulcer related studies involving paraplegic animals have been performed [20, 46, 50]. Results were however contradictory, caused, in part, by differences in time between spinal cord transection and experiments, which seemed to represent a critical factor.

In conclusion, this thesis presents a selection of MRI methodologies, each designed to identify specific mechanisms associated with the temporal profile of muscle tissue damage in an animal model. Derived MR parameters were examined in conjunction with histological analysis and FE simulation. As an example, the increase in T2 values following compression were shown to persist up to 20 hours, whilst the corresponding changes were transient in nature following ischaemia alone. This highlighted the importance of deformation, which was supported by evidence of complete disruption of muscle fibres. These methodologies represent a valuable tool for studying the aetiology of deep pressure ulcers.

References

[1]   Dealey C, The size of the pressure sore problem in a teaching hospital. *J Adv Nurs* 1991; 16: 663-70

[2]   Meehan M, Multisite pressure ulcer prevalence study. *Decubitus* 1990; 3: 14-7

[3]   Haalboom JRE, Medical perspectives in the 21st century, In *Pressure Ulcer Research Current and Future Perspectives*, edited by DL Bader, CVC Bouten , D Colin, CWJ Oomens. Springer- Verlag, 2005; 11-21

[4]   Gunningberg L, Are patients with or at risk of pressure ulcers allocated appropriate prevention measures? *Int J Nurs Pract* 2005; 11(2): 58-67

[5]   Byrne DW, Salzberg CA, Major risk factors for pressure ulcers in the spinal cord disabled: a literature review. *Spinal cord* 1996; 34(5): 255-63

[6]   Garber SL, Rintala, DH, Pressure ulcers in veterans with spinal cord injury: a retrospective study. *J Rehabil Res Dev* 2003; 40(5): 433-41

[7]   Yarkony GM, Matthews KP, Carlson C, Roth EJ, Lovell L, Classification of pressure ulcers. *Arch Dermatol* 1990; 126: 1218-9

[8]   Harker J, Pressure ulcer classification. *J Wound Care* 2000; 9: 275-7

[9]   Shea JD, Pressure sores classification and management. *Clin Orthop* 1975; 112: 89-100

[10] Witkowski JA, Parisch LC. Classification of pressure ulcers. *Arch Dermatol* 1991; 127: 907-8

[11] EPUAP, Guidelines on treatment of pressure ulcers. *EPUAP review* 1999; 2: 31-33

[12] EPUAP, Guide to pressure ulcer grading. *EPUAP review* 2002; 3: 75

[13] Maklebust J, Pressure ulcer staging systems. *Adv Wound Care* 1995; 8(4): suppl 11-4

[14] NPUAP, Position on reverse staging of pressure ulcers. *Adv Wound Care* 1995; 8: 32-3

[15] Bliss MR, Aetiology of pressure sores. *Reviews in clinical gerontology 1993;* 3: 379-397

[16] Bouten CVC, Oomens CWJ, Baaijens FPT, Bader DL, The etiology of pressure ulcers: skin deep or muscle bound? *Arch Phys Med Rehabil 2003;* 84(4): 619-9

[17] Donnelly J, Should we include deep tissue injury in pressure ulcer staging systems? The NPUAP debate. *J Wound Care* 2005; 14(5): 207-210

[18] Stekelenburg A, Oomens CWJ, Bader DL, Compression-induced tissue damage: animal models. In *Pressure Ulcer Research Current and Future Perspectives*, edited by DL Bader, CVC Bouten, D Colin, CWJ Oomens. Springer- Verlag, 2005; 187-204

[19] Peirce SM, Skalak TC, Rodeheaver GT, Ischemia-reperfusion injury in chronic pressure ulcer formation: a skin model in the rat. *Wound Repair Regen* 2000; 8(1): 68-76

[20] Daniel RK, Priest DL, Wheatley DC, Etiologic factors in pressure sores: An experimental model. *Arch Phys Med Rehabil* 1981; 62(10): 492-8

[21] Kosiak M, Etiology of decubitus ulcers. *Arch Phys Med Rehabil 1961; 42: 19-29*

[22] Dinsdale SM, Decubitus ulcers: role of pressure and friction in causation. A*rch Phys Med Rehabil* 1974; 55(4): 147-52

[23] Houwing R, Overgoor M, Kon M, Jansen G, Asbeck BS, Haalboom JRE, Pressure- induced skin lesions in pigs: reperfusion injury and the effects of vitamin E. *J Wound Care* 2000; 9(1): 36-40

[24] Barbenel JC, Pressure management. *Prosth Orth Int* 1991; 5: 225-31

[25] Dodd KT, Gross DR., Three-dimensional tissue deformation in subcutaneous tissues overlying bony prominences may help to explain external load transfer to the interstitium. *J Biomech* 1991; 24: 11-9

[26] Miller GE, Seale J, Lympatic clearance during compressive loading. *Lymphology* 1981; 14: 161-66

[27] Reddy NP, Cochran GV, Interstital fluid flow as a factor in decubitus ulcer formation. *J Biomech* 1981; 14: 879-81

[28] Bosboom EMH, Bouten CVC, Oomens CWJ, van Straaten HWM, Baaijens FPT, Kuipers H, Quantification and localisation of damage in rat muscles after controlled loading; a new approach to study the aetiology of pressure sores. *Med Eng Phys* 2001; 23(3): 195-200.

[29] Bouten CVC, Bosboom EMH, Oomens CWJ, The aetiology of pressure sores: A tissue and cell mechanics approach. In *Biomedical aspects of manual wheelchair propulsion,* edited by LHV van der Woude, MTE Hopman, CH van Kemenade, Amsterdam: IOS Press; 1999; 52-62

[30] Ryan TJ, Cellular responses to tissue distortion. In *Pressure sores: Clinical practice and scientific approach,* edited by DL Bader, London; Macmillan Press Ltd; 1990; 141-52

[31] Bliss MR, Aetiology of pressure sores. *Rev Clin Geront* 1993; 3: 379-97

[32] DeFloor, de Laat E, Schoonhoven L, Vanderwee K, PUCLAS software 2003, Available from http://www.epuap.org

[33] Bours GJ, Halfens RJ, Abu-Saad HH, Grol RT, Prevention, and treatment of pressure ulcers: descriptive study in 89 institutions in the Netherlands. *Res Nurs Health* 2002; 25(2): 99-110

[34] Lyder CHB, Battling pressure ulcers: consistency means success. Nursing homes long term care management 2004; 53(1): 72-3

[35] Srinivasan S, Krouskop T, Ophir J, A quantitative comparison of modulus images obtained using nanoindentation with strain elastograms. *Ultrasound Med Biol* 2004; 30(7): 899-918

[36] Sinkus R, Lorenzen J, Schrader D, Lorenzen M, Dargatz M, Holz D, High-resolution tensor MR elastography for breast tumour detection *Phys Med Biol* 2000; 45(6): 1649-64.

[37] May DA, Disler DG, Jones A, Balkissoon AA, Manaster BJ, Abnormal signal intensity in skeletal muscle at MR imaging: patterns, pearls and pitfalls. *Radiographics* 2000, 20 Spec No, S295-S315

[38] Hencey JY, Vermess M, van Geertruyden HH, Binard JE, Manchepalli S, Magnetic resonance imaging examinations of gluteal decubitus ulcers in spinal cord injury patients. *J Spinal Cord Med* 1996; 19: 5-8

[39] Ruan CM, Escobedo E, Harrison S, Goldstein B, Magnetic resonance imaging of nonhealing pressure ulcers and myocutaneous flaps. *Arch Phys Med Rehabil* 1998; 79: 1080-1088

[40] Bosboom EMH, Bouten CVC, Oomens CWJ, Baaijens FPT, Nicolay K, Quantifying pressure sore related muscle damage using high resolution MRI. *J Appl Physiol 2001;* 95: 2235-2240

[41] Hornak JP, The Basics of MRI. http://www.cis.rit.edu/htbooks/mri, 1996

[42] Vlaardingerbroek MT, den Boer JA, Magnetic Resonance Imaging, 2nd ed. Berlin: Springer –Verlag, 1999

[43] Haacke EM, Brown RW, Thompson MR, Venkatesan R, Magnetic Resonance Imaging, physical principles and sequence design. New York: John Wiley and Sons Inc. 1999: 513-552

[44] Patten C, Meyer RA, Fleckenstein JL, T2 mapping of muscle. *Semin Musculoskelet Radiol* 2003; 7(4): 297-305. Review

[45] Fleckenstein JL. Skeletal muscle evaluated by MRI. In: *Encyclopedia of nuclear magnetic resonance*, edited by DM Grant and RK Harris. 1996 Chichester, Wiley, p 4430-4436

[46] Groth KE, Klinische beobachtungen und experimentelle studien uber die entstehung des dekubitus. *Acta Cher Scand* 1942; 87: 198-200, supp 76

[47] Husain T, An experimental study of some pressure effects on tissues, with reference to the bed-sore problem. *J.Path. Bact* 1953; 66: 347-58

[48] Kosiak M, Etiology and pathology of ischemic ulcers. *Arch Phys Med&Rehabil 1959; 40(2): 62-9*

[49] Swaim SF, Bradley DM, Vaughn DM, Powesr RD, Hoffman CE, The greyhound dog as a model for studying pressure ulcers. *Decubitus* 1993; 6(2): 32-40

[50] Hyodo A, Reger SI, Negami S, Kambic H, Reyes E, Browne EZ, Evaluation of a pressure sore model using monoplegic pigs. *Plast Reconstr Surg* 1995; 96(2): 421-8.

[51] Goldstein B, Sanders J, Skin response to repetitive mechanical stress: a new experimental model in pig. *Arch Phys Med Rehabil 1998;* 79(3): 265-72

[52] Salcido R, Donofrio JC, Fisher SB, LeGrand EK, Dickey K, Carney JM, Schosser R, Liang R. Histopathology of pressure ulcers as a result of sequential computer-controlled pressure sessions in a fuzzy rat model. *Adv Wound Care 1994;* 7(5): 23-8

[53] Salcido R, Fisher SB, Donofrio JC, Bieschke M, Knapp C, Liang R, LeGrand EK, Carney JM, An animal model and computer-controlled surface pressure delivery

system for the production of pressure ulcers. *J Rehabil Res Dev 1995;* 32(2): 149-61

[54] Salcido R, Donofrio JC, Fisher SB, LeGrand EK, Carney JM, Schosser R, Rodgers J, Liang R, Evaluation of ibuprofen for pressure ulcer prevention: application of a rat pressure ulcer model. *Adv Wound Care 1995;* 8(4): 30-40

[55] Dinsdale SM, Decubitus ulcers in swine: light and electron microscopy study of pathogenesis. *Arch Phys Med Rehabil 1973*; 54(2): 51-6

[56] Daniel RK, Wheatley DC, Priest DL, Pressure sores and paraplegics: an experimental model. *Ann Plast Surg* 1985; 15: 41-9

[57] Sundin BM, Hussein MA, Glasofer S, El-Falaky MH, Abdel-Aleem SM, Sachse RE, Klitzman B, The role of allupurinol and deferoxamine in preventing pressure ulcers in pigs. *Plast Reconstr. Surg 2000;* 4: 408-21

[58] Patel S, Knapp CF, Donofrio JC, Salcido R, Temperature effects on surface pressure-induced changes in rat skin perfusion: implications in pressure ulcer development. *J Rehabil Res Dev 1999;* 36(3): 189-201

[59] Reger S, Negami S, Reyes E, McGovern T, Navarro R, Effect of DC electrical stimulation on pressure sore healing in pigs. *RESNA Conference*, Washington, DC, 1990; 379

[60] Reswick JB, Rogers JE (1976) in Kenedi RM and Cowden JM (eds) *Bedsore Biomechanics 1976*, university park press, Baltimore 301-310

[61] Lindan O, Etiology of decubitus ulcers: an experimental study. *Arch Phys Med Rehabil 1961; 42: 774- 83*

[62] Sacks, Theoretical prediction of a time-at-pressure curve for avoiding pressure sores. *J Rehabil Res Dev 1989;* 26(3): 27-34

[63] Reichel SM, Shearing force as a factor in decubitus ulcers in paraplegics. *J.A.M.A*. 1958; 66: 762-763

[64] Bennett L, Kavner D, Lee BK, Trainor FA. Shear vs pressure as causative factors in skin blood flow occlusion. *Arch Phys Med Rehabil* 1979; 60(7): 309-14

[65] McCord JM. Oxygen-derived free radicals in postischemic tissue injury. *N Engl J Med 1985;* 17; 312(3): 159-63. Review

[66] Kukreja RC, Janin Y, Reperfusion Injury: Basic Concepts and Protection Strategies. *J Thromb Thrombolysis* 1997; 4(1): 7-24

[67] Russell RC, Roth AC, Kucan JO, Zook EG, Reperfusion injury and oxygen free radicals: a review. *J Reconstr Microsurg* 1989; 5(1): 79-84

[68] Parks DA, Granger DN, Ischemia-reperfusion injury: a radical view. *Hepatology 1988;* 8(3): 680-2

[69] Unal S, Ozmen S, DemIr Y, Yavuzer R, LatIfoglu O, Atabay K, Oguz M. The effect of gradually increased blood flow on ischemia-reperfusion injury. *Ann Plast Surg* 2001; 7(4) 412-6

[70] Brown AC, Brengelmann G Energy metabolism. In P*hysiology and biophysics,* edited by RC Ruch, HD Patton, Philadelphia, 1965;1030-49

[71] Mahanty SD, Roemer RB, Thermal response of skin to application of localized pressure, *Arch Phys Med Rehabil* 1979*;* 60(12): 584-90

[72] Fisher SV, Szymke TE, Apte SY, Kosiak M. Wheelchair cushion effect on skin temperature. *Arch* Phys Med Rehabil 1978; 59(2): 68-72

[73] Kokate JY, Leland KJ, Held AM, Hansen GL, Kveen GL, Johnson BA, Wilke MS, Sparrow EM, Iaizzo P, Temperature-modulated pressure ulcers: a porcine model. *Arch Phys Med Rehabil 1995;* 76(7): 666-73.

[74] Iaizzo P, Kveen GL, Kokate JY, Leland KJ, Hansen GL, Sparrow EM, Prevention of pressure ulcers by focal cooling: histological assessment in a porcine model. *Wounds* 1995; 7(5): 161-9

[75] Herrman EC, Knapp CF, Donofrio JC, Salcido R., Skin perfusion responses to surface pressure-induced ischemia: implication for the developing pressure ulcer. *J Rehabil Res Dev* 1999; 36(2): 109-20

[76] Beltran J, MR imaging of soft-tissue infection, *Magn Reson Imaging Clin N Am* 1995; 3: 743-751

[77] Revelon G, Rahmouni A, Jazaerli N, Godeau B, Chosidow O, Authier J, Mathieu D, Roujeau JC, Vasile N, Acute swelling of the limbs: magnetic resonance pictorial review of fascial and muscle signal changes, *Eur J Radiol* 1999, 30, 11-21

[78] Vleet JF, Ferrans VJ, Pathological reaction of skeletal muscle to injury. in *Cardiovascular and musculoskeletal systems, Monographs in Pathology of laboratory animals, edited by* TC Jones, U Mohr, RD Hunt, New York: Springer-Verlag, 1991: 109-126

[79] Linder-Ganz E, Gefen A, Mechanical compression-induced pressure sores in rat hindlimb: muscle stiffness, histology, and computational models, *J Appl Physiol* 2004; 96; 2034-2049

[80] Gonzalez-Serratos H, Rozycka M, Cordoba-Rodriguez R, Ortega A, Membrane healing and restoration of contractility after mechanical injury in isolated skeletal muscle fibers in the frog. *Proc Natl Acad Sci* USA, 1996; 93; 5996-6001

[81] Rubin, E. and Farber, J.L., Eds. *Pathology*. Lippincott-Raven Co., Philadelphia, Pa. Third Edition, 1998

[82] Oomens CWJ, Bressers OFJT, Bosboom EMH, Bouten CVC, Bader DL, Can loaded interface charateristics influence strain distributions in muscle adjacent to bony prominences? *Comput. Methods Biomech. Biomed. Eng.* 2003; 6(3): 171-80

[83] Reger SI, McGovern TF, Chung KC, Biomechanics of tissue distortion and stiffness by magnetic resonance imaging. In Bader DL, editor, *Pressure sores: Clinical practice and scientific approach*, 177-190. 1990, The Macmillan Press Ltd

[84] Luo Y, Mohning KM, Hradil VP, Wessale JL, Segreti JA, Nuss ME, Wegner CD, Burke SE, Cox BF, Evaluation of tissue perfusion in a rat model of hind limb ischemia using contrast- enhanced magnetic resonance imaging, *J Magn reson Imaging* 2002, 16, 277-283

[85] Bar CA, The Response of tissues to applied pressure. Cardiff University of Wales College of Medicine, PhD thesis 1988, United Kingdom

[86]   Breuls RG, Bouten CV, Oomens CWJ, Bader DL, Baaijens FP, Compression induced cell damage in engineered muscle tissue: an in vitro model to study pressure ulcer aetiology. *Ann Biomed Eng* 2003*;* 31(11): 1357-64

[87]   Peters E, Swain ID, Evaluation of wheelchair cushions, static and dynamic. PS4 Norwich: Medical devices agency, department of health, 1997

[88]   Lieber RL, Fridén J, Mechanisms of muscle injury gleaned from animal models. *Am J Phys Med Rehabil 2002;* 81: S70-S79

[89]   Morgan DL, Allen DG, Early events in stretch-induced muscle damage. *J Appl physiol* 1999; 87(6): 2007-2015

[90]   Helliwell TR, Muscle damage in myopathies. In: *Muscle damage,* edited by Salmons S, Oxford university press, 1997; 168-214

[91]   Fridén J, Pedowitz RA, Thornell LE, Sensitivity of different types of fibres in rabbit skeletal muscle to pneumatic compression by tourniquet and to ischaemia. *Scand J Plast Reconstr Hand Surg* 1994; 28: 87-94

[92]   Heppenstall BM, Scott R, Sapega A, Park YS, Chance B. A comparative study of the tolerance of skeletal muscle to ischaemia. *J Bone Joint Surg* 1986; 68A: 820-828

[93]   Stekelenburg A, Oomens CWJ, Strijkers GJ, de Graaf L, Bader DL, Nicolay K, A new MR-compatible loading device to study in-vivo muscle damage development in rats due to compressive loading. *Med Eng Phys 2005;* in press

[94]   Scelsi R Skeletal muscle pathology after spinal cord injury: our 20 year experience and results on skeletal muscle changes in paraplegics, related to functional rehabilitation. *Basic Appl Myol* 2001; 11(2): 75-85

[95]   Lieber RL, Friden JO, Hargens AR, Feringa ER, Long-term effects of spinal cord transection on fast and slow rat skeletal muscle. II. Morphometric properties. *Exp Neurol* 1985; 91(3): 435-48

[96]   Lieber RL, Fridén J, Muscle damage is not a function of muscle force but active muscle strain. *J Appl Physiol* 1993; 74(2): 520-526

[97]   Fridén J, Lieber RL, Segmental muscle fibre lesions after repetitive eccentric contraction. *Cell Tissue Res* 1998; 293: 165-171

[98]   Best TM, McElhaney JH, Garretr WE Myers BS, Axial surface strains in skeletal muscle under various loading rates. *J Biomech Eng* 1995; 117: 262-5

[99]   Brooks SV, Zerba E, Faulkner JA, Injury to fibres after single stretches of passive and maximally stimulated muscles in mice. *J Physiol* 1995; 488: 459-69

[100] Nola GT and Vistnes LM, Differential response of skin and muscle in the experimental production of pressure sores. *Plast Reconstr Surg* 1980; 60: 728-33

[101] Bouten CV, Breuls RG, Peeters EA, Oomens CW, Baaijens FP, In vitro models to study compressive strain-induced muscle cell damage. Biorheology. 2003; 40: 383-8.

[102] Lutz AM, Weishaupt D, Amann-Vesti BR, Pfammatter T, Goepfert K, Marincek B, Nanz D, Assessment of skeletal muscle perfusion by contrast medium first-pass magnetic resonance imaging: Technical feasibility and preliminary experience in healthy volunteers, *J. Magn. Reson. Imaging* 2004; 20: 111-121

[103] Nygren AT, Greitz D, Kaijser L, Skeletal muscle perfusion during exercise using Gd-DTPA bolus detection. *J Cardiovasc Magn Reson* 2000; 2(4): 263-70.

[104] Hamer PW, McGeachie JM, Davies MJ, Grounds MD, Evans Blue Dye as an *in vivo* marker of myofibre damage: optimizing parameters for detecting initial myofibre membrane permeability. *J Anat* 2002; 200(1): 69-79

[105] Lebon V, Carlier PG, Brillault-Salvat C, Leroy-Willig A, Simultaneous measurement of perfusion and oxygenation changes using a multiple gradient-echo sequence: application to human muscle study. *Magn Reson Imaging* 1998; 16(7): 721-29

[106] Ostman B, Michaelsson K, Rahma H, Hillered L, Tourniquet-induced ischemia and reperfusion in human skeletal muscle. *Clin Orthop Relat Res* 2004; 418: 260-5

[107] Morikawa S, Kido C, Inubushi T, Observation of rat hind limb skeletal muscle during arterial occlusion and reperfusion by ^{31}P MRS and ^{1}H MRI, *Magn Reson Imaging* 1991; 9(3): 269-74

[108] Blum H, Schnall MD, Chance B, Buzby GP, Intracellular sodium flux and high-energy phosphorus metabolites in ischemic skeletal muscle. *Am J Physiol* 1988; 255: C377-C384

[109] Appell HJ, Glöser S, Duarte JA, Zellner A, Soares JMC, Skeletal muscle damage during tourniquet-induced ischaemia. The initial step towards atrophy after orthopaedic surgery? *Eur J Appl Physiol* 1993; 67: 342-7

[110] Pedowitz RA, Friden J, Thornell L-E, Skeletal muscle injury induced by a pneumatic tourniquet: An enzyme- and immunohistochemical study in rabbits, J *Surg Res* 1992; 52: 243-50

[111] Pedowitz RA, Gershuni DH, Fridén J, Garfin SR, Rydevik BL, Hargens AR, Effects of reperfusion intervals on skeletal muscle injury beneath and distal to a pneumatic tourniquet. *J Hand Surg* 1992; 17A: 245-55

[112] da Cruz CA, Massuda CA, Cherri J, Piccinato CE, Metabolic alterations of skeletal muscle during ischaemia and reperfusion, *J Cardiovasc Surg* 1997; 38: 473-477

[113] Harris K, Walker PM, Mickle DAG, Harding R, Gatley R, Wilson GJ, Kuzon B, McKee N, Romaschin AD, Metabolic response of skeletal muscle to ischaemia, *Am J Physiol* 1986; 250: H213-H220

[114] Welsh DG and Lindinger MI, Energy metabolism and edenine nucleotide degradation in twitch-stimulated rat hindlimb during ischemia-reperfusion. *Am J Physiol* 1993; 264: E655-E661

[115] Axel L, Dougherty L, MR imaging of motion with spatial modulation of magnetization. *Radiology* 1989; 171: 841-5

[116] Fischer SE, McKinnon GC, Maier SE, Boesiger, Improved myocardial tagging contrast. *Magn Reson Med* 1993; 30: 191-200

[117] Osman NF, Kerwin WS, McVeigh ER, Prince JL, Cardiac motion tracking using CINE harmonic phase (HARP) magnetic resonance imaging, *Magn Reson Med* 1999; 42: 1048-1060

[118] Geers MGD, de Borst R, Brekelmans WAM, Computing strain fields from discrete displacement fields in 2D-solids, *Int J Solids Structures* 1996; 33(29): 4293-4307

[119] Guus Segal. Sepran: Sepra Analysis. User guide. Ingenieursbureau SEPRA, Den Haag, The Netherlands, August 2004

[120] HSL (2002). A collection of Fortran codes for large scale scientific computation. http://www.numerical.rl.ac.uk/hsl

[121] Young AA, Axel L, Dougherty, Bogen DK, Parenteau CS, Validation of tagging with MR imaging to estimate material deformation. *Radiology* 1994; 188(1): 101-8

[122] Augenstein KF, Cowan BR, LeGrice IJ, Nielsen PM, Young AA, Method and apparatus for soft tissue material parameter estimation using tissue tagged Magnetic Resonance Imaging. *J Biomech Eng* 2005; 127(1): 148-57

[123] Liu W, Chen J, Ji S, Allen JS, Bayly PV, Wickline SA, Yu X, Harmonic phase MR tagging for direct quantification of Lagrangian strain in rat hearts after myocardial infarction. *Magn Reson Med* 2004; 52(6): 1282-90

[124] Bosboom EM, Hesselink MK, Oomens CW, Bouten CV, Drost MR, Baaijens FP, Passive transverse mechanical properties of skeletal muscle under in vivo compression *J Biomech* 2001; 34(10): 1365-8.

[125] Drummond D, Breed AL, Narechania R, Relationship of spine deformity and pelvic obliquity on sitting pressure distributions and decubitus ulceration. *J Pediatr Orthop* 1985; 5(4): 396-402

[126] Bader DL, White SH, The viability of soft tissues in elderly subjects undergoing hip surgery. *Age and Ageing* 1998; 27: 217-221

[127] Sangeorzan BJ, Harrington RM, Wyss CR, Czerniecki JM, Matsen FA, Circulatory and mechanical response of skin to loading, *J Orthop Res* 1989; 7(3): 425-31

[128] Bogie KM, Bader DL, Susceptibility of spinal cord-injure individuals to pressure ulcers. In *Pressure Ulcer Research Current and Future Perspectives*, edited by DL Bader, CVC Bouten , D Colin, CWJ Oomens. Springer- Verlag, 2005, p73-88

[129] Swain ID, Bader DL, The measurement of interface pressure and its role in soft tissue breakdown. *J Tissue Viability* 2002; 12(4):132-46

[130] Janssen TWJ, Smit C, Hopman MT, Prevention and treatment of pressure ulcers using electrical stimulation. In *Pressure Ulcer Research Current and Future Perspectives*, edited by DL Bader, CVC Bouten , D Colin, CWJ Oomens. Springer- Verlag, 2005, p89-107

[131] Gefen A, Gefen N, Linder-Ganz E, Margulies SS, In vivo muscle stiffening under bone compression promotes deep pressure sores. *J Biomech Eng* 2005; 127(3): 512-24

[132] Walker PM, Ischemia/reperfusion injury in skeletal muscle. *Ann Vasc Surg* 1991; 5(4): 399-402

[133] Sorichter S, Puschendorf B, Mair J, Skeletal muscle injury induced by eccentric muscle action: muscle proteins as markers of muscle fiber injury. *Exerc Immunol Rev* 1999; 5: 5-21. Review

[134] Hagisawa S, Ferguson-Pell MW, Palmieri VR, Cochran GV, Pressure sores: a biochemical test for early detection of tissue damage, *Arch Phys Med Rehabil* 1988; 69(9): 668-71

[135] Van Nieuwenhoven FA, Kleine AH, Wodzig WH, Hermens WT, Kragten HA, Maessen JG, Punt CD, Van Dieijen MP, Van der Vusse GJ, Glatz JF, Discrimination between myocardial and skeletal muscle injury by assessment of the plasma ratio of myoglobin over fatty acid-binding protein. *Clin Chem* 1995; 15; 92(10): 2848-54

[136] Muthupillai R, Ehman RL, Magnetic resonance elastography. *Nat Med* 1996; 2: 601-603

[137] Baur A, Reiser MR, Diffusion-weighted imaging of the musculoskeletal system in humans *Skeletal Radiol* 2000; 29: 555-62

[138] Le Bihan D, Breton E, Lallemand D, Grenier P, Cabanis E, Laval-Jeantet M, MR imaging of intravoxel incoherent motions: application to diffusion and perfusion in neurologic disorders. *Radiology* 1986; 161: 401-407

[139] Heemskerk AM, Strijkers GJ, Vilanova A, Drost MR, Nicolay K, Determination of mouse skeletal muscle architecture using three-dimensional diffusion tensor imaging. *Magn Reson Med* 2005; 53(6): 1333-40.

[140] Scelsi R Skeletal muscle pathology after spinal cord injury: our 20 year experience and results on skeletal muscle changes in paraplegics, related to functional rehabilitation. *Basic Appl Myol* 2001; 11(2): 75-85

[141] Lieber RL, Friden JO, Hargens AR, Feringa ER, Long-term effects of spinal cord transection on fast and slow rat skeletal muscle. II. Morphometric properties. *Exp Neurol* 1985; 91(3): 435-48

Samenvatting

Drukwonden, ook wel aangeduid als doorligwonden of decubitus, zijn locale degeneraties van huid en/of de onderliggende weefsels en worden veroorzaakt door langdurige mechanische belasting. Ze vormen een serieus en toenemend probleem in de gezondheidszorg. De prevalentiecijfers zijn hoog. Afhankelijk van welke wonden worden meegenomen in het onderzoek en van de groep patiënten die wordt onderzocht, ontwikkelen tussen de 8 en 23 % van de patiënten een drukwond. Drukwonden komen het meest voor bij ouderen en bij mensen met een dwarslaesie. Ook mensen die een prothese of orthese dragen kunnen last krijgen van drukwonden.

Drukwonden kunnen zowel in de huid beginnen als in dieper gelegen weefsels. In het eerste geval breiden ze zich uit van de huidlaag naar dieper gelegen weefsellagen, terwijl dit in de tweede situatie andersom gebeurt. Deze laatste wonden worden ook wel aangeduid met 'diepe weefselschade' of 'diepe drukwonden' en zijn gedefinieerd als 'druk-gerelateerde schade aan subcutaan weefsel onder een intacte huid'. Deze definitie geeft direct een van de grote problemen van deze wonden aan: vroegtijdige detectie. Dat is van belang omdat op het moment dat een diepe drukwond zichtbaar wordt, de schade al groot is en genezing zeer moeilijk. Daarnaast is het niet duidelijk welke mechanismen leiden tot diepe drukwonden. Dit proefschrift richt zich daarom op diepe drukwonden en specifiek op de schade die ontstaat in spierweefsel. Onze hypothese is dat schade in spierweefsel ontstaat door een locale mechanische overbelasting van spiervezels.

Onderzoek naar diepe drukwonden werd lange tijd belemmerd door een gebrek aan niet-invasieve technieken om initiële pathologische veranderingen in diepgelegen weefsels te onderzoeken. Er zijn nu echter nieuwe technieken ontwikkeld waarmee dit wel mogelijk is. In dit promotieonderzoek is gebruik gemaakt van MRI (magnetic resonance imaging) om het ontstaan en de ontwikkeling van schade in spierweefsel van Brown Norway ratten te meten tijdens en na een mechanische belasting. Daartoe werd een MR-compatibel belastingsapparaat ontworpen en geconstrueerd waarmee een belasting kan worden opgelegd en tegelijkertijd MR-data kunnen worden verzameld. Hiermee kan het moment van schadeinitiatie en de ontwikkeling daarvan in de tijd gemeten worden, gebruik makend van T2-gewogen MRI. Met dit belastingsapparaat kunnen ook andere MR-technieken gebruikt worden, zoals MR tagging om weefselvervormingen te onderzoeken en MRI in combinatie met een contrastvloeistof om perfusie in de spier te onderzoeken tijdens en na belasting. Om een onderscheid te kunnen maken tussen de verschillende factoren die bijdragen aan spierschade werd een aantal belastingsprotocollen gebruikt, waaronder ischaemische belasting en compressieve belasting. De relevantie van aanhoudende vervorming van cellen voor het schadeproces is onderzocht door de locatie

van schade, bepaald via een verhoogde T2, te vergelijken met locale rekvelden, bepaald uit MR tagging data. Daarnaast is een numeriek model ontwikkeld waarmee computer simulaties werden uitgevoerd om uiteindelijk objectieve schadedrempels en ontwerpcriteria voor drukverlagende systemen te kunnen bepalen.

Uit de experimenten blijkt dat het effect van 2 uur ischaemie op de T2 van spierweefsel reversibel is binnen 40 minuten na verwijdering van de belasting. Dit werd bevestigd met behulp van histologische technieken die slechts kleine afwijkingen lieten zien. Compressie van het weefsel leidt echter tot blijvend verhoogde T2-waarden en – zoals bleek uit histologisch onderzoek - necrotische gebieden. Dit impliceert dat de vervorming, bovenop de ischaemie, een belangrijke trigger is voor het ontstaan van schade. De toename in T2 tijdens ischaemische belasting duidt echter wel op weefselveranderingen veroorzaakt door ischaemie alleen. Deze veranderingen zullen zeer waarschijnlijk de schadeontwikkeling ten gevolge van vervormingen versnellen en/of vergroten. Het belang van de vervorming wordt verder bevestigd door de correlatie tussen de gebieden met hoge rekken, zoals bepaald uit de tagging MR data, en de schadelocatie.

In conclusie: dit proefschrift presenteert een aantal MRI methoden die effectief kunnen worden gebruikt om specifieke mechanismen te identificeren die een rol spelen bij het ontstaan van schade na mechanische belasting. Naast MRI is er gebruik gemaakt van histologische technieken en een eindige elementen methode. Het belang van vervorming is aangetoond door de specifieke locatie van de schade, het type schade en het verschil in reactie op ischaemische en compressieve belasting.

Dankwoord

Er zijn veel mensen die ik wil bedanken voor hun bijdrage aan dit proefschrift. Als eerste wil ik mijn copromotor Cees Oomens bedanken die me vijf jaar geleden vroeg om dit promotie-onderzoek te doen. Cees, bedankt voor de geweldige begeleiding, de ondersteunende woorden en je positivisme. Ik heb onze samenwerking altijd als zeer prettig ervaren en ik ben heel blij en vereerd dat hier een vervolg aan mag komen. Ik wil Carlijn Bouten bedanken voor haar steun aan het begin van mijn promotie periode, welke moeilijk was door de problemen met m'n rug. I would like to thank Dan Bader for teaching me so much about doing research. It was really an honour to work with you. Thank you for your confidence, your time and your beautiful British English (the one time I corrected you was an exceptional moment). I'm looking forward to continue our cooperation. Ik wil Klaas Nicolay bedanken voor zijn begeleiding en vertrouwen. De manier waarop je hier de MR-groep hebt opgezet bewonder ik zeer. Ik wil Frank Baaijens bedanken voor het mogelijk maken van dit project. Gustav Strijkers wil ik bedanken voor alle hulp bij de MR-metingen en voor het feit dat hij altijd tijd voor me had, of ik nu een moeilijke of een wat meer trivialere vraag had. Ik wil Maarten Drost bedanken voor de adviezen aan het begin van het project en het doen van de 'bestellingen'.

Ik heb het voordeel gehad deel uit te mogen maken van twee groepen, de MaTe groep en de biomedische NMR groep, wat veel collega's opleverde. Allereerst wil de decubitus-AIO's bedanken. Te beginnen met Mariëlle voor het mogen voortzetten van haar werk, wat mij een goede startpositie gaf. Roel, Emiel, Debby, Debbie, Karlien en Lisette, ontzettend bedankt. Het is zo belangrijk om samen aan een onderwerp te kunen werken! Vooral in het laaste jaar was de saamhorigheid groot. De 'alles-komt-goed'-borrels waren geweldig en zeer ontspannend. Een speciale dank voor Debby, Lisette en Karlien voor hun steun en hulp in de laatste periode. Jullie staan niet als mede-auteur op de kaft, en het is ook geen hele pagina in het dankwoord geworden, maar daarom is mijn dank niet minder oprecht. Ik zal er tegen die tijd voor jullie zijn. Met mijn kamergenoten Bram, Raoul en Ralf heb ik heel wat tijd doorgebracht. Ondanks dat ze mij altijd uitlachten om mijn 'paint-gebruik' en aanhoudende enthousiasme over mijn MR-plaatjes, heb ik jullie gezelschap zeer gewaardeerd. Ik zal jullie missen. De koffie-pauzes in de MaTe-corner waren twee keer per dag een welkome onderbreking. Iedereen bedankt voor de gezelligheid, de onzinnige verhalen en adviezen daar (Maartje en Sjoerd: schouderklopje). Grote dank voor Rob v/d Berg voor het maken van m'n opstelling en alle daaropvolgende kleine wijzigingen. Voor alle computer-hulp bedank ik Patrick en Leo (en ik weet dat je sommige dingen nie mot willen...). Dank aan Rob Petterson voor alle hulp, welk praktisch probleem dan ook , je was pas tevreden als het helemaal goed was.

Curriculum Vitae

Anke Stekelenburg werd geboren op 26 februari 1976 in Raamsdonksveer. In 1994 behaalde zij haar VWO diploma aan het Riethil College te Raamsdonksveer. Aansluitend studeerde zij Technische Natuurkunde aan de Technische Universiteit Eindhoven (TUE). Als onderdeel van deze studie heeft zij stage gelopen bij het Bakken Research Center van Medtronic in Maastricht, met als onderwerp Atomic Force Microscopy. (AFM) Tijdens haar afstudeerwerk heeft zij het effect van shear stress op endotheel cellen onderzocht met behulp van confocal laser scanning microscopy en AFM. Eind 2000 is zij begonnen met haar promotie onderzoek aan de faculteit Biomedische Technologie (BMT) van de TUE, resulterend in dit proefschrift. Het onderzoek maakte deel uit van het decubitus onderzoek dat bij de faculteit BMT gedaan wordt. Aansluitend aan het promotie-onderzoek zal zij haar onderzoek naar de etiologie van diepe drukwonden voortzetten aan de TUE als post-doc.

February 26, 1976	Born in Raamsdonksveer, the Netherlands
1988-1994	Secondary education, Riethil College, Raamsdonksveer
1994-2000	Master's degree, Applied Physics, Eindhoven University of Technology
2000-2005	PhD, Biomedical Engineering, Eindhoven University of Technology